Università degli Studi di Padova

Dipartimento dei Beni Culturali: Archeologia,
Storia dell'Arte, del Cinema e della Musica

Corso di Studio Magistrale in
SCIENZE ARCHEOLOGICHE
Curriculum in
APPLIED SCIENCES TO CULTURAL HERITAGE MATERIALS AND SITES

Double MASTER Degree with the

Université Bordeaux Montaigne

MASTER
Mention
ARCHEOLOGIE, SCIENCE POUR L'ARCHEOLOGIE
Parcours
ARCHEOMÉTRIE

Identification of Pigments on Ceramics from the Ánimas Altas Archaeological Complex, Paracas Culture (Peru, 300 BCE–50 CE)

Supervisors: Dr. Aïcha Bachir Bacha and Prof. Lara Maritan

Co-supervisor: Dr. Ayed Ben Amara and Prof. Rémy Chapoulie

Master Candidate

Sifatullah Hassin, 2121962

Academic Year 2024/2025

Table of Contents

ACKNOWLEDGMENTS 6

ABSTRACT 7

FORWARD 9

INTRODUCTION AND PROBLEM STATEMENT 10

1 PART ONE: CONTEXT AND STATE OF THE ART 12

1.1 Introduction to Paracas Culture 12

1.2 Chronological Framework 13

1.3 Research history of Ánimas Altas/Ánimas Bajas 13

1.4 The Archaeological Complex of Ánimas Altas/Ánimas Bajas 15

1.4.1 Architecture and Functional Zoning at Ánimas Altas and Ánimas Bajas 16

1.4.2 Ceramic Production and Style at Ánimas 18

1.5 Key Areas of the Site 20

1.5.1 Montículo 1: Material Culture in the Edificio de los Frisos 20

1.5.2 El Panteón 23

2 PART TWO: STUDY MATERIAL AND METHODOLOGY 24

2.1 Overview of the Sample Set 24

2.1.1 Montículo 1 24

2.1.2 Montículo 25 24

2.1.3 El Panteón 25

2.2 Analysis Protocols 26

2.2.1 Binocular loupe observations 27

2.2.2 Hyperspectral Imaging 28

2.2.3 Sample Preparation 30

2.2.4 SEM-EDS (Scanning Electron Microscopy with EDS) 30

2.2.5 Portable X-Ray Fluorescence (pXRF) 31

2.2.6 Raman Spectroscopy 32

2.2.7 Fourier Transform Infrared Spectroscopy 34

3 PART THREE: Experimental Results and Discussion 36

3.1 Imaging and Texture Analysis 36

3.1.1 Microscopic Imaging (Optical Microscope and SEM) 36

3.1.1.1 Surface Features and Condition 36

3.1.1.2 Paste texture 39
3.1.1.3 Decorative Layers 42
3.1.2 Hyperspectral Imaging 53
3.1.2.1 Red Decorations 53
3.1.2.2 Black Decorations 54
3.1.2.3 Yellow Decorations 56
3.1.2.4 RGB and Infrared False Color (IRFC) Imaging 56
3.2 Colorimeter 58
3.2.1.1 Black Color Areas 58
3.2.1.2 Red Color Areas 58
3.2.1.3 Yellow Color Areas 58
3.2.1.4 Orange Color Areas 59
3.2.1.5 Cream Color Areas 60
3.2.1.6 Gray Color Areas 60
3.2.1.7 Beige and Brown Color Areas 60
3.3 Chemical Analyses 64
3.3.1 Analysis of the Ceramic Matrix 64
3.3.1.1 pXRF 64
3.3.1.2 SEM-EDS 69
3.3.2 Pigment and Decoration Analysis 71
3.3.2.1 SEM-EDS 71
3.3.2.2 pXRF 79
3.3.3 Raman Spectroscopy 82
3.3.4 FTIR Analysis 91
4 Conclusions and Future Perspectives 93
5 Bibliography 95
6 Appendix 104

ACKNOWLEDGMENTS

I would like to express my heartfelt appreciation to my supervisors, Dr. Aïcha Bacha Bachir and Prof. Lara Maritan, for their invaluable support and guidance throughout this Double Degree program between Bordeaux Montaigne University and the University of Padua. I am especially grateful to Dr. Aïcha Bacha Bachir, for her expertise, insightful advice, and thought-provoking discussions, all of which have been priceless to the creation and shaping of this work. I also sincerely thank Prof. Lara Maritan for coordinating the Double Degree program and for her dedication, which ensured a smooth and enriching academic experience across both institutions.

I would like to wholeheartedly thank my co-supervisors, Dr. Ayed Ben Amara and Prof. Rémy Chapoulie. I am especially thankful to Dr. Ayed Ben Amara for his close supervision during the entire internship and thesis process. His patience, generosity, and availability were the instruments behind every step of this research. I also sincerely thank Prof. Rémy Chapoulie for his important role in the Double Degree program, for his help in defining my research topic, and for his constant support during my time at Archéosciences Bordeaux.

I express my sincere appreciation to Christelle Lahaye and Christian Gensbeitel, director and deputy director respectively of Archéosciences Bordeaux, for accepting me to the laboratory and arranging for me to work on my research in the prestigious academic environment.

I would like to thank Dr. François-Xavier Le Bourdonnec for his helpful pXRF training, Dr. Stéphan Dubernet for his expert technical assistance regarding Raman spectroscopy, and Yannick Lefrais for his instrumental SEM training.

Special thanks go to Dr. Aurélie Mounier for her guidance in interpreting hyperspectral imaging data and to Sarah Petitcolas for her help with FTIR and imaging techniques. I am also deeply grateful to Dr. Mohamed Sofiane Djerad for the careful preparation of ceramic samples, which was fundamental to the success of this work.

This work was made possible thanks to the financial support of the LTC Sarea (Laboratories in Transfrontier's Collaboration) frame which links the laboratory Archéosciences Bordeaux (Pr. R. Chapoulie) to the GPAC laboratory in the University of the Basque Country at Vitoria-Gasteiz (Dr J.G. Iñañez).

Lastly, I must thank my family for their endless encouragement throughout the entire process. Being far from home, trying to adjust to a new environment, and immersing myself in another culture was not always easy. On solitary days, their constant presence—through phone calls, messages, and unwavering support—kept me from ever feeling lonely. Their encouragement and inspiration gave me the strength to continue and complete this piece of writing.

ABSTRACT

This master thesis presents a multidisciplinary archaeometric analysis of 19 monochrome and polychrome ceramic sherds from the Ánimas Altas archaeological complex, Paracas culture (300 BCE–50 CE). This study was conducted as part of a double degree program between the University of Padova and Bordeaux Montaigne University. It combines colorimetry and hyperspectral imaging with analytical techniques including SEM-EDS, pXRF, Raman spectroscopy, and FTIR to characterize the compositions of ceramic decorations and investigate their production technologies. Results show that monochrome decorations were applied before firing, whereas polychrome decorations were applied post-firing. Red, brown, and orange areas were found to contain red ochre (hematite); yellow and cream areas show presence of arsenic sulfides (orpiment); and black decorations showed evidence of amorphous carbon, manganese compounds, and indigo. Future research should include expanded use of advanced techniques such as mass spectrometry alongside a larger sample set and natural organic reference materials to better understand the provenance of pigments and the associated technological practices.

Résumé

Ce mémoire de master présente une analyse archéométrique pluridisciplinaire de 19 tessons de céramique monochromes et polychromes provenant du complexe archéologique d'Ánimas Altas, attribué à la culture Paracas (300 av. J.-C. – 50 apr. J.-C.). Cette étude a été réalisée dans le cadre d'un programme de double diplôme entre l'Université de Padoue et l'Université Bordeaux Montaigne. Elle combine la colorimétrie et l'imagerie hyperspectrale avec des techniques analytiques telles que la SEM-EDS, la pXRF, la spectroscopie Raman et la FTIR, afin de caractériser la composition des décorations céramiques et d'examiner leurs technologies de production. Les résultats montrent que les décorations monochromes ont été appliquées avant la cuisson, tandis que les décorations polychromes l'ont été après la cuisson. Les zones rouges, brunes et orangées contiennent de l'ocre rouge (hématite) ; les zones jaunes et crème révèlent la présence de sulfures d'arsenic (orpiment) ; et les décorations noires présentent des traces de carbone amorphe, de composés de manganèse et d'indigo. Des recherches futures devraient inclure un recours accru à des techniques avancées telles que la spectrométrie de masse, ainsi qu'un ensemble d'échantillons plus large et des matériaux de référence organiques naturels, afin de mieux comprendre la provenance des pigments et les pratiques technologiques associées.

Riassunto

Questa tesi magistrale presenta un'analisi archeometrica multidisciplinare di 19 frammenti ceramici monocromi e policromi provenienti dal complesso archeologico di Ánimas Altas, attribuito alla cultura Paracas (300 a.C. – 50 d.C.). Lo studio è stato svolto nell'ambito di un programma di doppio titolo tra l'Università di Padova e l'Université Bordeaux Montaigne. L'analisi integra la colorimetria e l'imaging iperspettrale con tecniche analitiche quali SEM-EDS, pXRF, spettroscopia Raman e FTIR, al fine di caratterizzare la composizione delle decorazioni ceramiche e investigare le relative tecnologie di produzione. I risultati mostrano che le decorazioni monocrome sono state applicate prima della cottura, mentre quelle policrome dopo la cottura. Le aree rosse, marroni e arancioni contengono ocra rossa (ematite); le aree gialle e crema mostrano la presenza di solfuri di arsenico (orpimento); e le decorazioni nere evidenziano tracce di carbonio amorfo, composti del manganese e indaco. Le ricerche future dovrebbero prevedere un uso più esteso di tecniche avanzate come la spettrometria di massa, insieme a un campione più ampio e a materiali di riferimento organici naturali, per comprendere meglio la provenienza dei pigmenti e le pratiche tecnologiche associate.

FORWARD

This study is part of the Ánimas Atlas/Ánimas Bajas archaeological program in Ica, Peru, directed by Aïcha Bachir Bacha and Oscar Daniel Llanos, supported by the French Ministry for Europe and Foreign Affairs (MEAE) and the School for Advanced Studies in the Social Sciences (EHESS), and authorized by the Peruvian Ministry of Culture.

The physical-chemical analysis of ceramic sherds collected from the site is conducted at Archéosciences Bordeaux (UMR 6034, Université Bordeaux Montaigne – CNRS) under the supervision of Dr. Ayed Ben Amara.

The ceramic sherds selected for analysis originate from the Ánimas Altas archaeological complex, a major Paracas settlement in the Ica Valley dated between 300 BCE and 50 CE. Paracas culture is known for its polychrome ceramics, notably Paracas Cavernas/Ocucaje, characterized by incised ornamentation and post-firing technique. The technique reflects an advanced understanding of pigment preparation and uses that allow for a broad color range.

These polychrome ceramics, traditionally associated with ritual and ceremonial settings, found in several Paracas settlements, including civic-ceremonial structures, tombs, workshops, and residential areas. Their wide distribution beyond the Peruvian south coast suggests their importance in elite political and religious networks and maybe their function as part of long-distance trade exchanges.

While Paracas textiles have been researched more (*Protective Perimeters*, 2017; Sabatini et al., 2020), the composition and application of pigments in Paracas ceramics remain comparatively under-researched. To address this lack, this study applies a multi-analytical approach to examine mineralogical and organic components of ceramic decoration. The goal is to reconstruct the techniques used in ceramic colorant production and identify the raw material.

Finally, this study contributes to a broader understanding of ancient Andean ceramic technologies, symbolic uses of color, and the socio-economic dimensions of Paracas craftsmanship, enhancing our knowledge of this fascinating pre-Columbian civilization.

INTRODUCTION AND PROBLEM STATEMENT

The study of ancient times ceramic is a rich source of data on past civilizations' technological activity, social structure, and economies. Among the pre-Columbian Andean cultures, Paracas culture (800 BCE – 50 CE) stands out for its exceptional polychrome ceramics with a sophisticated post-firing technique of painting. Despite the central role these ceramics play in Paracas art, the composition and application of their decorations remain insufficiently understood.

The Ánimas Altas/Ánimas Bajas archaeological complex in the Ica Valley is an important site for understanding the Paracas culture by providing a significant collection of ceramics used in both domestic and ceremonial contexts. Excavations carried out by Bachir Bacha and Oscar Daniel Llanos Jacinto since 2007 at the site have revealed a diverse range of Paracas polychrome ceramics, which are notably found beyond the southern Peruvian coast, indicating their potential association with elite political and religious spheres, as well as their involvement in broader exchange networks(Bachir Bacha & Llanos Jacinto, 2021, p. 26).

However, the precise technology of ceramics decoration and color technology remain unstudied. The current research seeks to bridge these gaps by using archaeometric methods in the study of the compositional and technological characteristics of the applied pigments on the ceramics.

1- Technological Aspects of Color Application:

- What were the materials and techniques used in the preparation and application of color in the ceramics discovered at Ánimas, excavated by A. Bachir Bacha and Oscar Daniel Llanos?
- Are the colorants more mineral based or do they include organics?

2- Archaeometric Characterization of ceramic decoration:

- What are the chemical and mineralogical compositions of the color decoration used in Paracas ceramics?
- What types of binding agents were used in the production of these pigments and colorants, and how were they processed?
- Are there variations in color composition between the different archaeological sites (Ánimas and El Panteón), and between the architectural structures within Ánimas (e.g., Montículo 1 and Montículo 25)?

To fulfill these objectives, the present work employs a multi-disciplinary methodology that integrates Optical Microscopy (OM), Scanning Electron Microscopy coupled with Energy Dispersive X-ray Spectroscopy (SEM-EDS), portable X-ray Fluorescence (pXRF), Raman spectroscopy,

Hyperspectral Imaging (HSI), and Fourier Transform Infrared Spectroscopy (FTIR). These advanced techniques provide microstructural and compositional data, which can help us to reconstruct the methods used to produce ceramic decoration. The analytical methodologies took place at Archéosciences Bordeaux (https://www.archeosciences-bordeaux.fr), Pessac, France.

By uniting archaeometric data and technological and material analyses, this research aims to refine our understanding of Paracas ceramic traditions, paying particular attention to the technological processes of pigment production and application. The study will enlighten the raw materials and processing methods utilized in the production of these ceramics and contribute to the overall knowledge of the technological prowess of Paracas culture.

1 PART ONE: CONTEXT AND STATE OF THE ART

1.1 Introduction to Paracas Culture

The Paracas culture is among the most distinctive and influential of the ancient Peruvian coastal civilizations, occypying an vast area that extended along the whole southern coastal region of the country (Fig. 1). Paracas is not only the name of the culture but also the name of a seasonal wind blowing in winter. According to Bachir Bacha (2018), the name probably originated from the Quechua terms para (rain) and acco (sand), meaning "rain of sand."

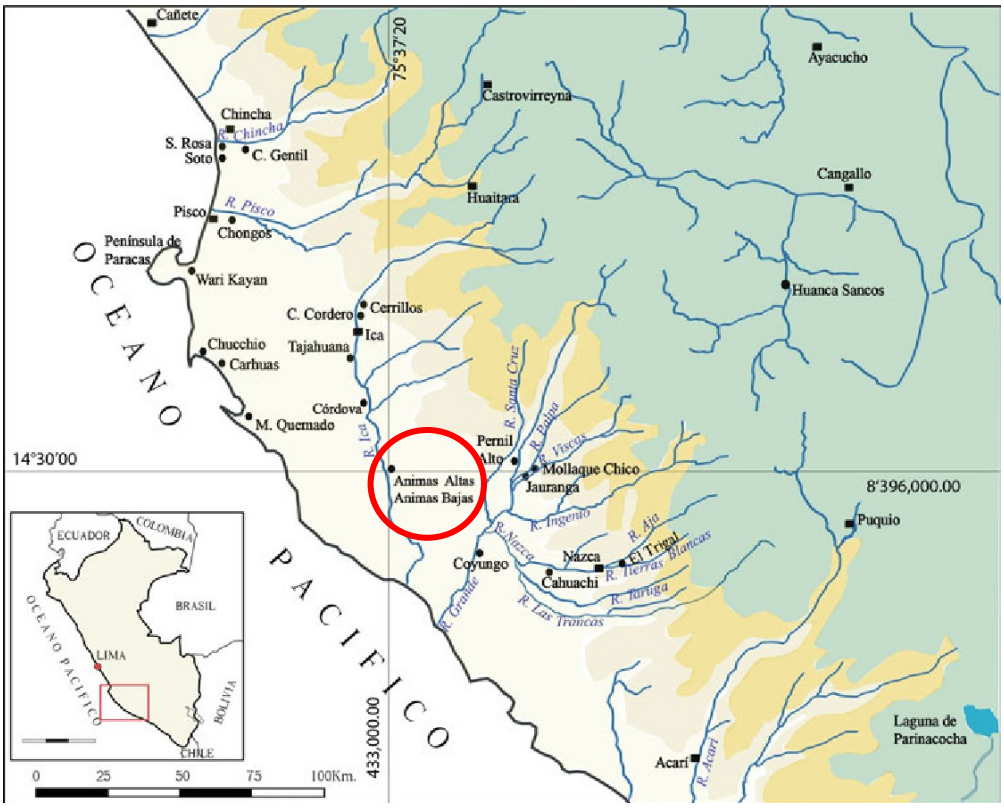

Figure 1. Map showing the south coast of Peru and the location of the Animas Altas/Animas Bajas archaeological complex. Adapted from Bachir Bacha (2018).

Paracas became widely recognized in academic literature after the discovery of highly well-preserved funerary bundles on the Paracas Peninsula that showcased the technical and artistic prowess of the culture. Paracas is most renowned for painted ceramics and polychrome textiles, which are marked by skillful craftsmanship and elaborate iconography (Fig. 2). Their architectural, pyramids, platforms, and ritual areas and ceremonial spaces were built from unbaked adobe and clay that show examples of Paracas cultural and ritual sophistication (Bachir Bacha, 2018, p. 2).

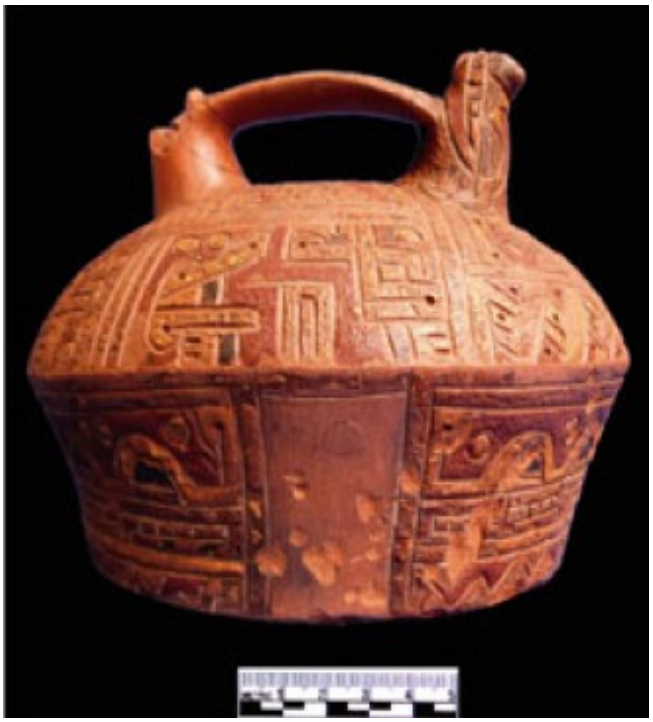

Figure 2. Polychrome ceramic discovered at León Dormido 3, Paracas (Lucia Balbuena).

1.2 Chronological Framework

The Paracas culture, active along Peru's south coast during the Early Horizon, is now commonly divided into four chronological phases following the framework proposed by P.H. Carmichael (2019), as adapted in Bachir Bacha (2022) and shown in (Fig. 3a): Early Paracas (ca. 800–500 BCE), Middle Paracas (ca. 500–300 BCE), Late Paracas (ca. 300–200 BCE), and Final Paracas (ca. 200 BCE–50 CE). Even though these are used for analytical clarity, some researchers for example, Aïcha Bachir Bacha considers the entire period from 300 BCE to 50 CE as a single continuous Late Paracas phase, due to the cultural and stylistic continuity observed across this span. The Ánimas Altas ceramic assemblages are so dominated by Phases 9 and 10 of Ocucaje that they clearly indicate a primary occupation during the Late phase (ca. 300 BCE–50 CE)(Bachir Bacha, 2022, pp. 58–59). Ánimas Bajas, particularly Montículo 127, has yielded ceramics associated with Phases 7 and 8 of Ocucaje, indicating an earlier occupation during the Middle and early Late Paracas periods.

1.3 Research history of Ánimas Altas/Ánimas Bajas

The earliest references to the Ánimas Altas/Ánimas Bajas complex can be traced back to Julio C. Tello and later William D. Strong, who surveyed the broader Callango region in the mid-20th

century. Lawrence E. Dawson later identified the site under the name “Media Luna” and conducted preliminary excavations. The site was subsequently catalogued by researchers from the University of California, including John Rowe and Dorothy Menzel, who associated the ceramics with the Ocucaje 8 and 9 phases (Bachir Bacha, 2017, pp. 195–196).

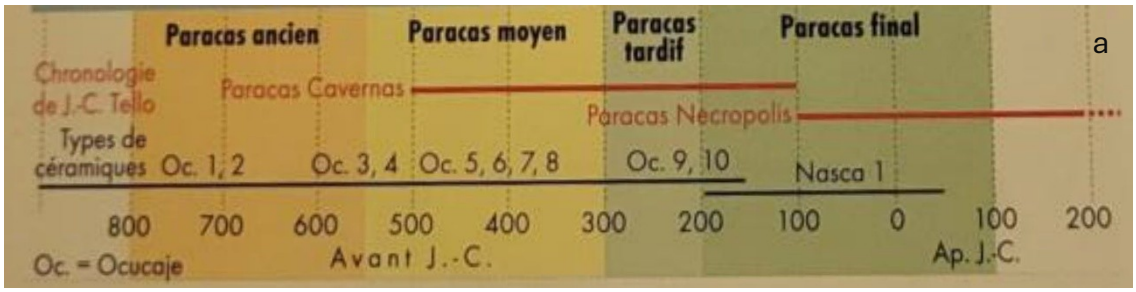

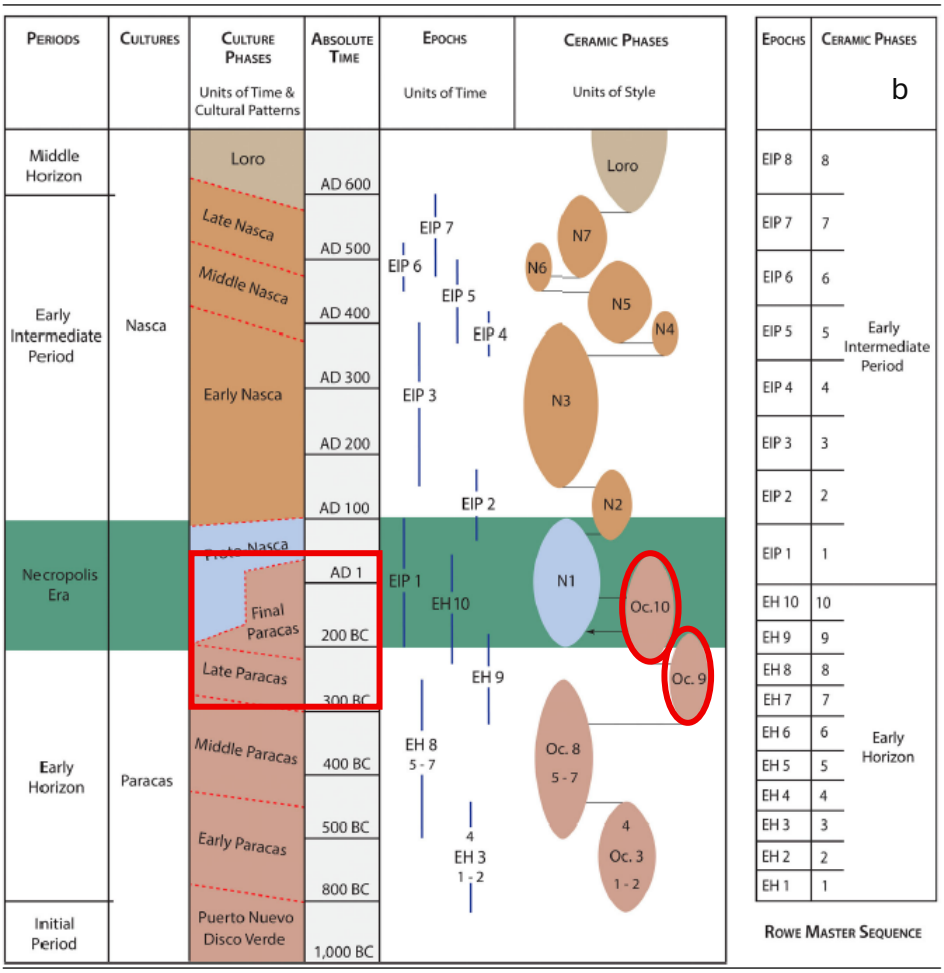

Figure 3.(a) Chronology of the Paracas culture and distribution of principal sites at Ánimas Altas. Bachir Bacha (2022).

(b) Chronology of the South Coast of Peru (Carmichael, 2019).

In the decades that followed, scattered investigations by archaeologists such as Sarah Massey and Anita Cook provided some additional data, particularly on architectural features and ceramic

sequences. However, these initial interventions were limited in scope and lacked comprehensive contextual documentation (Bachir Bacha, 2017, pp. 195–196).

A more intense and methodical approach began in 2007 with the French Peruvian mission directed by Aïcha Bachir Bacha and Óscar Daniel Llanos Jacinto. Their works were a significant shift by locating Ánimas Altas/ Ánimas Bajas not as just two distinct settlements but as a unified, complex urban center. Excavations and mapping revealed that Ánimas was a multipurpose center that combined ritual, productive, and funerary spaces (Bachir Bacha & Llanos Jacinto, 2021, pp. 26–29).

This new phase of research not only more extensively elaborated our understanding of Paracas spatial planning and architectural techniques but also contradicted past interpretations primarily based on ceramic typologies. Stratigraphic evidence points to a more complex and superimposed series of occupations, with iconographic elements suggesting connections to earlier coastal traditions. The project also highlighted Ánimas' integration into broader regional systems, revealing links with both highland and coastal areas. Simultaneously with these research objectives, the team considered preserving the grand architectural and decoration elements, particularly the friezes, that are still vulnerable to human impacts and environmental degradation(Bachir Bacha & Llanos Jacinto, 2021, pp. 26–29).

1.4 The Archaeological Complex of Ánimas Altas/Ánimas Bajas

The Ánimas Altas and Ánimas Bajas site in the lower Ica Valley near the Ocucaje district (Fig. 1) is the most significant Paracas settlement in southern Peru, along the coastal area. It occupies over 100 hectares in the Pampa del Cacique, near the left bank of the Ica River and is located approximately 53 km south of the city of Ica (Bachir Bacha & Llanos Jacinto, 2021, p. 19).

Ánimas is strategically located between inland valley and coastlines, making it have access to agricultural lands, marine resources, and desert ecosystems, thus making it an ideal location for long-term habitation and social development (Bachir Bacha, 2018).

Other than these advantages, the surrounding environment also offered varied raw materials such as clayey soils, natural pigments, and mineral deposits in surrounding dunes and hills (Bachir Bacha & Llanos, 2013, p. 173) Ánimas' material culture establishes this close connection with the environment, particularly the colors of its textiles and the use of locally sourced colorants in ceramics.

The site organization resembles a complex urban structure made up of more than 100 mounds (Fig. 4) that are arranged across distinct architectural and functional zones including large ceremonial platforms, plazas, domestic areas, and workshops. While earlier interpretations suggested a chronological difference between Ánimas Bajas in the south and Ánimas Altas in the north, the former

being an older ceremonial center and the latter a later residential hub; more recent excavations have indicated that both were occupied contemporaneously. Ánimas Bajas contains both monumental and domestic architecture, while Ánimas Altas has higher public architecture, cemeteries, and plazas. The spatial organization of the site reveals a dual structure deeply embedded in Andean cosmology, two complementary yet contrasting halves, Ánimas Bajas and Ánimas Altas, bound together into a systematic and purposefully constructed settlement (Bachir Bacha & Llanos Jacinto, 2021, p. 27).

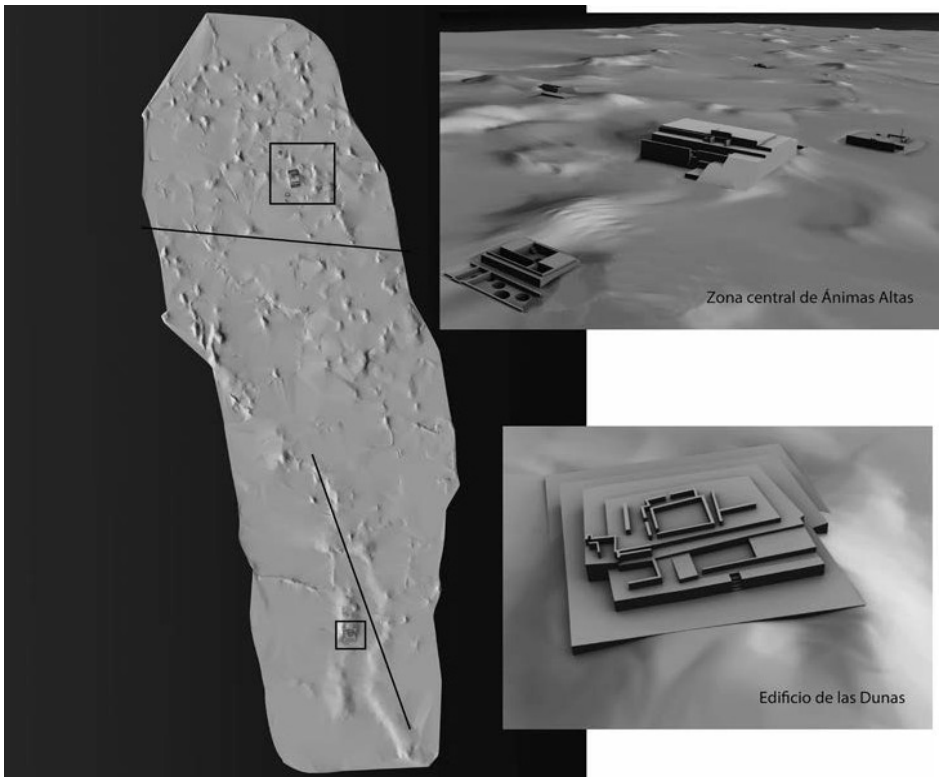

Figure 4. 3D construction of the Ánimas Altas/Ánimas Bajas archaeological complex (Bachir Bacha, 2018).

1.4.1 Architecture and Functional Zoning at Ánimas Altas and Ánimas Bajas

The Ánimas Altas and Ánimas Bajas architectural design reflects a sophisticated level of organization that combined ceremonial and residential and domestic functions. In contrast to other Paracas sites using adobe bricks in their constructions, Ánimas structures were built from semi-rectangular blocks of local clay sediment (Fig. 5). They were joined together by mortar composed of clay and straw and were usually finished with a smooth or textured plastered surface(Bachir Bacha & Llanos, 2013; Bachir Bacha, 2018, pp. 7–9) .

Ánimas Bajas stands out for its ritual offerings and layered construction phases; for example, Mound 127 (building of the Dunes) (Fig. 4). At the same time, Ánimas Altas features larger

ceremonial buildings like Mound 26 (building of Banquettes) (Fig. 6) and Mound 71, known for its mausoleum and friezes with Paracas and highland imagery(Bachir Bacha & Llanos, 2013).

In addition to public monuments, domestic and production areas, such as the D1 sector (Fig.7) and Mound 30, storage pits, textile tools, and ceramic debris indicate that daily and ritual life were spatially intertwined. Overall, Ánimas appears to have been a deliberately organized settlement where ceremonial, domestic, and productive spaces were functionally distinct although closely connected, reflecting an integrated and cohesive urban layout (Bachir Bacha & Llanos, 2013).

Figure 5. Sedimentary clay blocks of Ánimas commonly used for construction (Bachir Bacha & Llanos, 2013).

Figure 6. Mound 26 (building of Banquettes) (Bachir Bacha & Llanos Jacinto, 2021).

1.4.2 Ceramic Production and Style at Ánimas

The archaeological site of Ánimas presents an exceptional case for understanding Paracas ceramic production, not only due to the scale of its occupation and architectural complexity but also due to the richness and diversity of its ceramic assemblages. Excavations conducted by Bachir Bacha and Llanos since 2007 in different mounds and architectural zones, such as the Edificio de los Frisos and the Edificio de las Dunas, have provided important evidence regarding ceramic typologies, techniques, decorative systems, and production contexts, offering valuable information regarding the artistic and technological features of Paracas pottery during the Ocucaje 8, 9, and 10 phases (Bachir Bacha, 2017).

Figure 7. Sector D1, a domestic area showing architectural and occupational features across multiple construction phases, the hearth is highlighted in red and storage pits in blue, indicating key domestic area (adapted from Bachir Bacha & Llanos Jacinto, 2021).

Different forms were distinguished, such as short-necked ollas, bowls with negative decoration, bowls with incised and post-firing painted decoration, as well as a small number of jars and bottles (Fig. 8)(Bachir Bacha, 2017, pp. 208–209). These vessels had different domestic and ceremonial functions, such as food preparation, storage, distribution, and consumption.

Surface treatments show a range of techniques, including burnishing, smoothing with fingers or textile tools, and the application of reddish-brown or gray slips. While oxidizing atmospheres predominate in firing, evidence of both reducing and mixed atmospheres was observed (Bachir Bacha, 2017, pp. 208–209).

Decorative techniques included incising and post-firing painting (Fig. 9 left), and negative painting (Fig. 9 right) (Bachir Bacha, 2017, pp. 210–211). Most of these painted ceramics featured a range of geometric or anthropomorphic designs like stepped designs, pyramids, or serpents, which were executed in red, orange, and yellow pigments on black or dark brown backgrounds. Negative-painted ceramics often display dark designs on orange backgrounds, with dominant patterns such as vertical bands and concentric circles(Bachir Bacha & Llanos, 2013).

Technologically, ceramic production appears to have been organized around several workshops. There were five distinctive groups of clay pastes, suggesting the existence of relatively standardized production of transport and storage vessels and more variability with serving and consumable wares (Bachir Bacha & Llanos, 2013).as was observed in pottery over the Ocucaje periods 8, 9, and 10 (Bachir Bacha, 2017).

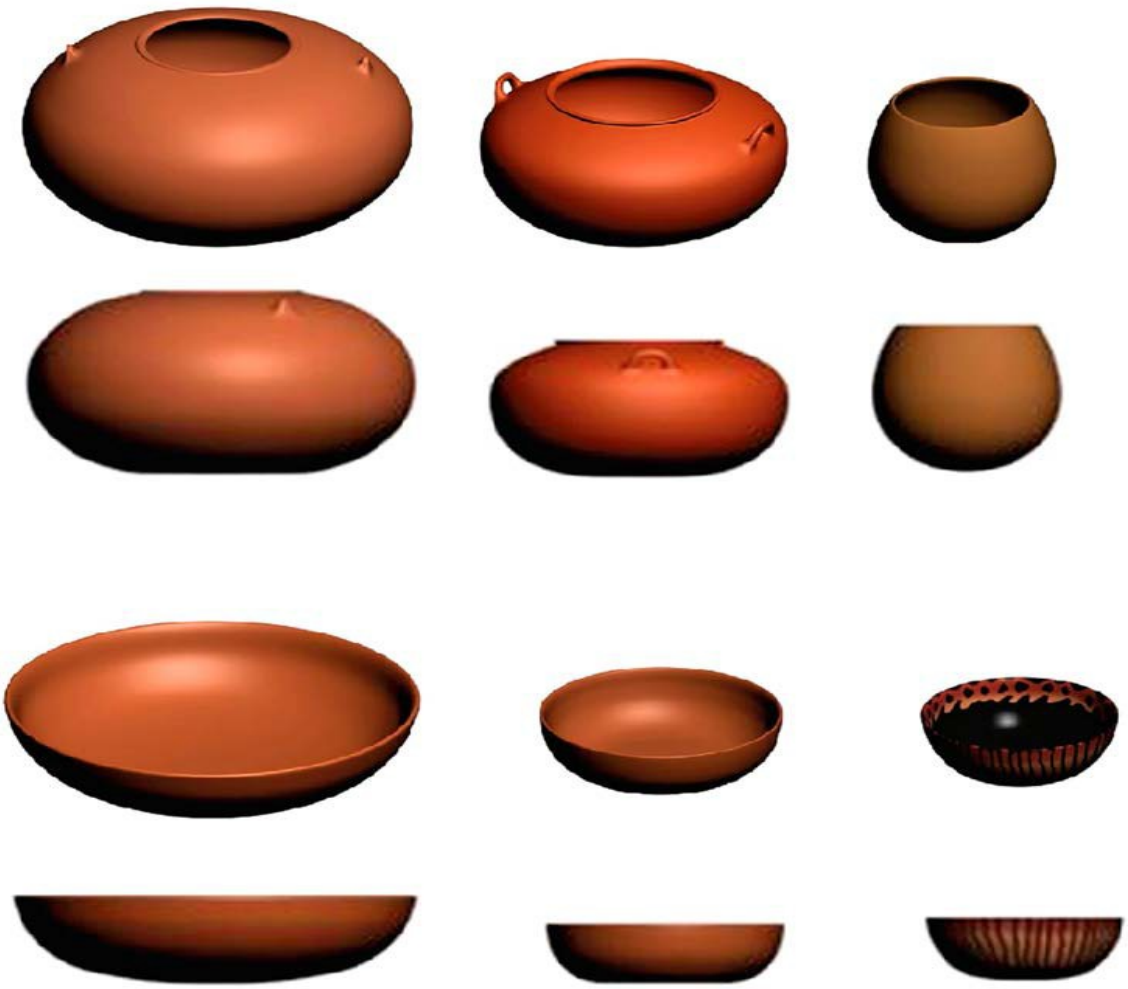

Figure 8. Reconstruction of Paracas vessels found in the Frieze Building (Bachir Bacha & Llanos Jacinto, 2021).

Figure 9. On the left, BDX27680, polychrome post-firing painting; on the right, BDX27678, negative painting decoration from Montículo 1(Sifatullah Hassin).

The evidence of production contexts complements these stylistic and technological observations. At Montículo 30, Plaza 1, and Area D1 in southern Ánimas Altas, features such as clay lumps with fingerprints, potters' plates, burnishing tools, and stratified burning zones were uncovered, pointing to onsite ceramic production. In these zones a lot of utilitarian ceramic sherds, grinding stones, and pigments residues discovered, linking ceramic production with broader artisanal practices (Bachir Bacha & Llanos, 2013, pp. 194–196).

Ánimas ceramics also exhibit sub-stylistic diversity, reflecting broader patterns of exchange and political tactics. Diversity of icons throughout phases suggests the employment of ceramics to mark identity and power, linking domestic life with ceremonial practice (Bachir Bacha & Llanos, 2013, pp. 196–197)).

1.5 Key Areas of the Site

This section presents the key archaeological contexts from which ceramic samples were selected: *Montículo 1* and *Montículo 25*, both located within the Ánimas Altas archaeological site, and *El Panteón*, a distinct Paracas site situated nearby. While Montículo 1 has been published and contextualized, Montículo 25 and El Panteón remain unpublished; however, ceramic material from both is included in this study.

1.5.1 Montículo 1: Material Culture in the Edificio de los Frisos

Montículo 1, also known as the Edificio de los Frisos (Fig. 10), is a civic-ceremonial structure located in the northern part of Ánimas archaeological complex. While it stands out for its complex architectural sequence and richly carved friezes, the archaeological excavations carried out between

2014 and 2016 by Bachir Bacha and Llanos Jacinto (2017) revealed an abundance of material culture, notably ceramics, textiles, and organic offerings, which provide essential insight into its ritual function and its broader socio-political role in the Paracas world (Bachir Bacha, 2017, pp. 196–197) .

Figure 10. Montículo 1 (Edificio de los Frisos) showing the architectural sequence of the building. The engraved friezes are shown in green box, while the ramp fill, corrals, and tomb—where ceramics, textiles, and organic materials were discovered are highlighted in red (Bachir Bacha, 2017).

The ceramic assemblage recovered in Montículo 1 is primarily associated with the Ocucaje 9 and 10 phases (Fig. 11) and only rarely Ocucaje 8, placing the structure within the Late Paracas period (Bachir Bacha, 2017, p. 201; Bachir Bacha & Llanos Jacinto, 2021, pp. 50–66).

Among the ceramics, plenty of the sherds were decorated using negative painting techniques, incised post-firing (Fig. 9), and plain utilitarian wares. The shapes most identified are bowls and cooking vessels, with decorative pieces more related to ceremonial use (Bachir Bacha, 2017, p. 209; Bachir Bacha & Llanos Jacinto, 2021, p. 49). Some deposits' finding like an upside-down container or burned vessels, that imply ritual use in connection with closure or offering events. Other offerings were more symbolic: miniature figures made from raw clay or carved bone appeared in fills and on floor surfaces. Materials such as pigments (ochre), obsidian projectile points, and textile fragments with polychrome embroidery were also discovered, complementing the impression that Montículo 1 was not only a sacred space but a politico-religious integration point in material culture use (Bachir Bacha, 2017, p. 201; Bachir Bacha & Llanos Jacinto, 2021, pp. 49–60).

Apart from ceramics, notable amounts of textile remain were excavated, especially in the context of burials and enclosure infill. They included camelid fiber, tufts of cotton, embroidered cloth, and spindle whorls (Bachir Bacha, 2017, p. 197; Bachir Bacha & Llanos Jacinto, 2021, p. 66). The fact that they were associated with offerings, rather than domestic context, means they had symbolic rather than practical uses in this context. The persistent accumulation of ceramics, organic remains, and symbolic figurines at every subsequent stage of construction confirms that Montículo 1 was ritually charged with significance, since burial, sacrifice, and symbolic closure overlay every architectural intervention.

Figure 11. Ceramics sherds (BDX27679 left and BDX27682 right) from phases 9 and 10 found at Montículo 1 (Sifatullah Hassin).

The friezes (Fig. 12) at Montículo 1 combine Paracas iconography from the Ocucaje 9–10 phases with earlier stylistic influences, such as those from Cupisnique and Chavín traditions. According to Bachir Bacha and Llanos, their geometric designs, featuring repeated rhomboids and

nested pyramids, symbolize ideas of time, space, and ancestral power. These patterns visually support the ceremonial and political role of the structure (Bachir Bacha, 2017, p. 206).

Figure 12. Detail of the frieze discovered in Mound 1 (Bachir Bacha & Llanos Jacinto, 2021).

1.5.2 El Panteón

The site of El Panteón is located on the left bank of the Río Ica, 800 meters west of Ánimas. Surveyed in 2013, the site covers more than one hectare and consists of five mounds with roughly oval shapes. The largest, Mound A, measures 60 meters in length, 50 meters in width, and 4 to 5 meters in height. The architecture is built from natural sedimentary clay blocks, and decorated ceramic sherds from Ocucaje Phases 8 and 9 have been found. Similar to the mounds identified at Ánimas, Mound A contains several superimposed and modified structures, covered by layers of fill, giving the final construction the form of a truncated pyramid topped with a series of enclosures and corridors (Bachir Bacha, 2017).

2 PART TWO: STUDY MATERIAL AND METHODOLOGY

2.1 Overview of the Sample Set

The ceramic assemblage analyzed in this study includes in total 19 samples collected from two architectural structures of the archaeological site of Ánimas Altas, Montículo 1 and Montículo 25, and El Panteón site. In total there are 9 polychromes, while the remaining samples are monochrome ceramics showing gray and orange surface.

2.1.1 Montículo 1

This sector has the largest number of samples (11) seen (Fig. 13), which exhibit a wide range of surface finishes and decorative techniques.

a. Polychrome decoration is prominent, with multiple colors showing red, yellow, black, white, cream or beige, and occasionally brown (e.g., BDX27677, BDX27679, BDX27680, BDX27682, BDX27683 and BDX27698).
b. Negative painting is visible in BDX27678, in which an orange and black motif extends onto the internal face. BDX27681 is a shiny yellow monochrome sample. This shiny surface can suggest the use of resin-based decoration.
c. BDX27674 and BDX27675 are monochrome samples and show gray coloration on both interior and exterior surfaces, which may be suggestive of reducing or mixing atmospheres.

2.1.2 Montículo 25

From Montículo 25, four samples were analyzed: three display monochrome decoration, and one is polychrome (Fig. 14).

a. BDX27684 and BDX27687 are coated in orange slip on both sides. There are potential traces of soot and incised marks on BDX27687 interior face. BDX27685 shows undecorated surfaces.
b. BDX27686 is polychrome decoration in red, black, and yellowish, with a brown slip on the internal face.

2.1.3 El Panteón

Out of the four samples, only one features polychrome decoration, while the remaining three are monochrome with orange surfaces (Fig. 14).

a. (BDX27688, BDX27689, BDX27691) samples show a predominance of orange slips, typically applied to both faces and several show soot traces (BDX27689, BDX27691), possibly linked to cooking or ceremonial fire exposure.
b. BDX27690 is exceptional in this group for its rich polychrome decoration, using red, yellow, cream white, and black, with a dark brown slip on the external and internal faces.

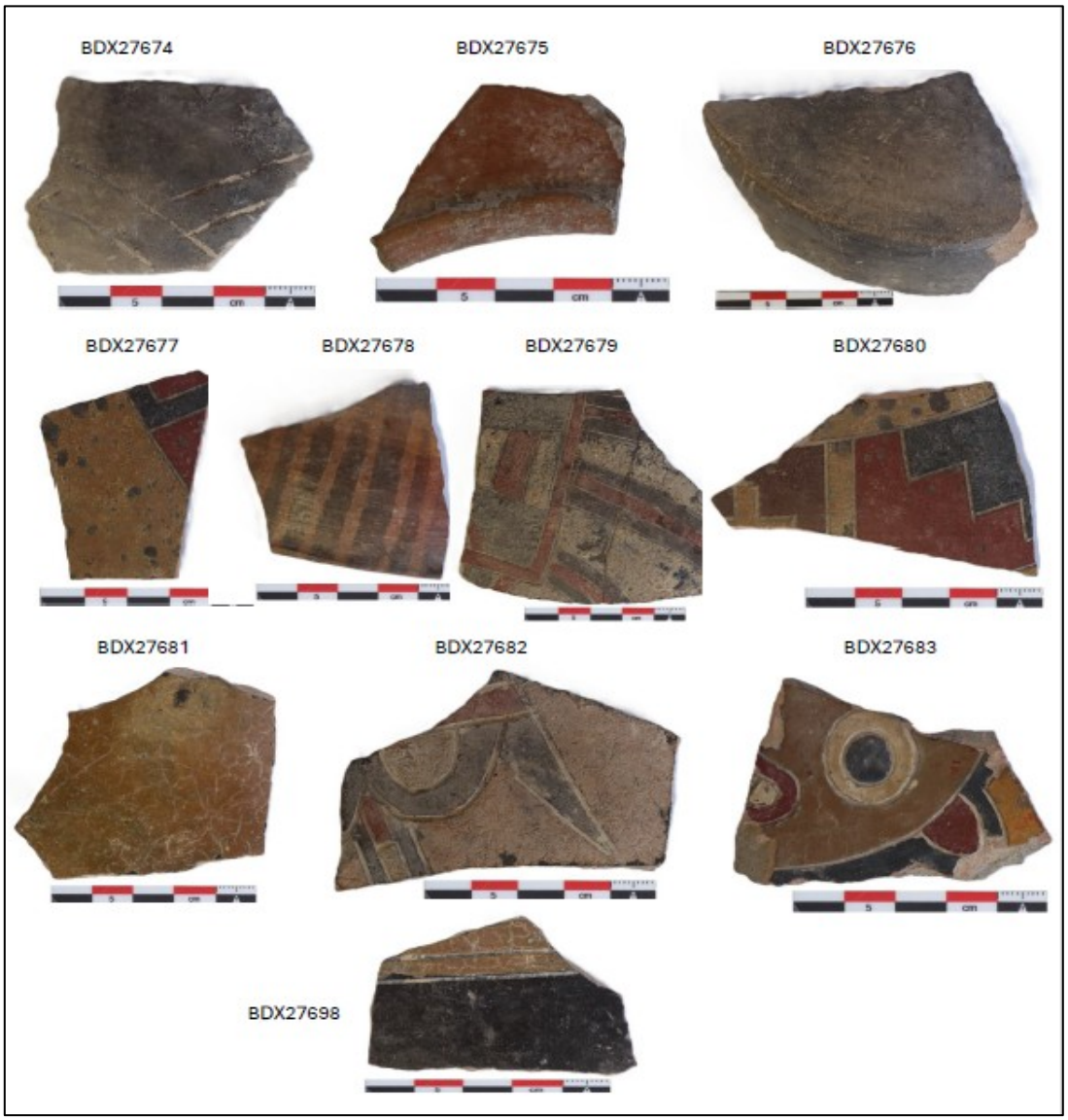

Figure 13. Ceramic samples collected from Montículo 1, showing the exterior decorated surfaces (Sifatullah Hassin).

Figure 14. Ceramic samples collected from Montículo 25 and El Panteón showing the exterior surfaces (Sifatullah Hassin).

2.2 Analysis Protocols

To address this study's research questions and hypotheses, a set of analytical techniques was employed. These techniques were chosen because of their ability to provide detailed information on the chemical composition, methods of production, and patterns of decoration for the ceramic samples. The non-destructive and destructive analyses, which were adopted, allowed proper comprehension of the materials and their characteristics.

2.2.1 Binocular loupe observations

Binocular loupe observations were conducted to examine the ceramic sherds to identify markers of manufacturing techniques, such as methods of slip or pigment application, the superposition of layers, and traces of shaping and finishing techniques.

The LEICA MC125 optical microscope was used for these observations, offering magnification range from 8x to 100x (Fig. 15). This microscope is equipped with stereo vision, allowing for a three-dimensional view of the ceramic surfaces. The stereo vision was particularly useful for visualizing fine surface details, such as texture, cracks, and decoration patterns.

Photographs were taken using a CCD camera attached to the microscope, providing high-resolution images of the ceramic surfaces. The images were processed and analyzed using the Leica Application Suite (LAS) software, which facilitated documentation and measurement of the observed features, such as colorant layering, surface texture, and any tool marks.

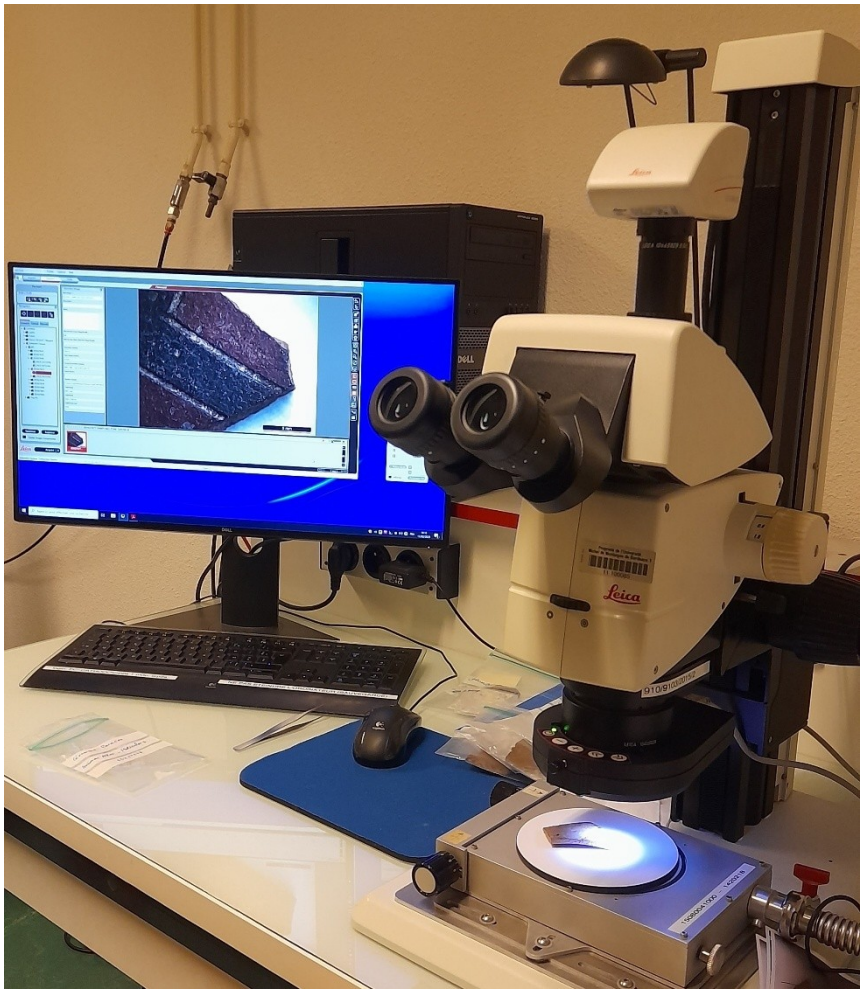

Figure 15. LEICA optical microscope used for the observation of ceramic surface treatments (Sifatullah. Hassin).

2.2.2 Hyperspectral Imaging

Hyperspectral imaging was applied on the ceramics prior to cutting carried out in order to facilitate enhanced surface area for analysis with the capability of scanning all the colors on the sample surface. The purpose was primarily to determine the to determine the nature of the decoration used, whether they are organic or mineral, and to see the variation and distribution of decoration across different samples.

For spectral analysis, two hyperspectral camera models were used:

- HSI VNIR Camera (Fig.16): It works between visible and near infrared (400-1000 nm) with 2.8 nm spectral resolution. It is fitted with a coupled ImSpector V10E spectrograph with CCD sensor that can cover 1600 spatial pixels and 840 spectral pixels.
- HSI SWIR Camera (Fig. 17): This camera covers the near-infrared spectrum (1000-2400 nm). It features an N25E spectrograph and an MCT detector with a spatial resolution of 384 pixels and spectral resolution of 288 bands.

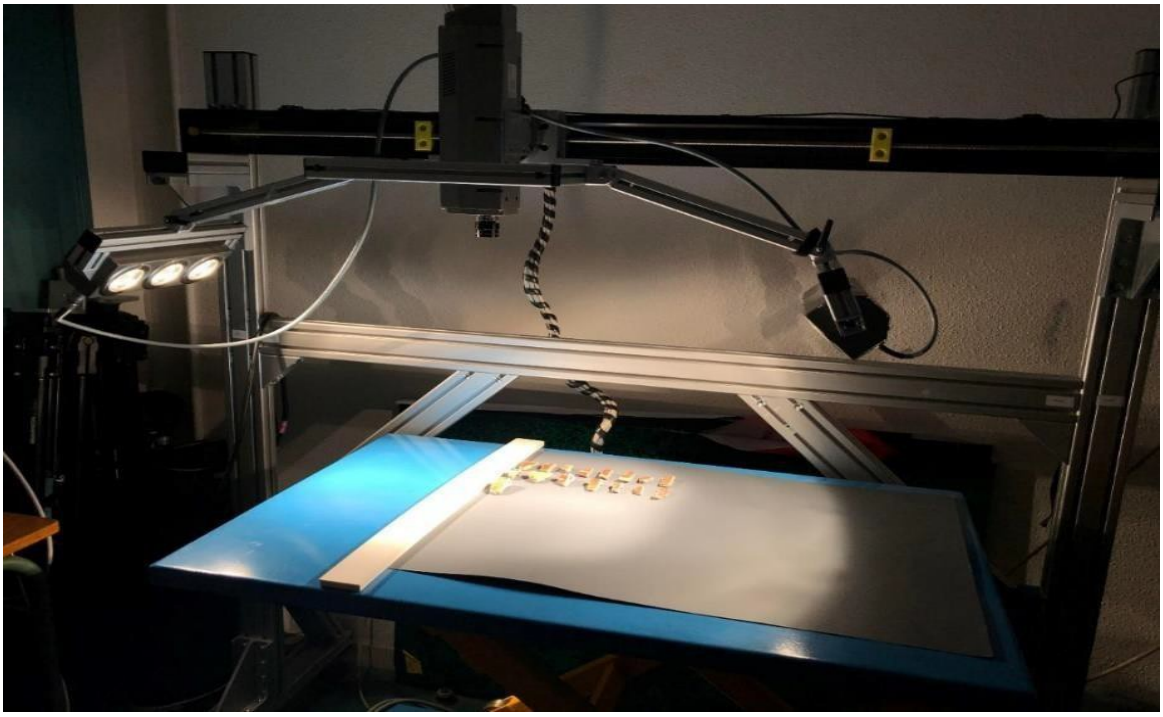

Figure 16. HSI VNIR hyperspectral camera (LEMAIRE Alice 2022).

During each measurement, a white reference was positioned on the sample surface to normalize reflectance data, and a black reference was captured by obstructing the camera lens. The images were normalized in RGB (R = 650 nm, G = 540 nm, B = 450 nm) and in false-color infrared (R = 900 nm, G = 650 nm, B = 540 nm) to establish a fair basis for comparison between spectra.

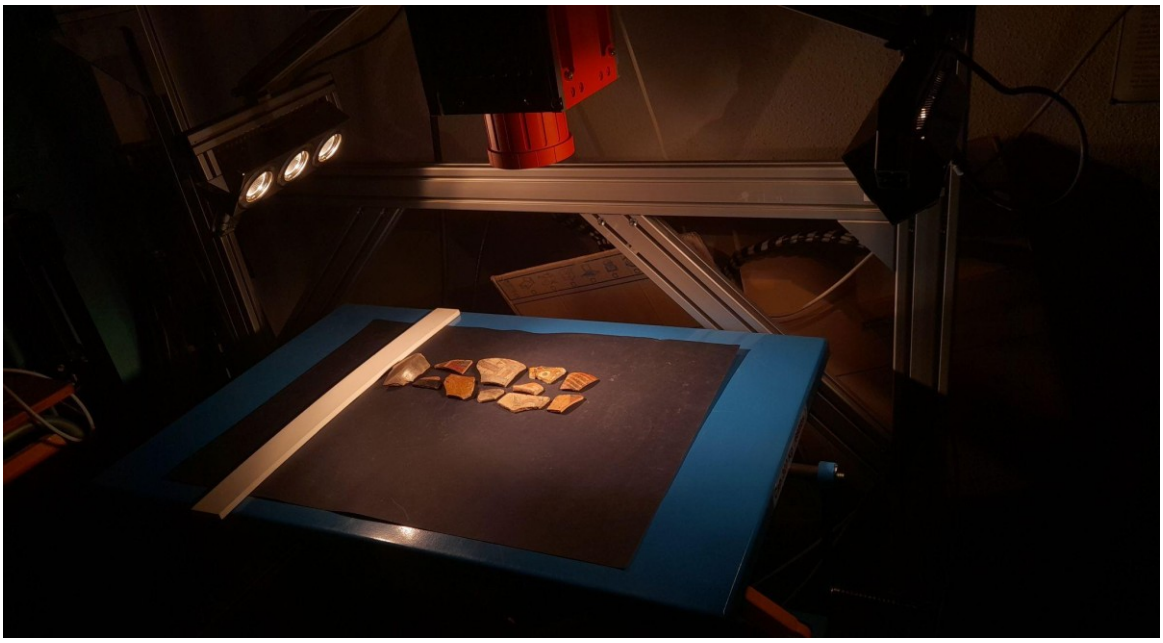

Figure 17. HSI SWIR Hyperspectral Camera (Sifatullah Hassin)

ENVI Classic data analysis software was used to the acquired spectral data. The data were smoothed by averaging over a 10 x 10-pixel window to eliminate noise and enhance the quality of the spectra. Additional spectral processing was done using Python in the Anaconda environment, using Matplotlib library to plot graphs and SciPy to apply the Savitzky-Golay filter to smooth the spectra and enhance signal quality.

Along with spectral analysis, colorimetric observations were made on the hyperspectral image to investigate the decoration features more closely. RGB color data were extracted from the hyperspectral images to quantify the color variation in the ceramic decorations. From the PIL (Python Imaging Library), the RGB values of selected regions of the sample were recorded, focusing on the decorative areas of interest. These values were then translated into Lab color space for a more standardized and consistent color comparison between samples.

We also carried out colorimetric measurements using the Konica Minolta CM-2600d spectrophotometer in reflection mode (D65 illuminant, 10° observer, SCI + SCE geometry, UV component at 100%) in order to be able to compare them with RGB values obtained from hyperspectral images. Two measurements for each sampling zone were done using the SCE (Specular Component Excluded) geometry and their mean used for analysis. This approach is more in line with the visual appearance of matte ceramic surfaces and is more representative with human color perception. The comparison was made to validate the color data obtained from the imaging process as well as to assess the consistency and reliability of decoration characterization by different analytical methods.

2.2.3 Sample Preparation

For sampling, the stiffer ceramic samples were cut by the Chainsaws Escil LD350 with diamond saw Ø350 mm disc and water-cooling system for ensuring clean and high-precision sampling. The fragile samples were sectioned by the ESCIL ATM Brillant 221 with finer control and less vibration, allowing careful sectioning without damaging to the surface layers. After cutting, the samples were cleaned with water and dried for approximately 12 hours in an oven set at 40°C so that they would be free from moisture.

Following drying, the samples were embedded in a transparent epoxy resin, Araldite 2020 A/B, which was mixed in a proportion of 100 g resin and 30 g hardener. The samples were then placed in a pressure chamber to allow the resin to penetrate into the pores of the ceramics for about 8 minutes. The samples were later left for about one day to polymerize, so to make sure the resin was fully cured.

After the process of polymerization, the samples were first subjected to an initial polishing procedure with TisseDiam 75 μm for 15 minutes at 70 RPM. Pre-polishing with different supports was further carried out in a stepwise fashion in order to progressively smoothen the surface. The pre-polishing procedures involved the use of support P240 (58.5 μm), P400 (35 μm), P1200 (15.3 μm), and P2400 (10 μm), each for 5 minutes.

The final polishing step was carried out with diamond suspensions of 6 μm, 3 μm, and 1 μm each for 15 minutes. To have clean and contamination-free surfaces, the samples were placed in an ultrasonic bath after every polishing step. This was to ensure that any remaining particles or contaminations of the polishing solutions were removed so that no small particles were introduced into the samples that could interfere with the subsequent analysis.

2.2.4 SEM-EDS (Scanning Electron Microscopy with EDS)

The ceramic sample sections were analyzed using a JEOL JSM-IT 500 HR scanning electron microscope (FEG-SEM) (Fig.18). The analyses were conducted in low vacuum mode with a pressure of 30 Pa, a working distance of 10 mm, and an acceleration voltage of 20 keV. It is equipped with two SDD X-MAX 20 detectors to allow for rapid energy-dispersive X-ray spectroscopy (EDS) analysis.

Detailed examination of the ceramic materials, i.e., the paste, inclusions, and decorations, was carried out. Five areas per sample, each approximately (1250 × 900 μm in size) were examined for the global characterization of the paste to account for the inherent heterogeneity of the material. For the pigment and decoration analysis, typically, three representative areas approximately between 20

to 200 µm were selected; in some exceptional decorations, however, only two were analyzed since the painted layer was too thin. In a few cases, the pigment layers were so thin that they could not be observed in cross-section in the SEM. For these samples, the analyses were consequently performed directly on the surface rather than on polished sections.

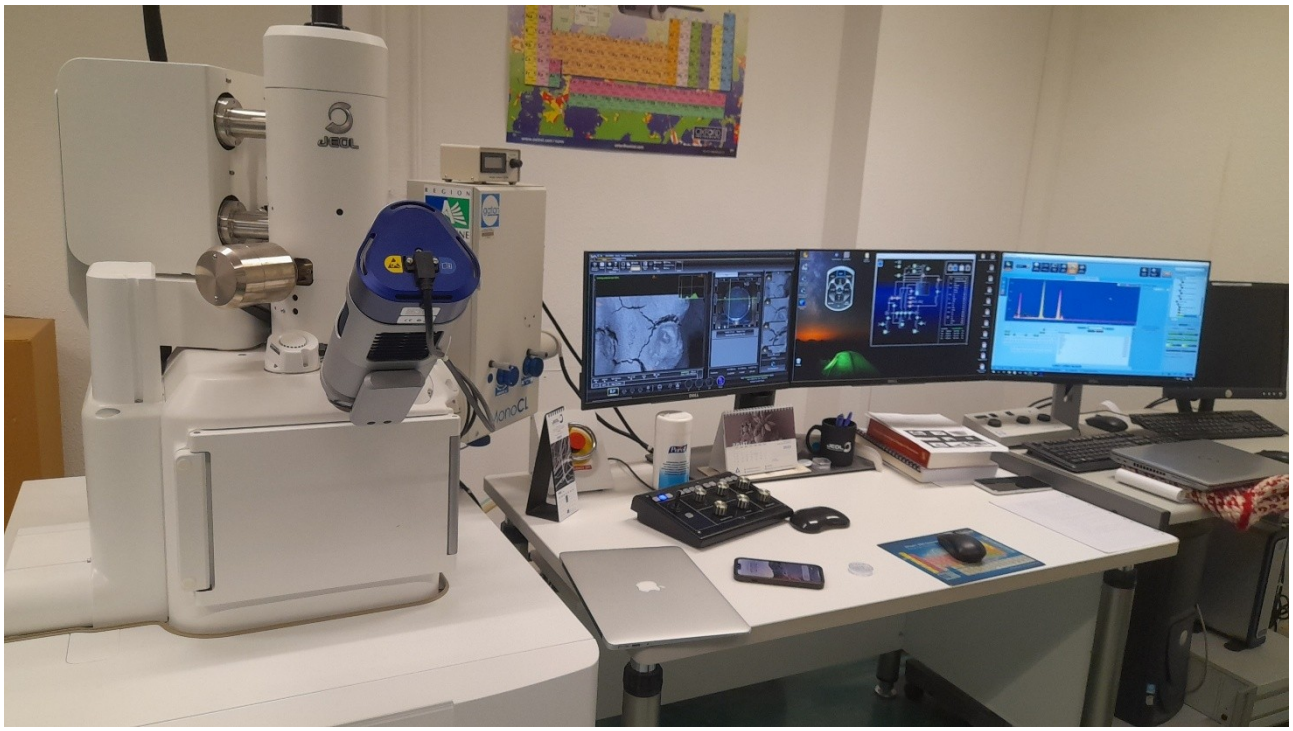

Figure 18. JEOL JSM-IT 500 HR scanning electron microscope equipped with 2 EDS detectors (Sifatullah Hassin).

For better resolution and clarity of the analysis, images were obtained at multiple magnifications, capturing various aspects of the samples, such as decoration and pigment distribution. SEM images were captured by backscattered electron imaging to provide high contrast and surface detail morphology of the samples.

A detailed map of pigment distribution was also created, outlining the spatial variation across the samples. The thus obtained spectra were treated on Oxford Instruments AZtec software, and the data were normalized and expressed in mass percentages.

2.2.5 Portable X-Ray Fluorescence (pXRF)

All the ceramic samples were analyzed using a portable X-ray fluorescence (pXRF) spectrometer from Olympus (Fig. 19), with data collected via the Venta App software. The

experimental parameters followed the protocol established by Kouakou Koffi (2022, University of Bordeaux Montaigne).

The ceramic sherds were analyzed once on their cross-sections with three distinct areas examined per section to account for variability in the ceramic matrix.

A second round of pXRF analysis was carried out directly on the surface decorations, aiming to detect elemental signatures, including potential trace elements, and to compare these results with SEM-EDS data. As with the paste analysis, three specific areas were selected for each decorated surface.

To ensure precision and consistency across all analyses, the collimator was used throughout the study. For surface decorations, this was essential because some painted layers were small, and the collimator allowed precise targeting of the decorations. Similarly, on cross-sections, certain samples had very narrow or uneven sections, and the use of the collimator ensured that the measurement focused on the intended ceramic body region.

The pXRF analysis was conducted using two X-ray beams: one at 40 kV for 60 seconds to target heavier elements and another at 10 kV for 90 seconds to detect lighter elements.

To ensure the repeatability, accuracy and precision of our measurements, one in-house obsidian standard (named MAOA.STD) was systematically analyzed at the beginning and at the end of each run. The composition of MAOA.STD, as determined by Inductive Coupled Plasma - Mass Spectrometry (ICP-MS) and Inductive Coupled Plasma - Optical Emission Spectrometry (ICP-OES), is given in Table 1 in appendix.

Figure 19. Olympus Vanta XRF analyzer mounted on a fixed lab stand used for the analysis (Sifatullah Hassin).

2.2.6 Raman Spectroscopy

Raman spectroscopy was performed using a BWTeK i-Raman Plus portable spectrometer with two excitations lasers: 532 nm (i-Raman Plus 532s) (Fig. 20) and 785 nm (i-Raman Plus 785s). The analysis was focused on identification of the decoration materials used on ceramics. Spectra were measured in backscattering mode to obtain high spectral resolution and prevent sample damage. No preparation of samples was needed to preserve the integrity of the original surfaces. Measurements

were taken from different points across the decorated areas to accommodate compositional heterogeneity. Various acquisition settings were tested to acquire good signal quality and preserve sensitive materials. These included short-time configurations such as 3 acquisitions of 1 seconds at 30% and 30% laser power, along with high intensity setups such as 3 × 5 seconds at 50% and 3 × 10 seconds at 70% laser power. This approach offered flexible adjustment based on the stability and fluorescence response of each sample. These conditions were selected with caution to achieve maximum spectral quality while preventing thermal degradation, particularly for sensitive or highly pigmented layers.

Spectral data processing began with BWSpec software for initial acquisition and preprocessing. Baseline correction, peak fitting, and spectral visualization were then performed using SpectraGryph and Omnic. The resultant spectra were subsequently compared with reference databases, such as the RRUFF Raman spectral library, to assist identification of both the mineral and organics within the decorative layers.

Figure 20. BWTek i-Raman Plus 532s Raman spectrometer set up, showing (a) the power supply unit, (b) the optical fiber probe for laser delivery and signal collection, and (c) the laptop with dedicated software for data acquisition (Sifatullah Hassin).

In addition to the portable systems, Benchtop Raman spectroscopy with 532 nm, 633 nm, and 785 nm laser excitations were also performed (Fig. 21). This setup was employed to enhance spectral acquisition conditions, particularly where surface properties required greater sensitivity and control. Spectra were collected with a 50× objective, which offered higher spatial resolution and signal intensity. A set of acquisition parameters was also attempted to fit the varying thermal and optical sensitivities of the materials. These included short acquisitions, such as 1 × 10 seconds at laser power,

and extended acquisitions up to 5× 100 seconds at 100% power. Laser settings were carefully adjusted based on the response of each sample to avoid surface damage, especially in pigment-rich or thermally sensitive areas. This flexible approach ensured high-quality spectral data while preserving the integrity of the original surfaces.

Figure 21. Benchtop Raman spectroscopy performed with 532 nm, 633 nm, and 785 nm laser excitations (Sifatullah Hassin).

2.2.7 Fourier Transform Infrared Spectroscopy

FTIR spectroscopy was used to determine the molecular composition of the decorations. Specular reflectance mode surface analysis of the samples was carried out using a Bruker Optics Alpha portable FTIR spectrometer (Fig.22). The external reflectance mode (specular) allowed direct, non-destructive surface analysis of the samples without preparation.

Spectra were acquired over a wavenumber range of 4000–400 cm^{-1} with a spectral resolution of 4 cm^{-1}. For better signal quality and to reduce noise, various scan settings (100, 70, and 50 scans) were first attempted; 32 scans per measurement were ultimately selected as the most effective setting, as this setting had already been employed earlier to get good data in similar studies(López Puértolas et al., 2024). A gold mirror was used to acquire background reference spectra prior to each series of acquisitions.

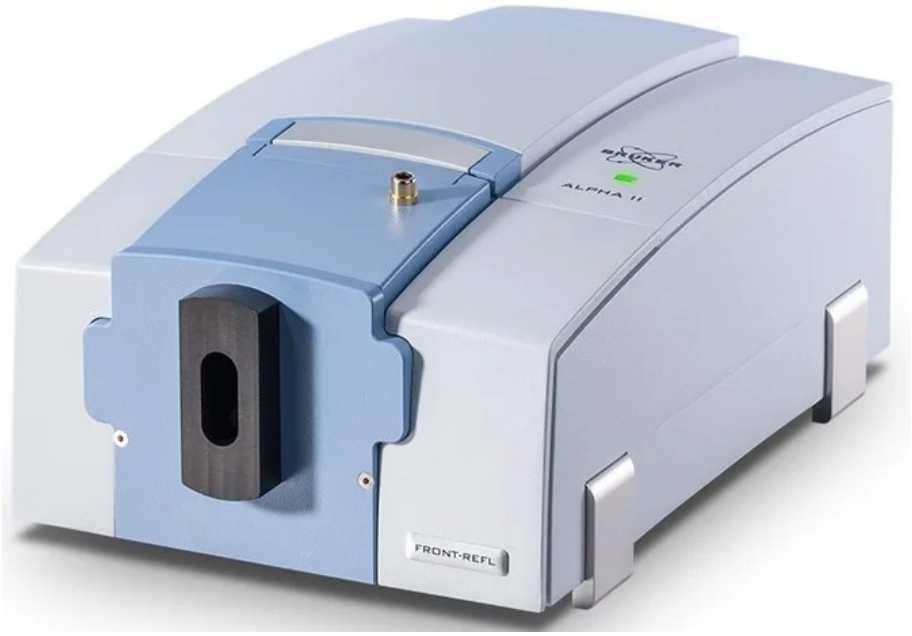

Figure 22. Bruker Optics Alpha portable FTIR spectrometer with front-reflection module (azom.com).

The objective of the analysis was to identify organic and inorganic functional groups related to decorative coatings, or binders. Special attention was given to absorption bands that might suggest the presence of resins or other post-firing organic materials.

Data collection was performed using OPUS software. For further spectral processing, including Kramers–Kronig transformation, baseline correction, normalization, smoothing, and peak assignment spectra were exported and analyzed using OMNIC software, referencing established spectral libraries for compound identification.

3 PART THREE: Experimental Results and Discussion

This chapter presents the results and discussion of the analyses performed on the ceramic samples. As the ceramic assemblage has both polychrome and monochrome decorations, the results from SEM-EDS and pXRF, Raman spectroscopy, and FTIR were grouped and discussed accordingly. This approach was taken to assess whether compositional or technological differences exist not only between polychrome and monochrome decorations, but also among samples of both types from different archaeological contexts. The distinction helps avoid conflating data from materials applied using different techniques and at different stages of the production process. Raman spectroscopy and FTIR analyses were conducted exclusively on polychrome samples.

On the other hand, hyperspectral imaging and colorimetric analyses were performed across all without separating them because these methods deal with visual properties and surface reflectance rather than compositional stratigraphy.

3.1 Imaging and Texture Analysis

This section presents the imaging approaches used to examine the ceramic samples, focusing on surface texture and decorative features.

3.1.1 Microscopic Imaging (Optical Microscope and SEM)

The optical (stereomicroscope) and (SEM) were used to examine the surfaces and structural features of the ceramics. The stereomicroscope allowed for the identification of surface treatments, tool marks, and paint application patterns. SEM analysis provided more detailed information on the ceramic matrix, including grain texture and size, the quantity and distribution of inclusions, and features indicative of the firing atmosphere (oxidizing or reducing). and the surface texture of the applied decoration.

3.1.1.1 Surface Features and Condition

Stereomicroscopic examination in natural light allowed us to observe fine surface detail on polychrome as well as monochrome samples, e.g., horizontal striations and tool marks typical of hand-working technique.

✓ **Polychrome**

The horizontal striations and finishing marks on Polychrome surfaces show typical coil construction and subsequent refinement to the surface (Courty & Roux, 1995). These traces are consistent with visual evidence (Fig. 23) and correspond with archaeological materials recovered during excavation, such as smoothing tools and burnishers (Bachir Bacha & Llanos, 2013). These features are especially visible in undecorated areas, particularly on interior surfaces where decorative layers are absent (Fig. 24).

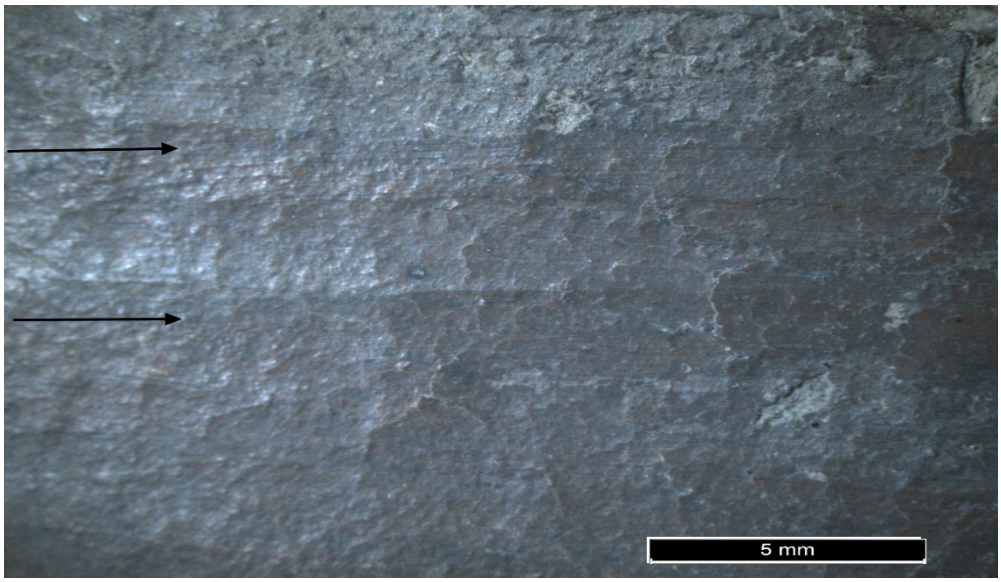

Figure 23. Surface showing visible striations that suggest manual smoothing after coil construction (BDX27690, El Panteón, 8× magnification).

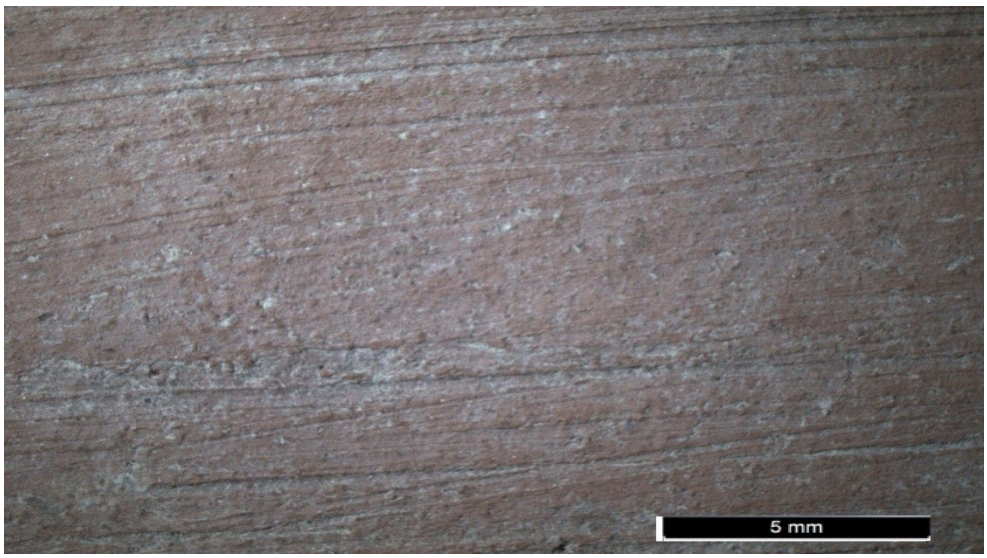

Figure 24. Detail of the interior surface in an undecorated area, showing clearer visibility of horizontal striations in the absence of surface decoration (BDX27677, Montículo 1, 8× magnification).

The state of color preservation varies in some samples, the decorative layers are more degraded (Fig. 25a), while in others, they remain remarkably well-preserved (Fig. 25b). Polychrome decorations are clearly defined, showing no evidence of pigment mixing between colors. Fine incisions, with a width of approximately 0.75 mm (Fig. 26), likely helped and guided the painting application and kept the decorations within defined boundaries(Senserrich, 2017). Such would show usage of a brush or similar tool for painting which allows precise and layered application of pigment(Mardi, 2014).

In some samples, a black layer seems to have been applied first, followed by additional colors like yellow and red (Fig. 26).

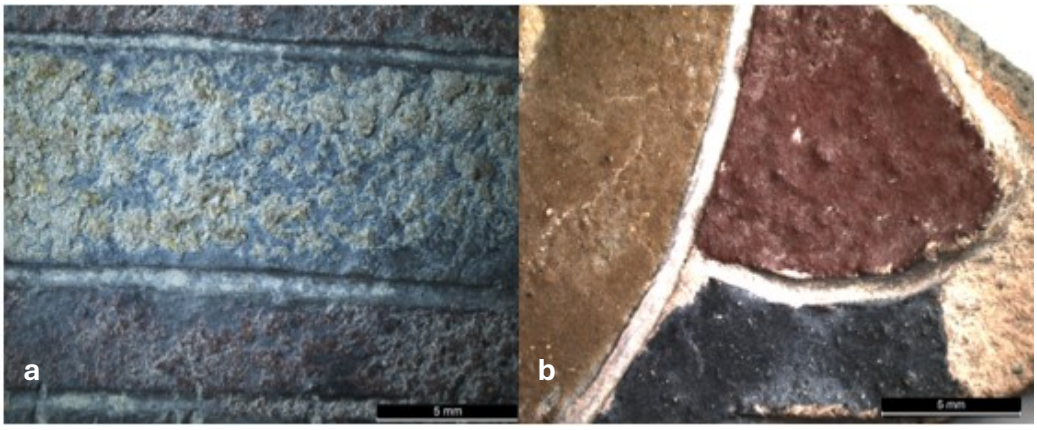

Figure 25. (a) With significantly degraded colorant layer; (b) Showing well-preserved decoration (a: BDX27679, Montículo 1; b: BDX27683, Montículo 25).

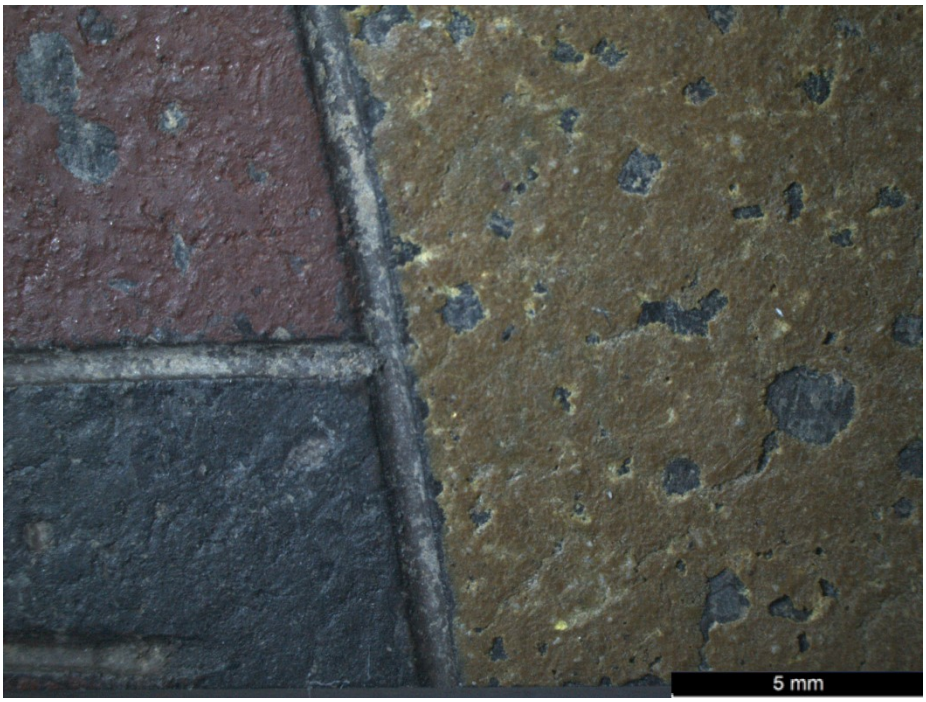

Figure 26. Fine incisions (~0.75 mm) on the surface, with a blackish layer visible beneath the yellow and red decorations (BDX27677, Montículo 1).

✓ **Monochrome**

The monochrome ceramics lack any incision marks visible. However, their surface features and construction techniques are the same as those visible in the polychrome samples, particularly the use of coiling.

Certain monochrome samples show the presence of black deposits on their surfaces (Fig. 27). These are recognized as soot residues, likely resulting from contact with fire or smoke during use. These residues are generally associated with household activities such as cooking or heating and were not observed on polychrome ceramics (Teetaert, 2017).

Figure 27. Soot residue on the surface of a ceramic fragment (BDX27689, El Panteón).

3.1.1.2 Paste texture

The ceramic pastes of polychrome and monochrome samples are not entirely homogeneous, as both contain inclusions of varying sizes, from fine grains up to 0.5 mm, to medium grains ranging from 0.5 to 1 mm, and occasionally coarse particles greater than 1 mm, as shown in (Fig.28). However, inclusions larger than 1 mm are rare, indicating that the paste is predominantly fine to medium in texture.

The ceramic sherds of monochrome and polychrome both exhibit evidence of variable firing conditions seen in (Fig.29), as indicated by their color variations. Paste colors range from reddish or orange, characteristic of complete oxidation, to gray and dark black, which suggest incomplete

oxidation or full reduction. This variation is a mixture of reducing and oxidizing atmospheres during the firing and cooling(Maritan et al., 2006; Felipe et al., 2019; Perttula, Timothy K, 2022). Most sherds contain intermediate firing profiles, with both reduced and oxidized zones. But three samples BDX 27685 (Montículo 25, monochrome), BDX 27690 (El Panteón, polychrome), and BDX 27698 (Montículo 1, polychrome) appear to have been fired entirely under reducing conditions.

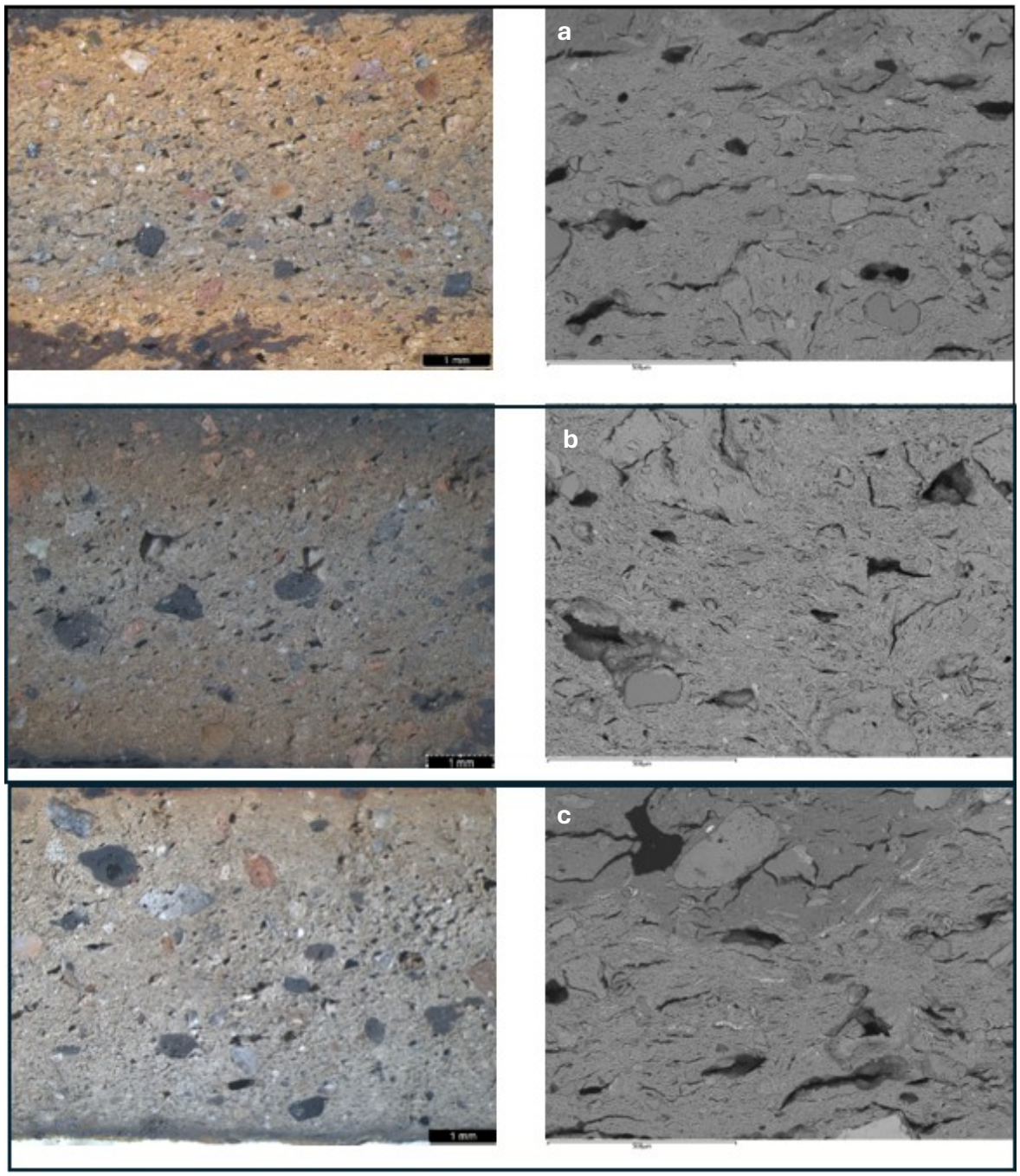

Figure 28. Examples of ceramic paste textures: (a) fine paste, (b) medium paste, and (c) coarse paste. (a) BDX27676, monochrome; (b) BDX27682, polychrome;(c) BDX27679, polychrome; all from Montículo 1. Left: binocular microscope, 20× (scale: 1 mm); right: SEM, 100× (scale: 500 µm).

The absence of kilns and the presence of hearths at the site also provide additional evidence for the interpretation that firing took place in open or semi-closed environments, which typically produce such variable and less controlled atmospheres(Amicone et al., 2021).

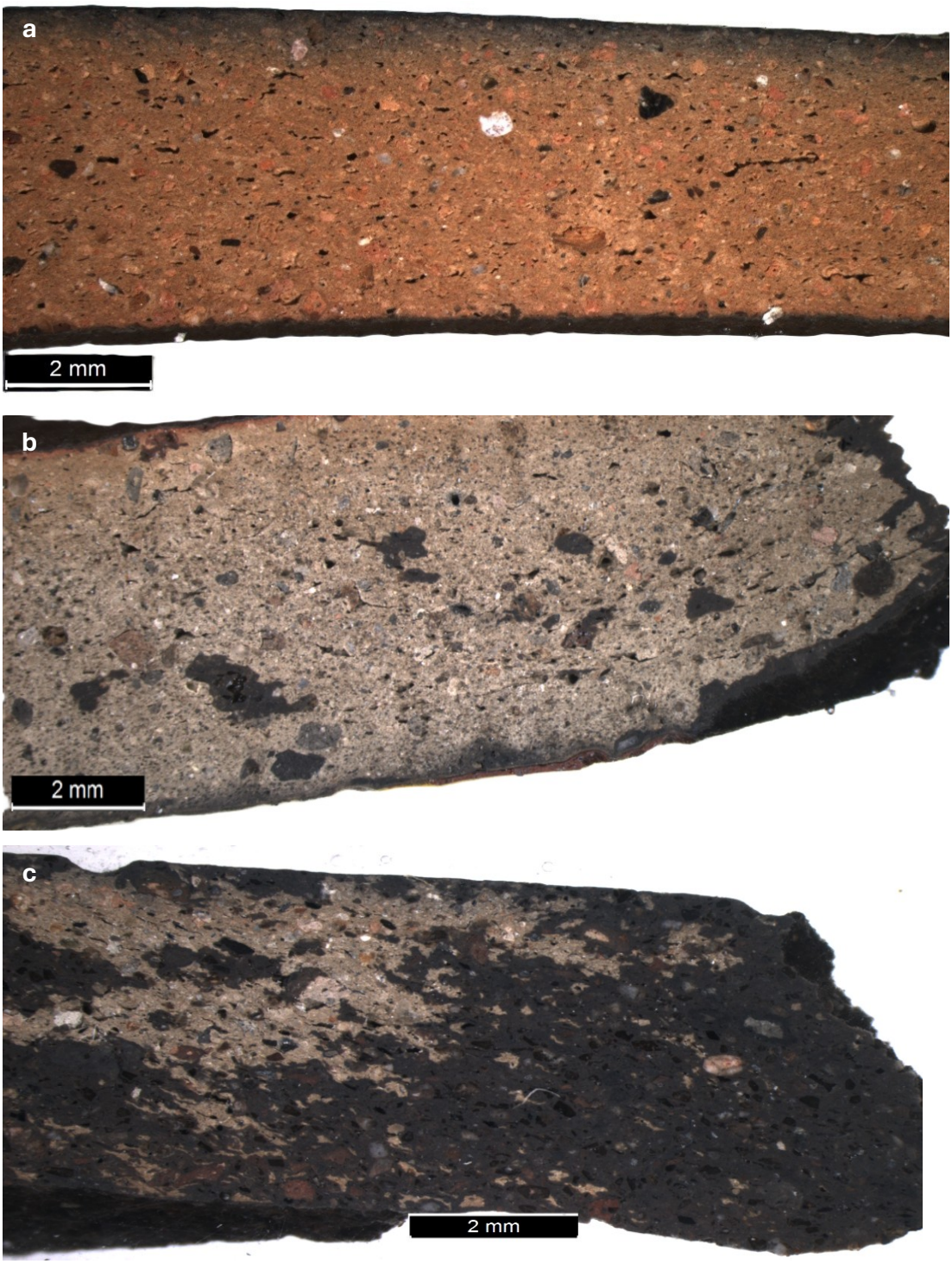

Figure 29. Firing atmosphere variation in polychrome ceramic samples from Montículo 1: (a) BDX27680, completely oxidized; (b) BDX27679, partially oxidized; (c) BDX27698, fully reduced.

3.1.1.3 Decorative Layers

This section examines the observable decorative layers in cross-sections, including surface treatment, color application, layer thickness, the size and distribution of decorative inclusions, and elemental mapping.

- ✓ **Polychrome**

Red, yellow, black, and cream are the most common colors observed for polychrome samples. As mentioned earlier, in some cases it appears that a dark layer (likely black) (Fig.26) was first applied across the surface, followed by additional colors, particularly yellow and red.

Although the layering is apparent in surface-level observations, it could not be confirmed in cross-section under SEM (Fig 30). Further stereomicroscopic examination revealed that the black layer does not originate from the applied decoration but rather from the ceramic paste itself—likely the result of firing in a reducing atmosphere (Fig.31)(Zhushchikhovskaya, Irina S, 2022). The space visible between the paste and the decoration likely corresponds to a separation line, as shown in (Fig. 32).

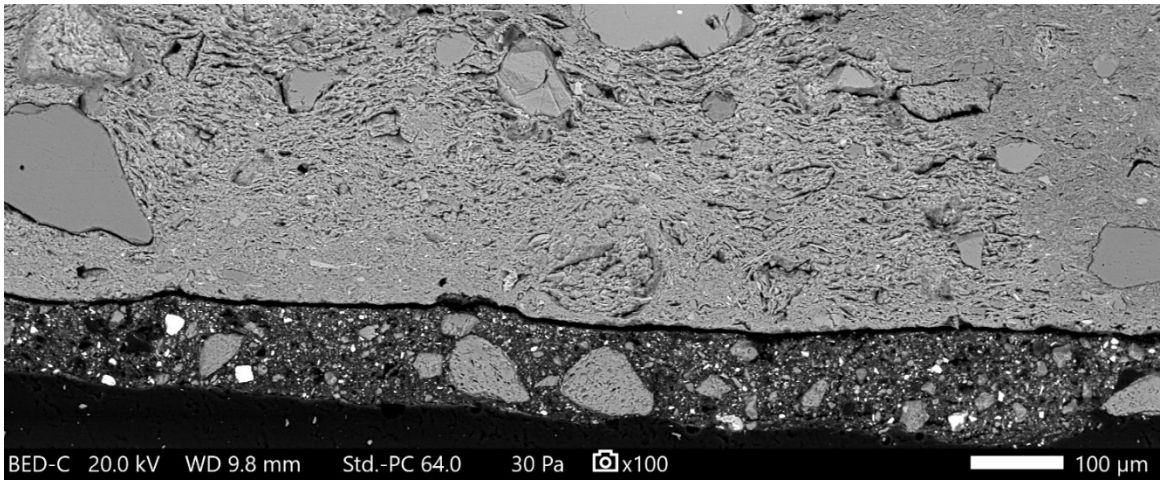

Figure 30. SEM backscattered electron (BSE) image of yellow decoration, shown at 100× magnification. No discrete decorative pigment layer is visible beneath the yellow decoration (BDX27677, Montículo 1).

The decorative layers observed across the ceramic samples significantly vary in thickness and size of inclusion, exhibiting heterogeneous raw material preparations and surface treatments. The red color pigment layers exhibit a significant difference in their thickness (6–105 µm) and the presence of inclusions as large as 50 µm, indicating differences in composition and tools used for color application (Fig. 32)

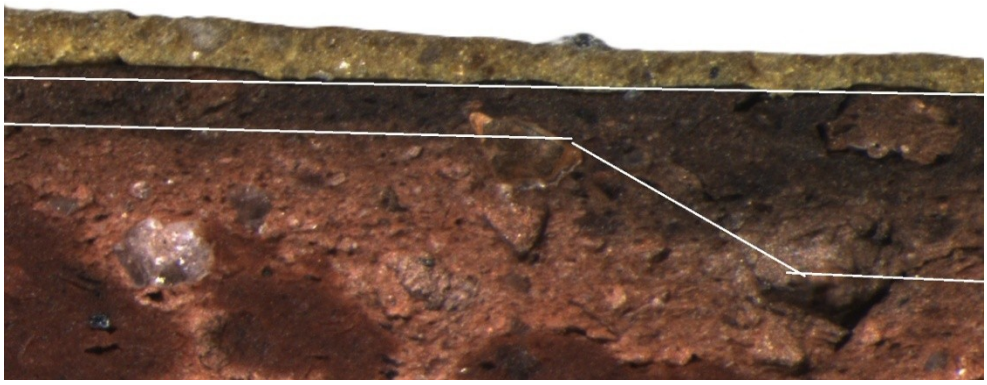

Figure 31. Stereomicroscopic image showing that no black decorative layer is observed beneath the yellow pigment. The dark coloration in some areas is attributed to the ceramic paste itself, likely resulting from firing in a reducing atmosphere (BDX27677, Montículo 1).

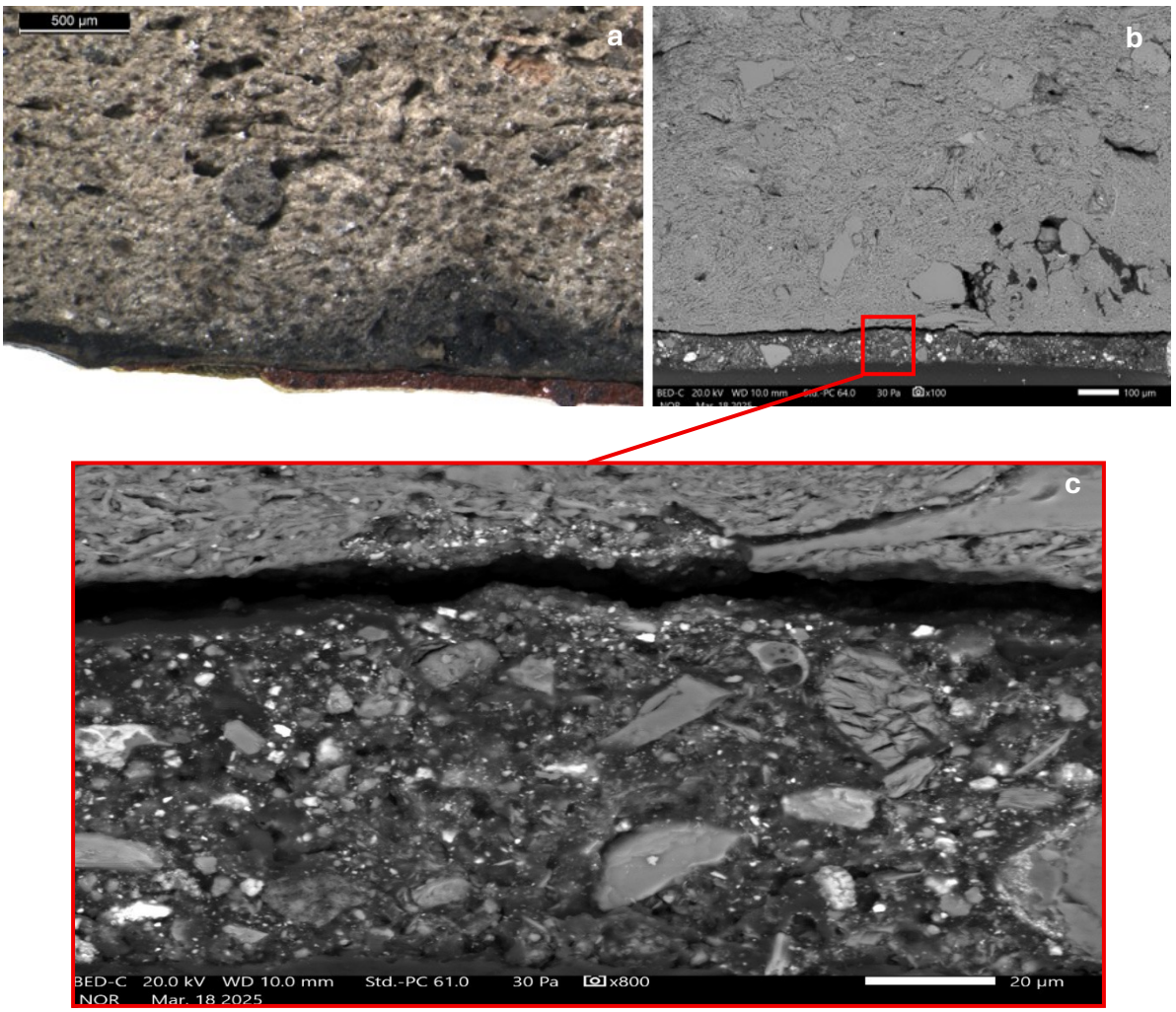

Figure 32. Red pigment observed under the stereomicroscope (a) and in SEM (b, c), showing increasing magnifications (a: 500 µm; b: 100 µm; c: 20 µm; BDX27679, Montículo 1).

The elemental mapping confirms that the red decorative layer is rich in iron and is clearly differentiated from the ceramic body (Fig.33.a). The pigment layer is very dark because of the carbon. The combined appearance of Fe and C proves that the layer was applied intentionally.

The strong carbon signal, seen in (blue color) on the EDS map (Fig. 33.b), substantiates this interpretation. Al, Si, and K in the red pigment layer do not contribute directly to the reddish color, but are part of the clay-rich matrix or extender used to apply the iron-based pigment(Pendleton et al., 2014).

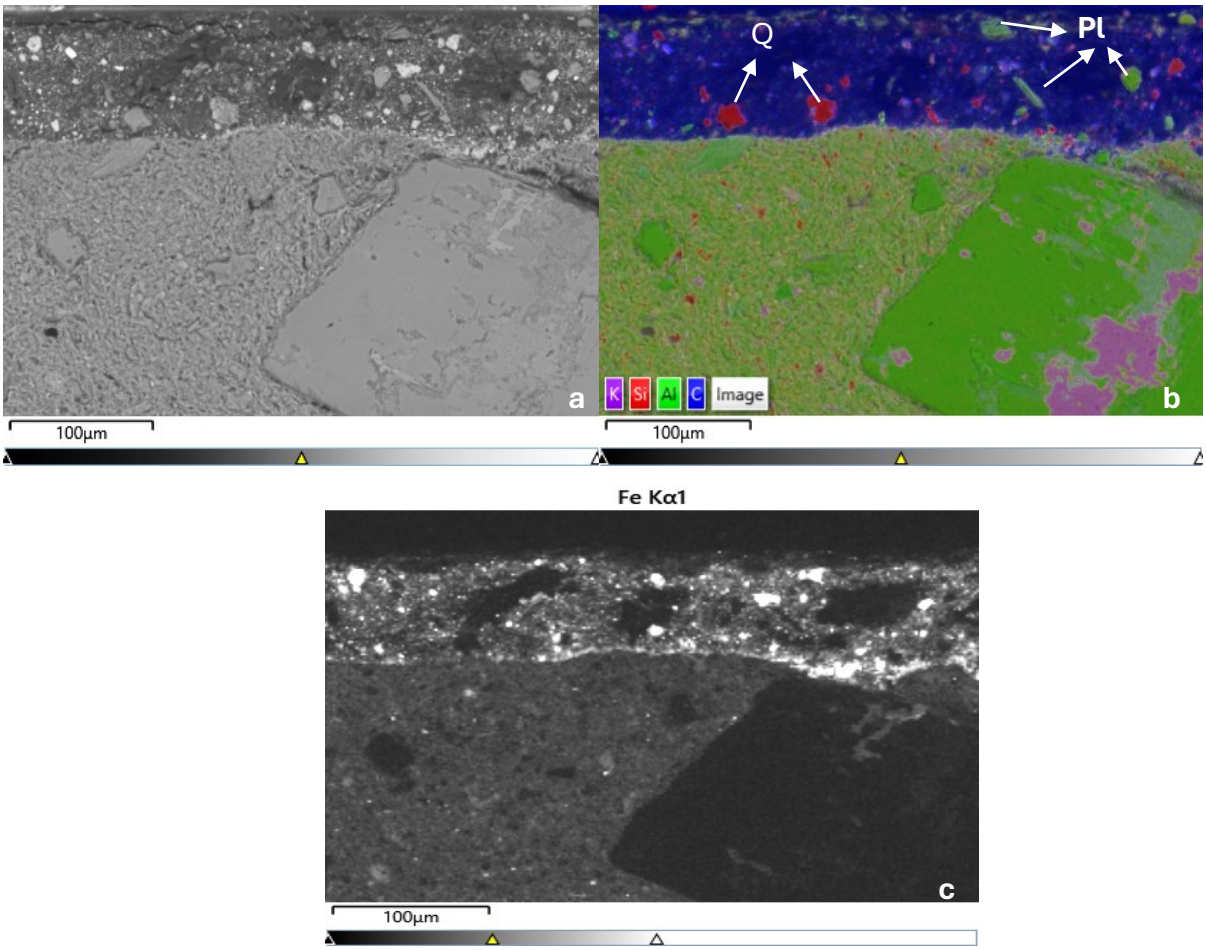

Figure 33. Elemental mapping (SEM-EDS) of the red surface decoration showing co-localization of carbon (C) and iron (Fe). The decoration is clearly stratified and distinct from the ceramic body, supporting its identification as an applied surface layer. The strong carbon signal (blue) suggests the presence of organic matter mixed with iron oxide. (a) BSE image of the same area (b); Carbon (C) map; (c) Iron (Fe) map (BDX27683, Monticulo1).

Yellow pigments are thick (140 µm maximum) and often have coarser inclusions, occasionally as large as 90 µm in diameter, which suggest either coarse material or intentionally texture effect (Fig. 34). The elemental mapping study in yellow layers shows a mixture of sulfur and arsenic (Fig.35), which is likely to be the result of the use of orpiment(As_2S_3) or pararealgar(As_4S_4) as a yellow pigment (Vermeulen et al., 2015; De Keyser et al., 2024). Like the red decoration, the yellow layer is also dark due to high amount of carbon on BSE image that contains dispersed As- and S-rich inclusions and quartz grains.

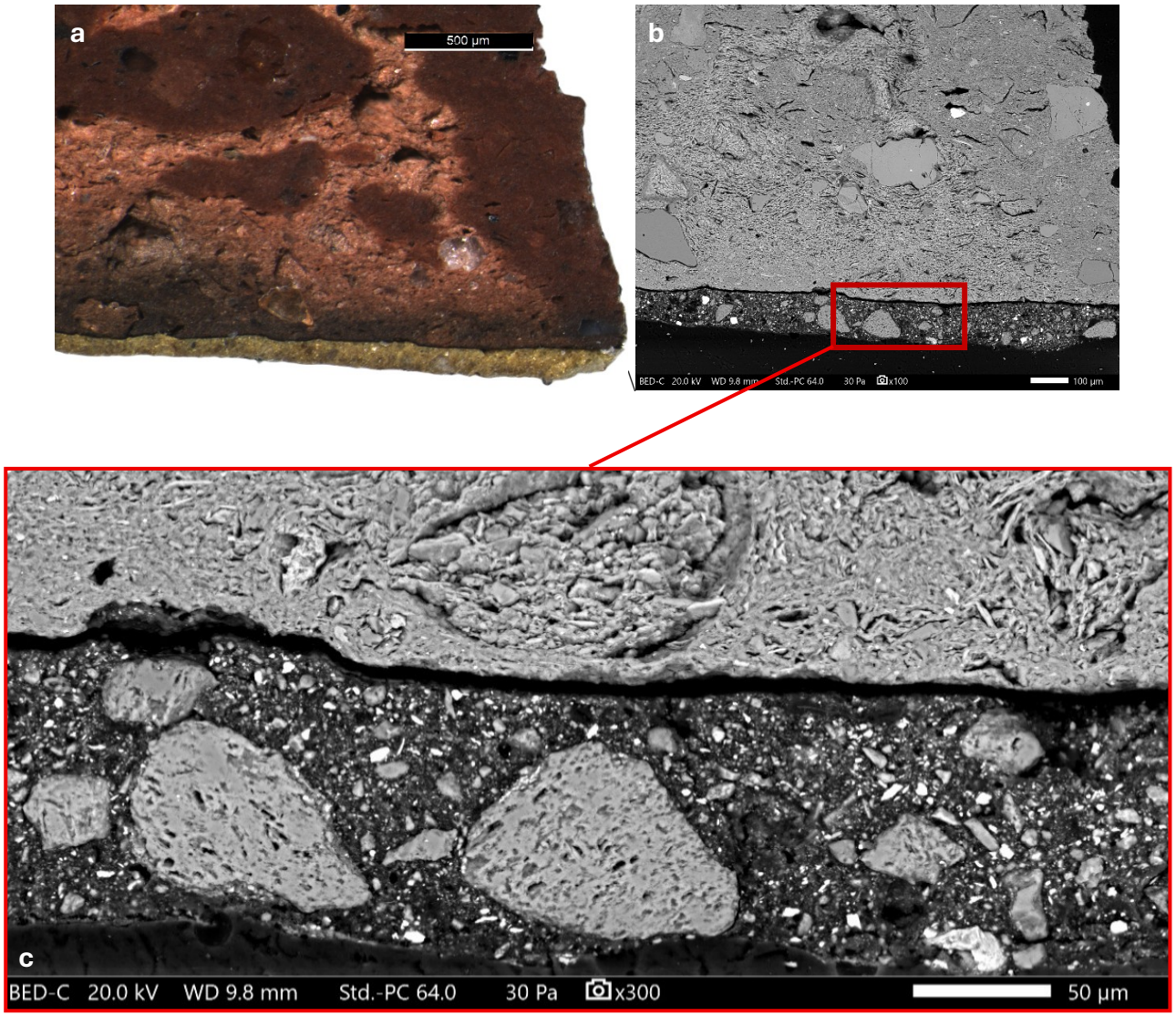

Figure 34. Yellow pigment observed under (a) under stereomicroscope, (b) under SEM at 100x magnification (50 µm) and (c) under SEM at 300x magnification (50 µm) (BDX27677, Monticulo1).

Black is thinner (9–80 µm) and more homogeneous compared to yellow and red decorations, with inclusions occasionally larger than 20 µm (Fig. 36). SEM-EDS mapping of the black layer reveals the presence of small grains of Fe_2O_3, feldspar, and quartz, whereas the remaining part of the layer is completely dark and porous of amorphous carbon.

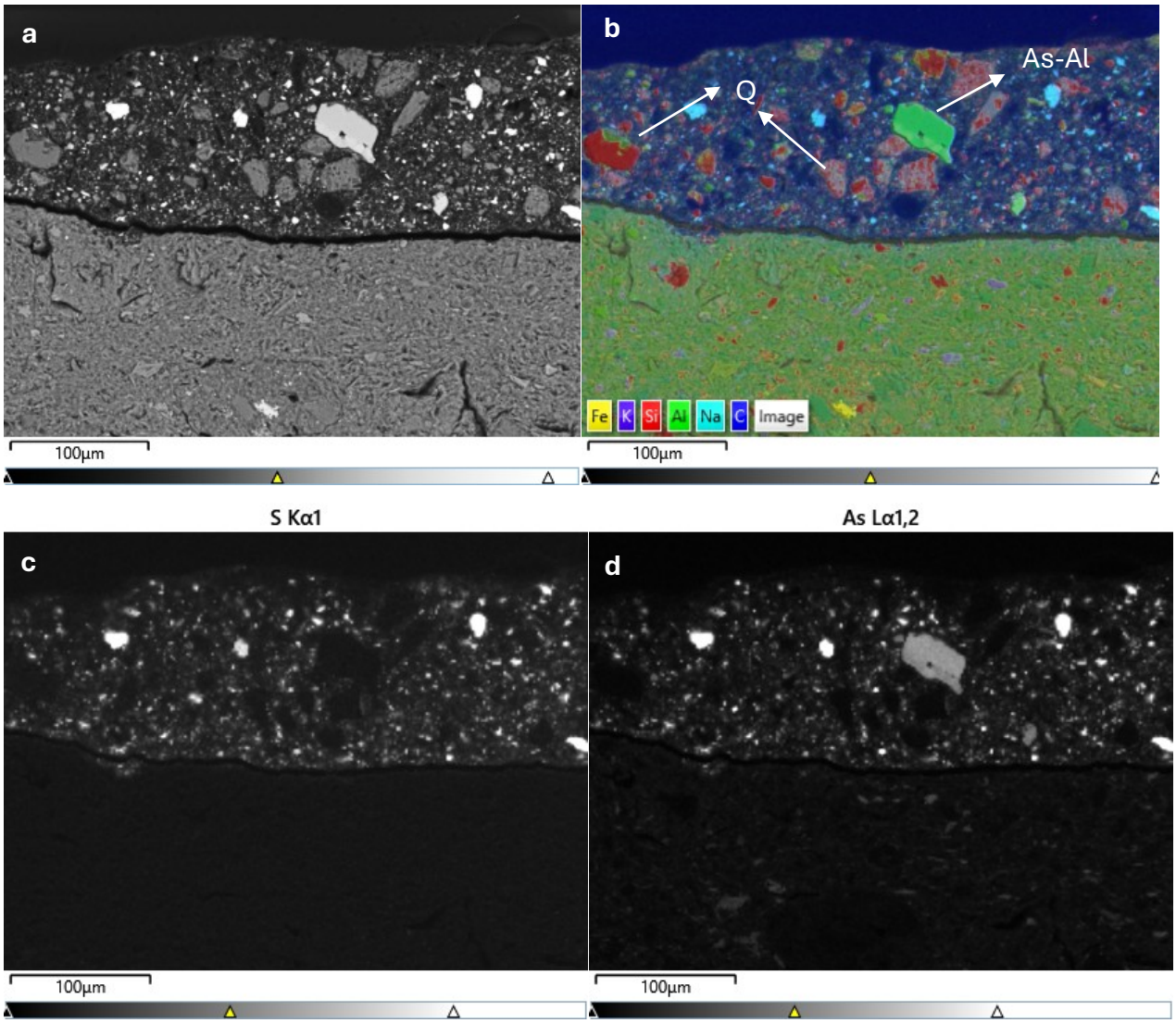

Figure 35. Elemental mapping (SEM-EDS) of the yellow surface decoration reveals a distinct layer separated from the ceramic body, characterized by the co-localization of organic matter, arsenic (As), and sulfur (S). (a) BSE image of the yellow pigment; (b) composite elemental map showing Fe, K, Si, Al, Na, and C; (c, d) elemental maps of arsenic (As) and sulfur (S), respectively (BDX27680, Montículo 1)

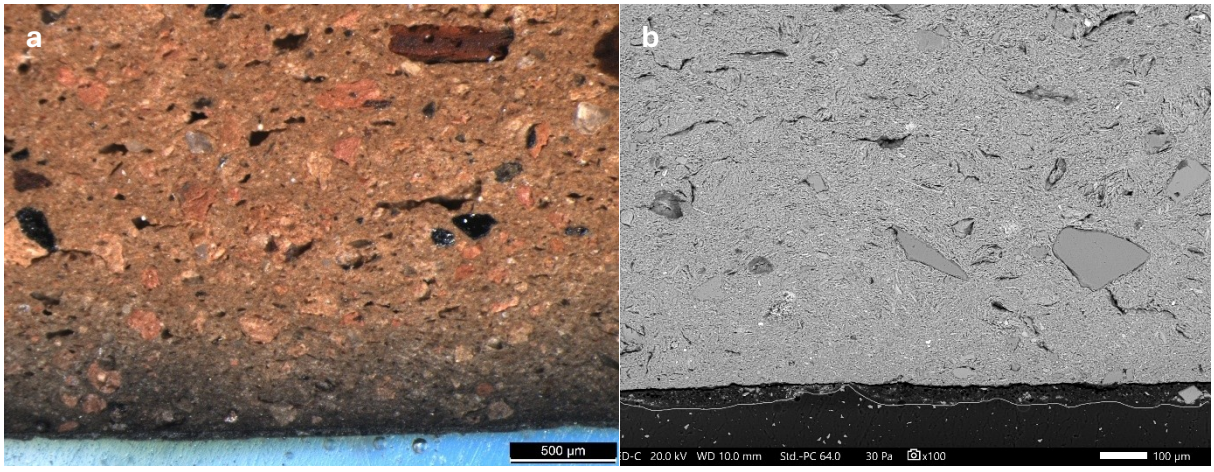

Figure 36. Black decoration observed in (a) under stereomicroscope (500 µm), and (b) under SEM (100 µm) showing very thing black decoration layer compared to other polychrome decoration layers (BDX27680, Montículo 1).

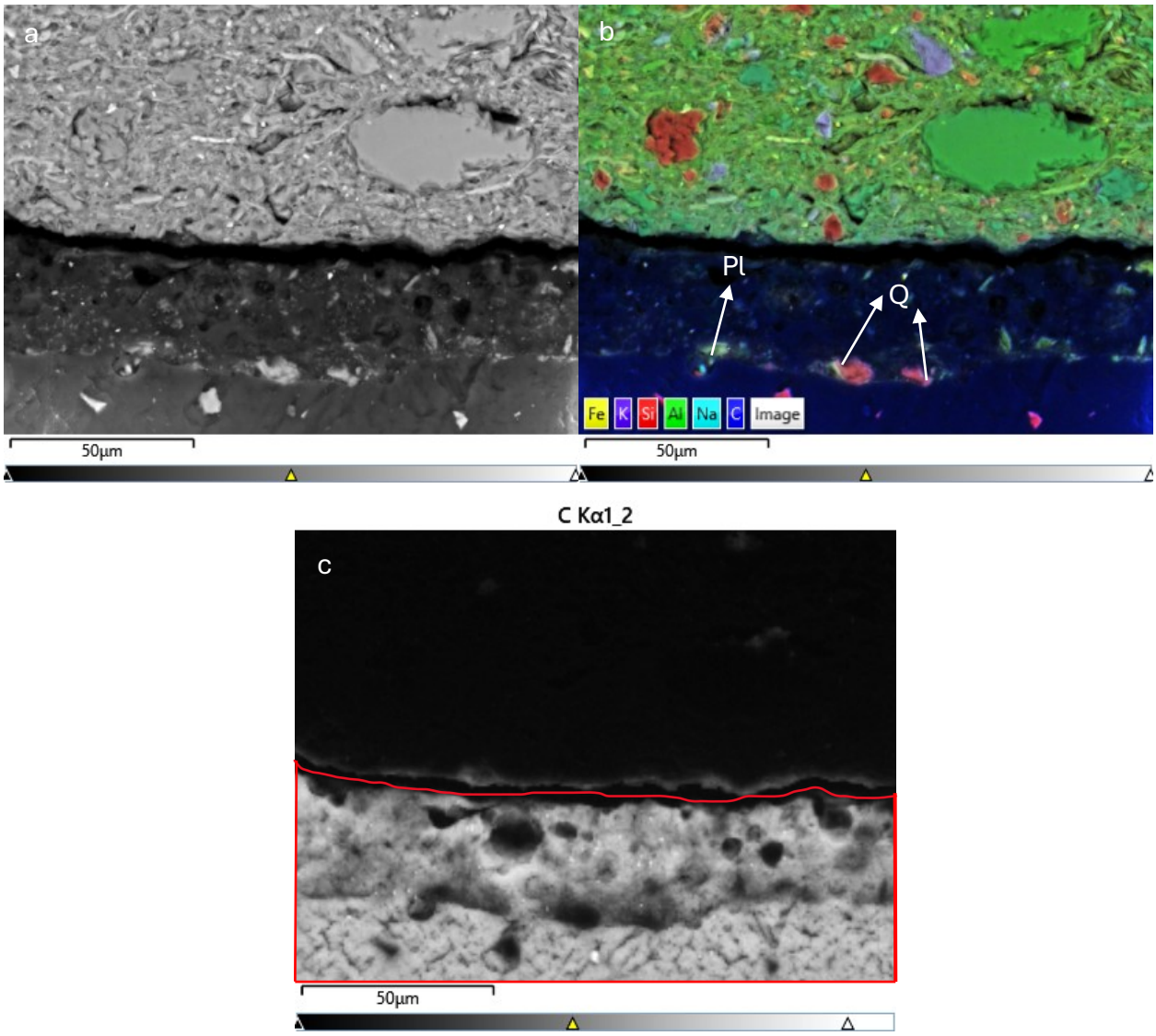

Figure 37. Elemental mapping of the black surface decoration shows a distinct dark carbon-rich layer separate from the ceramic body: (a) BSE image of the black decoration; (b); composite map showing Fe, K, S, Al, Na, and C, and (c) carbon map showing in red (BDX27680, Montículo 1).

In the polychrome sample BDX27678 (Montículo 1), decorated using the negative painting technique, the decorative layer is clearly visible; however, unlike other polychrome ceramics, there is no distinct separation line or gap between the decorative layer and the ceramic body (Fig. 39). In contrast, other samples within the polychrome group exhibit a well-defined, often empty boundary clearly separating the two layers. In BDX27678, the pigment layer appears more continuous with the ceramic matrix, though its presence is still evident—likely due to the application of an iron-rich clay slip. SEM-EDS elemental mapping of the orange-colored area reveals very little carbon, in contrast to other pigment layers within the polychrome group. Additionally, the orange layer does not appear dark in backscattered electron (BSE) images, differing from the typical appearance of other decorative layers in this group (Fig. 40).

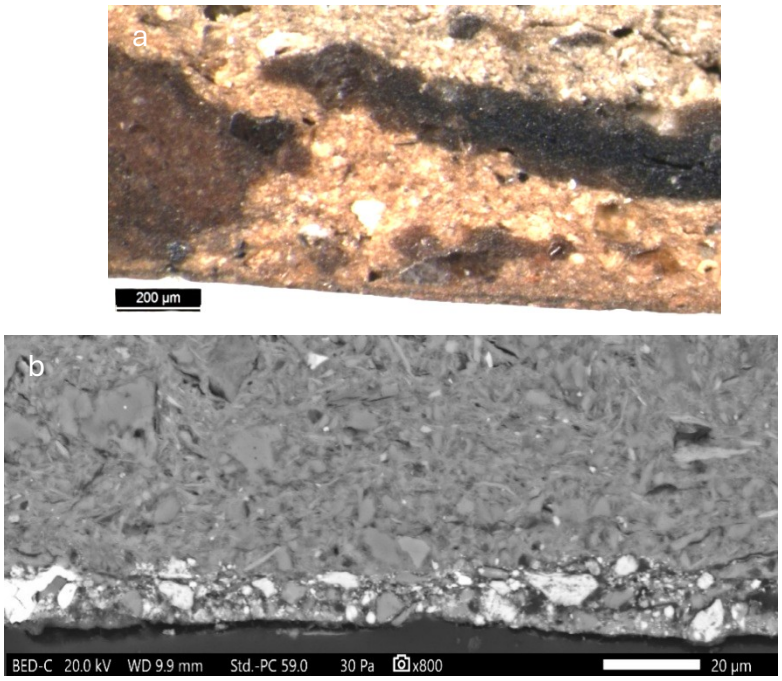

Figure 38. Cross-section on the negative painting ceramic, showing a decorative layer that appears more integrated with the ceramic body. Unlike other polychrome samples, no distinct separation gap is visible, likely due to the use of an iron-rich slip applied on the surface (BDX27678, Montículo 1).

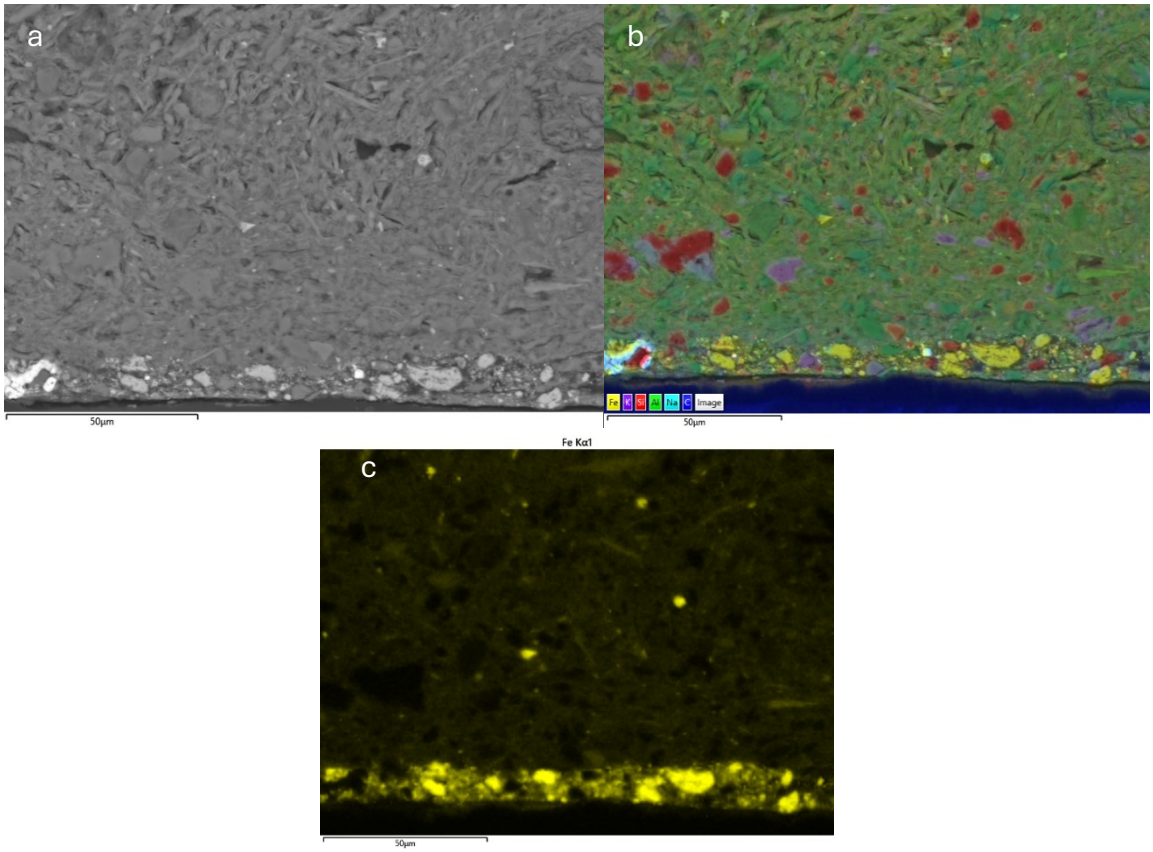

Figure 39 SEM-EDS mapping of the orange decorative layer, showing a low carbon signal and a lighter appearance in BSE images compared to other pigment layers in the polychrome group: (a) BSE image; (b), C, Si, Al, and Na map, and (c) iron (Fe) map (BDX27678, Montículo 1).

- ✓ **Monochrome**

Monochrome ceramics are primarily decorated in orange or gray tones, with one exception: BDX27681 (Montículo 1), which displays a yellow surface. Out of the ten monochrome samples, six are orange, two are gray, one is yellow, and one does not exhibit any visible coloration. The surface appearance of these ceramics appears to result from either surface treatments (such as polishing or smoothing) or the application of slips that were added before firing.

Based on SEM imaging and SEM-EDS analysis, three samples show evidence consistent with the application of a slip, while five are better explained by surface treatments (BDX27684, BDX27688, BDX27689 orange, and BDX27674, and BDX27676, gray). For example, under SEM imaging sample (BDX27676, Monticulo1), shows no visible decorative layer is observed (Fig. 40), suggesting that the color may result from surface treatment or firing conditions, such as reducing atmosphere, rather than from the application of a pigment.

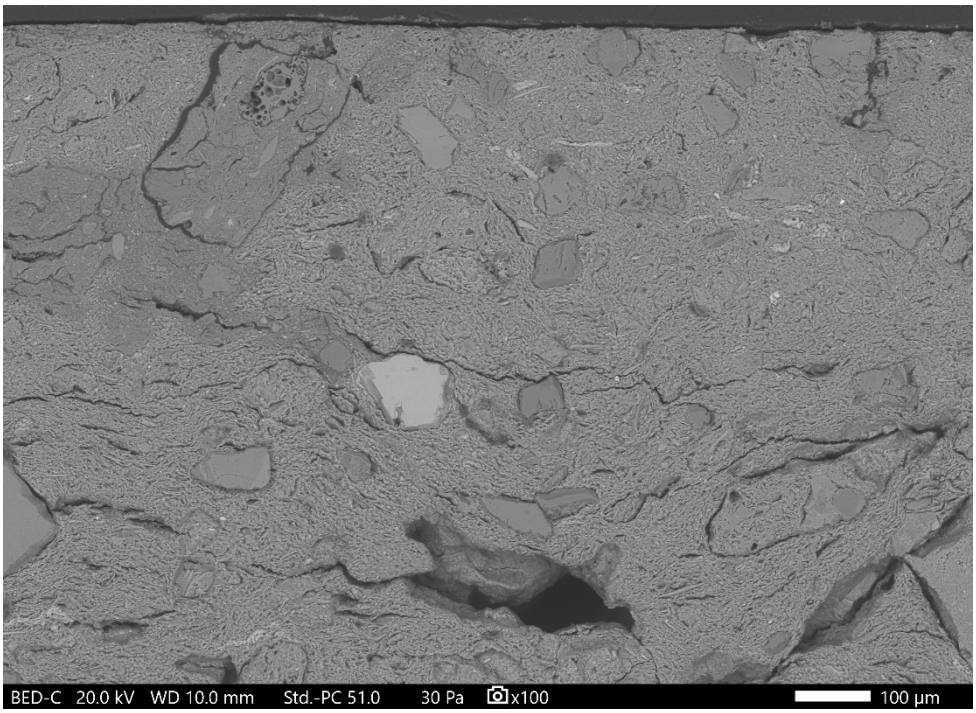

Figure 40. Gray decor observed in SEM shows no distinct pigment layer, probably it's due to surface treatment like polishing or smoothing (BDX27676, Monticulo1).

In contrast, some samples present a surface layer that appears to result from the use of naturally colored clay sediment. For example, (BDX27675, Montículo 1) shows a distinct layer, as seen in Fig. 41, containing inclusions of quartz and feldspar up to 180 µm. Elemental mapping (Fig. 42) of this area reveals a widespread distribution of iron near the surface, indicating the use of Fe-rich clay. No carbon signal is detected, and the surface does not appear dark in backscattered electron

(BSE) images—supporting the interpretation that no organic or carbon-based material was added. The external zone most likely consists of a Fe-rich slip of clay sediment applied during manufacturing.

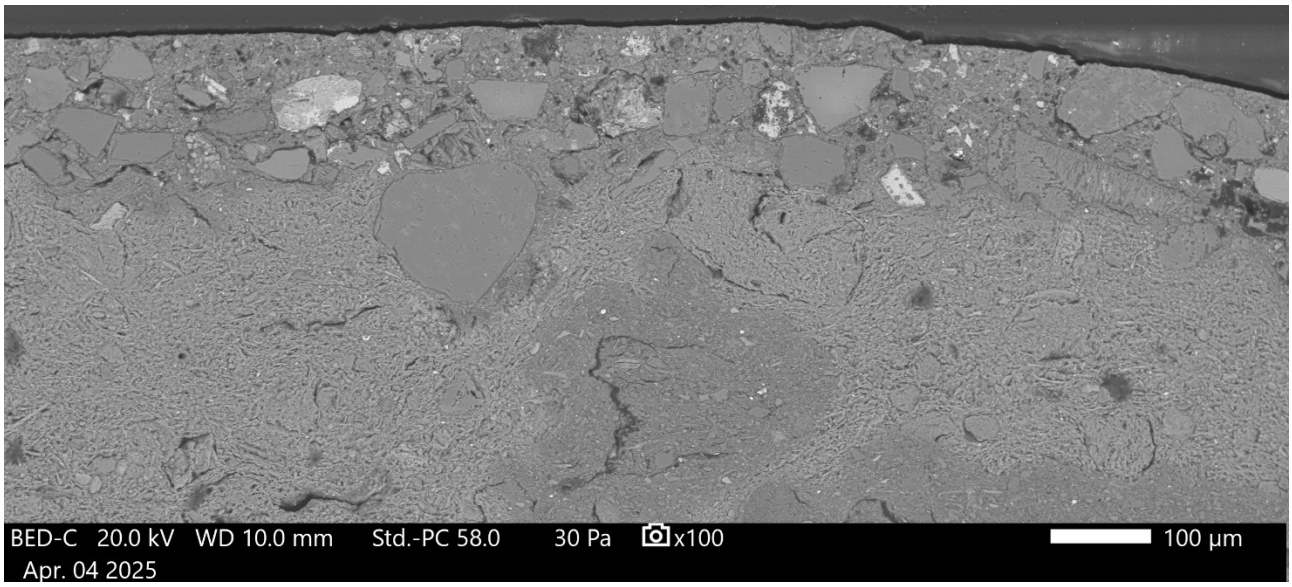

Figure 41. Cross-section of orange education in SEM, showing a surface layer with mineral inclusions up to 180 µm, including quartz and feldspar. The layer corresponds to a naturally colored, Fe-rich clay sediment slip applied during manufacture (BDX27675, Montículo 1)

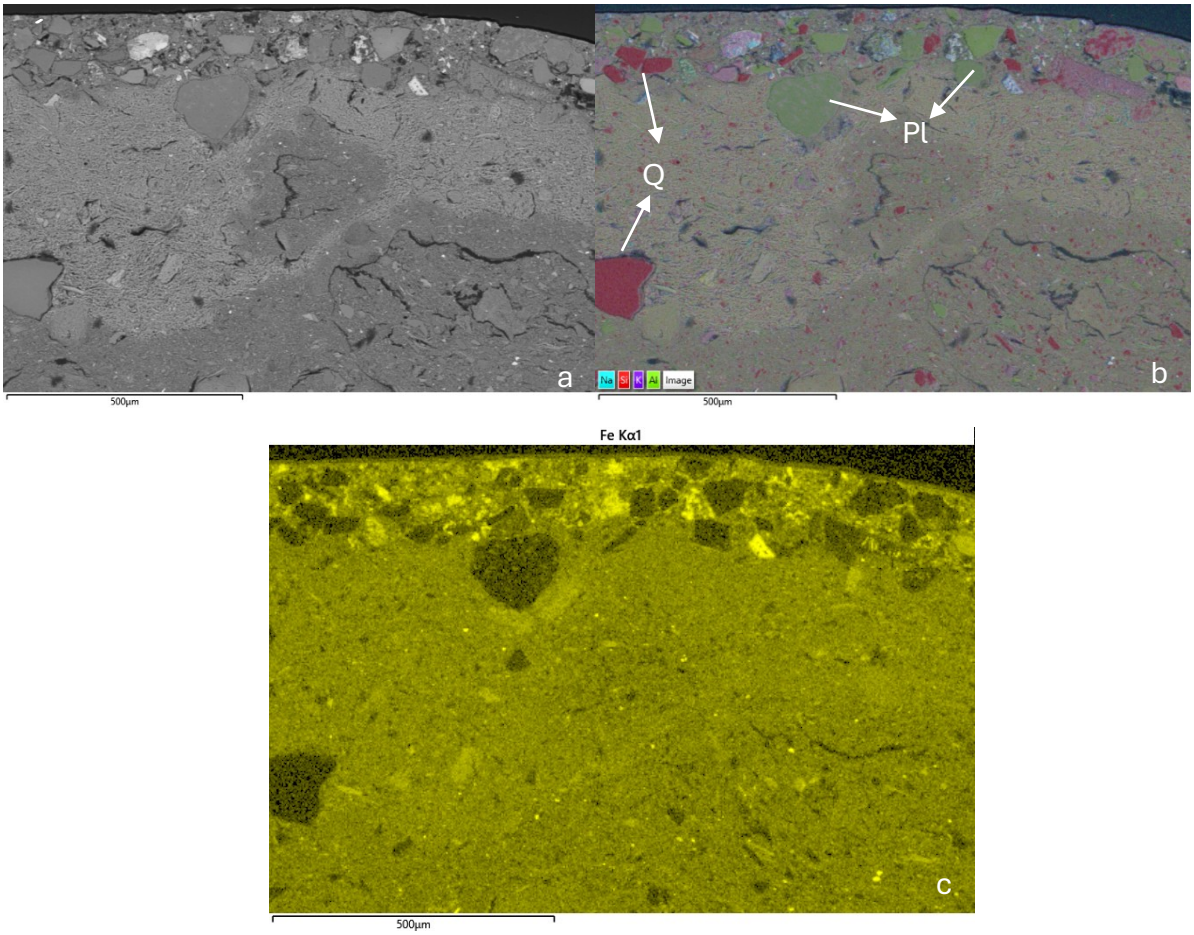

Figure 42. SEM-EDS elemental mapping of an orange decoration, showing a widespread distribution of iron near the exterior, consistent with the use of an Fe-rich clay slip. The outer zone does not appear dark in BSE imaging, suggesting the absence of organic materials. (a) BSE image; (b) composite map showing K, S, Al, and Na; and (c) Iron (Fe) map (BDX27675, Montículo 1).

Within the monochrome group, BDX27681 stands out due to its yellow decoration and the presence of a well-defined separation line between the decorative layer and the ceramic body. This raises the question of whether its yellow coloration is comparable to that of the polychrome group—or if it may have been misclassified and represents a sherd from a polychrome ceramic.

SEM and stereo imaging observations (Fig. 43) confirmed the presence of a well-defined yellow layer above the ceramic body—something that is not present in other monochrome samples, which lack such well-defined layers.

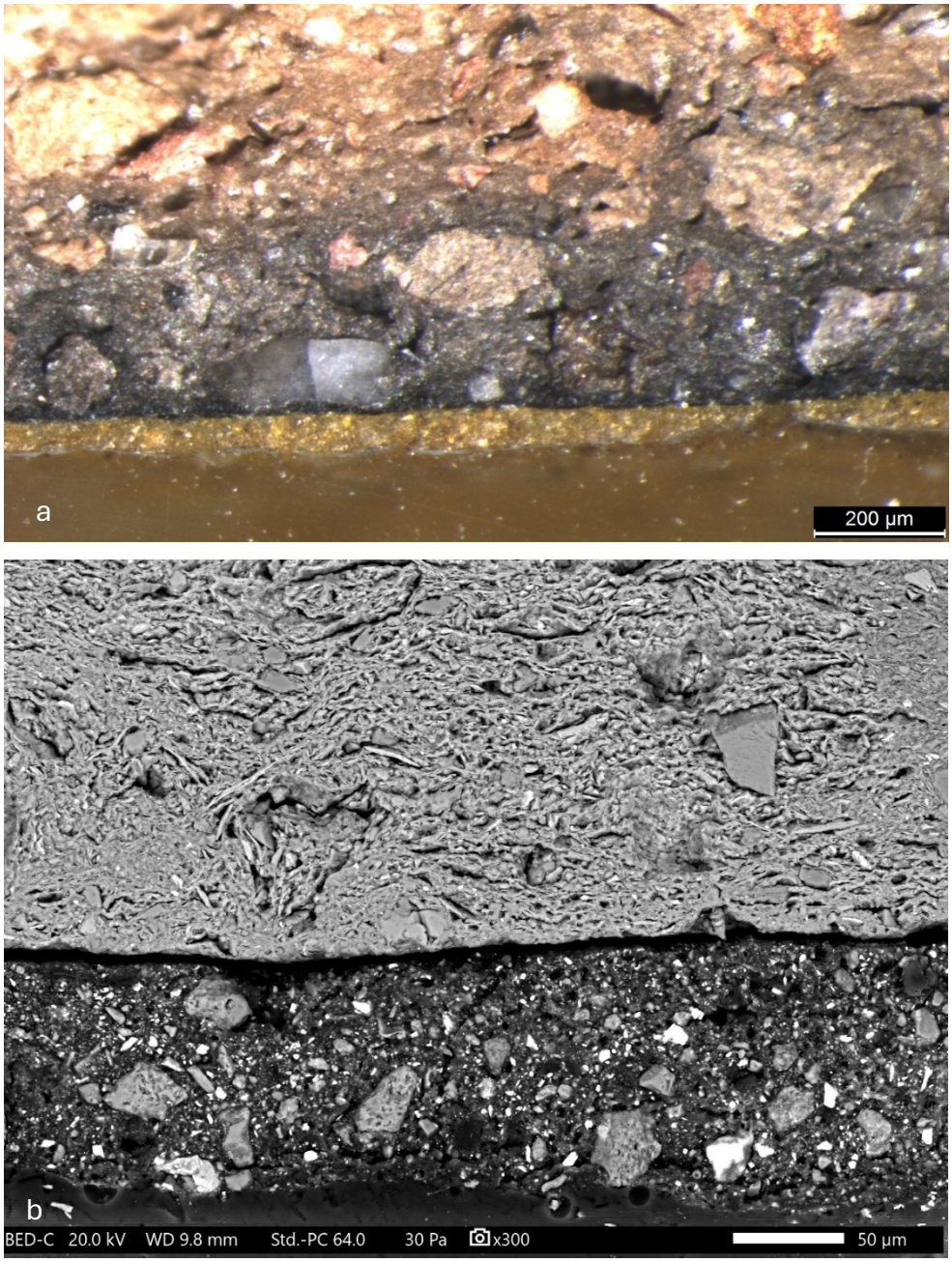

Figure 43. Stereomicroscope (a) and SEM (b) images of yellow decorative layer shows a clear separation from the ceramic body—resembling polychrome ceramics and raising questions about its classification (BDX2768, Montículo 1).

Elemental mapping (Fig. 44) also indicates a very high carbon content that aligns it more closely with the polychrome group than with other monochromes. Additionally, the distribution of sulfur (S) and arsenic (As) within the yellow layer supports the use of similar mineral-based pigments to those employed in the polychrome decorations.

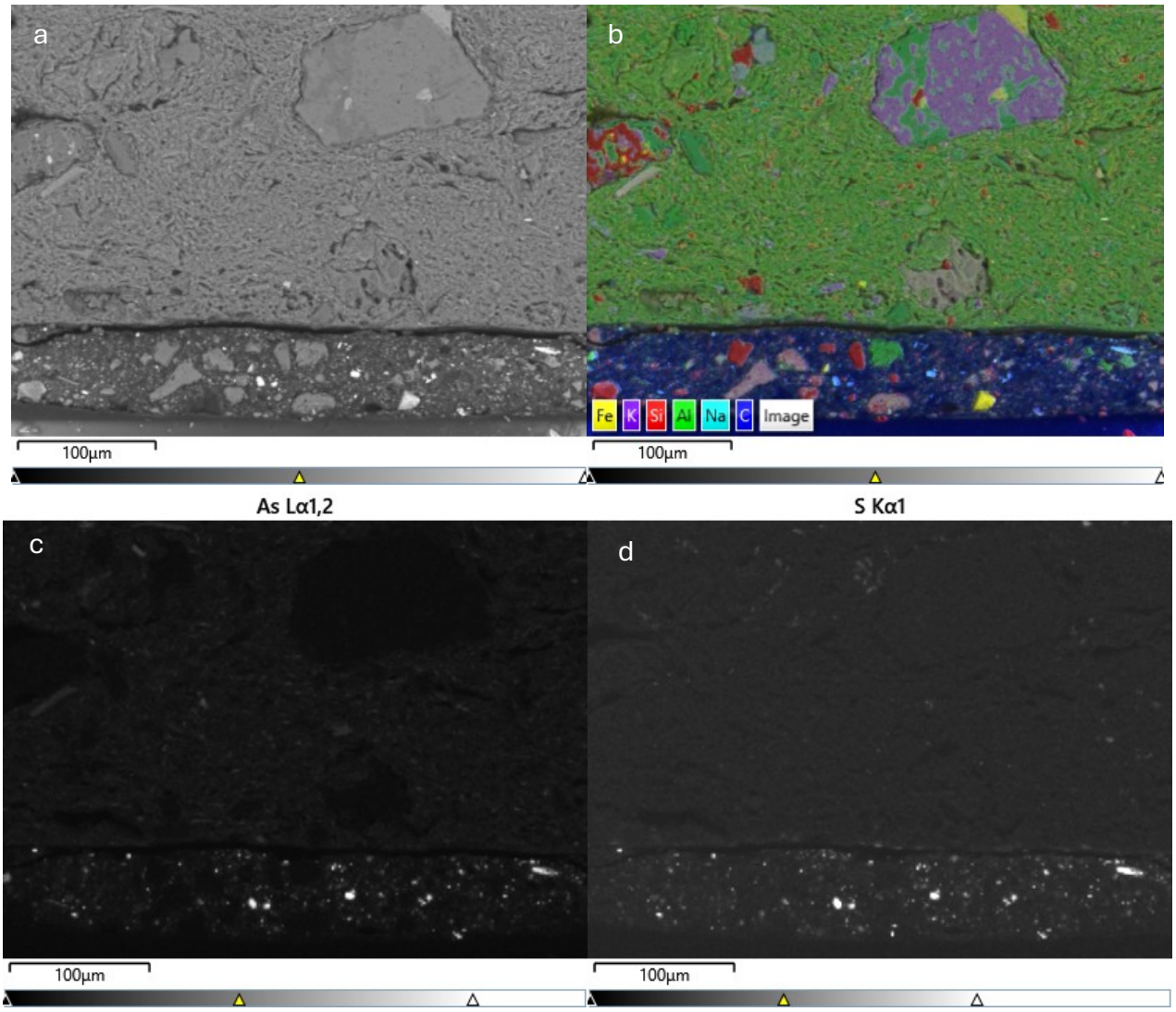

Figure 44. SEM-EDS analysis of yellow decoration. (a) BSE image of the yellow decorative layer; (b) elemental mapping of Fe, K, Ai, Al, C, and Na; (c) arsenic (As) map; (d) sulfur (S) map. The high carbon content suggests the presence of organic material, aligning this sample more closely with the polychrome group than with other monochrome (BDX27681, Montículo 1).

Briefly, comparative analysis of monochrome and polychrome ceramics shows that generally polychrome decorations were added post-firing. This is clear due to high amount of carbon content along with distinct boundaries between decoration and ceramic body—suggesting the employment of organic components and separate layers of pigments(Li et al., 2025). An exception is sample

BDX27678 (Montículo 1), that bears a negative decoration without carbon and lacks a sharp border, suggesting that the decoration had been applied before firing.

There is no post-firing application of the color in monochrome ceramics: they lack carbon signals and a clear separation line between declaration layers and ceramic body, suggesting that the coloring was applied before firing, either through surface treatments such as polishing or smoothing, or through the application of slips, possibly enhanced by firing regimes acting on naturally colored clays (Ion et al., 2024). But sample BDX27681 (Montículo 1) is an exception in the monochrome, as it has a clear yellow layer, rich in carbon, with a glossy surface, all of which are typical of post-firing application.

3.1.2 Hyperspectral Imaging

Hyperspectral imaging is a valuable non-destructive for characterization of nature of decoration. With collecting of spectral data over a wide range of wavelengths, it provides precise information on the optical properties of pigments and dyes and investigates changes in material composition(Kubik, 2007; Mounier et al., 2014; Picollo et al., 2020; Vasco et al., 2024).

By comparing the resultant spectra with known reference libraries, it is possible to identify pigments and recognize the colorants utilized in the decorations. However, all dyes and pigments such as lead white, calcium carbonate, gypsum, and certain black pigments cannot be detected with certainty in the near-infrared to visible (VIS–NIR) range (400–1000 nm) (Capobianco et al. 2024).

Different decorative colors like red, yellow, black, and orange were investigated under two architectural structures: Montículo 1, Montículo 25, and El Panteón site.

3.1.2.1 Red Decorations

The spectrum of the red decoration is characterized by a broad reflectance increase beginning near 580–600 nm, with a gentle slope around 600 nm and a noticeable absorption band between 850 and 900 nm (Fig. 45)(Elias et al., 2006; Aceto et al., 2014; Hayem-Ghez et al., 2015). This spectral signature is characteristic of iron oxide-based pigments such as hematite or red ochre. It is noteworthy that the orange and red decorations, such as those of BDX27675, BDX27691 (orange) and BDX27677, BDX27679 (red), exhibit very similar spectral behaviors with overlapping reflectance curves and with similar features between the visible and near-infrared range. This suggests that the two colors belong to the same iron oxide-based pigments. The variations in tone that are observed are

likely attributable to variations in pigment concentration, grain size, or mode of application, rather than to fundamentally different materials.

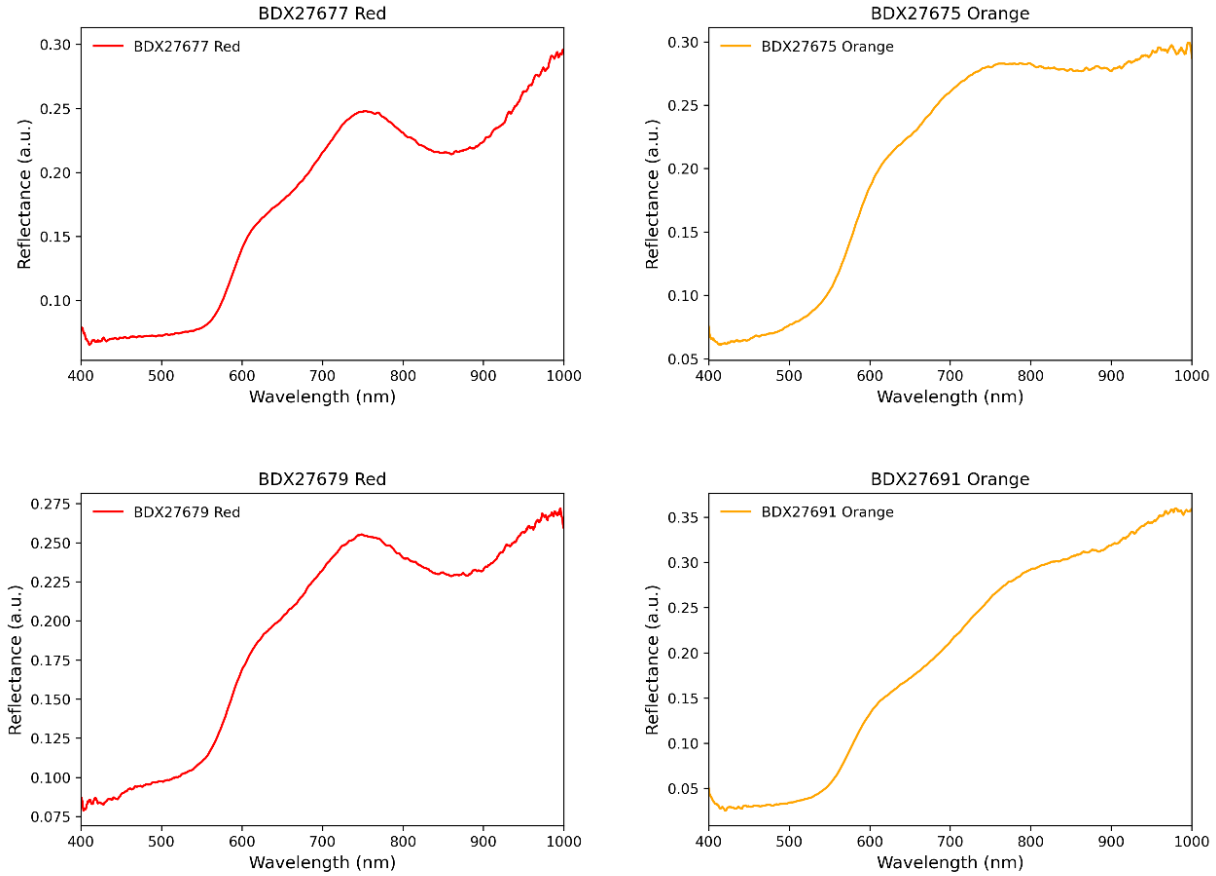

Figure 45. Reflectance spectra of the red (left)and orange(right) decorations obtained with the HSI VNIR camera.

3.1.2.2 Black Decorations

Black colors are extremely difficult to distinguish by hyperspectral imaging alone because they tend to have flat, featureless spectra with near zero reflectance, especially for carbon blacks such as lampblack or bone black (Aceto et al., 2014; Kastenholz et al., 2024).

The samples BDX27698, BDX27682, and BDX27679 in f(fig.46) are all very similarly shaped spectrally, featureless and smooth across the VIS–NIR range, following the overall shape of carbon-based black.

More distinctly, three samples—BDX27677, BDX27680, and BDX27683 (Fig. 47), which appeared black to the naked eye, were identified by HSI as containing indigo. Their reflectance spectra (Fig. 46) reveal a characteristic rise starting around 700 nm, a known spectral signature of indigo(Pei et al., 2023). Between 400 and 700 nm, the curve is flat, similar to that of carbon black, but after that, it rises sharply, which differentiates these from carbon blacks alone. This suggests use

of indigo at high concentration, either alone or mixed with carbon black, most likely to produce a deep, saturated black with more visual or symbolic effect. This spectral profile matches reference indigo spectra in previous studies, wherein high absorption within the visible and rising slope in the NIR are typical (Casanova-González et al., 2020).

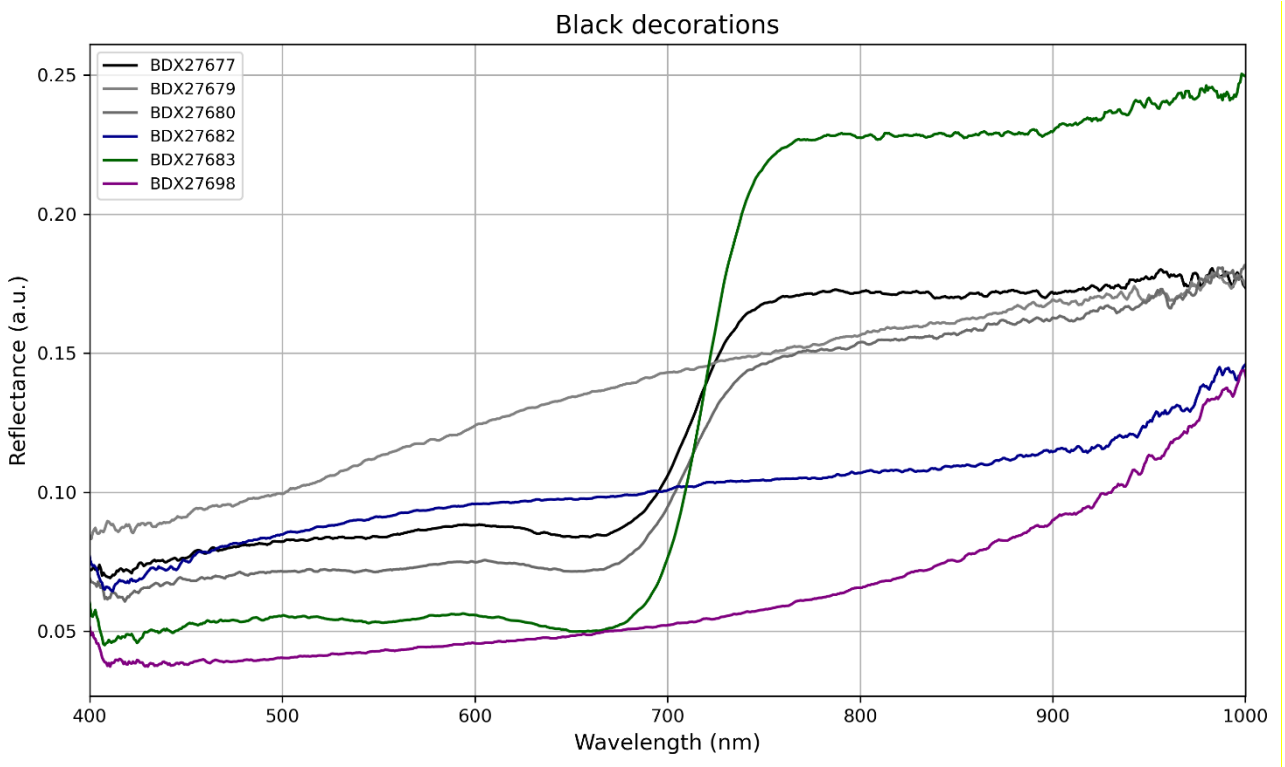

Figure 46. Reflectance spectra of the black decorations obtained with the HSI VNIR camera.

Figure 47. Black decorative areas on ceramic fragments from Montículo 1 which revealed the presence of indigo through hyperspectral imaging analysis.

In contrast, neither indigo was detected in the pigments of black from Montículo 25 or El Panteón, pointing to differences in pigment selection or preparation between site contexts. Such

differences could have arisen due to different workshop traditions, functional requirements, or social connotations given to black colors across architectural sectors.

The presence of indigo is especially important since the first recognized application of this dye in the world was found in Peru and dates back more than 6,000 years at the Preceramic site of Huaca Prieta(Splitstoser et al., 2016).

3.1.2.3 Yellow Decorations

The yellow-painted ceramics reveal a consistent pattern of reflectance behavior visually comparable to that of orpiment, an arsenic sulfide paint (Fig. 48).

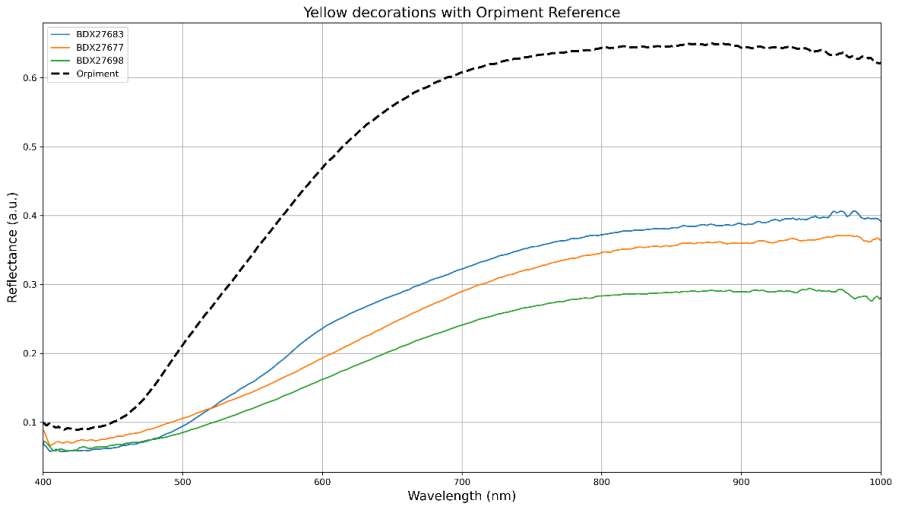

Figure 48. Reflectance spectra of the yellow decorations obtained with the HSI VNIR camera.

In these samples, the reflectance curves have a steady rise beginning around 480–500 nm and rising uniformly to over 800 nm, a profile characteristic of semiconducting yellow pigments such as orpiment (Aceto et al., 2014).

While absolute reflectance is lower than for the pure orpiment standard that likely arises from dilution, particle size differences, or surface alteration, the shape of the spectrum is characteristic of Orpiment as a primary component.

3.1.2.4 RGB and Infrared False Color (IRFC) Imaging

Aside from hyperspectral spectral analysis, RGB and IRFC images derived from the hyperspectral data cube provided visual information about surface variations not necessarily visible

under ordinary visible light (Fig.49)(Mounier et al., 2014; Hayem-Ghez et al., 2015). Red ochre, for instance, appears greenish on IRFC images, and some black areas, which were spectrally known to be made of indigo highlighted in red (Fig.49) shift towards reddish tones. This color shift in IRFC results from the manner materials reflect in the near-infrared range: iron-based red pigments, such as hematite, reflect more strongly in the NIR, producing a greenish hue when NIR is overlaid on the red channel. Indigo also reflects more strongly in the NIR than carbon black, and so indigo-dense regions appear lighter—typically reddish or pink—in IRFC(Mounier & and Daniel, 2015). These are the color changes that agree with the spectral data, further validating the identification of iron- and indigo-based pigments and showing how false-color imaging helps with pigment discrimination.

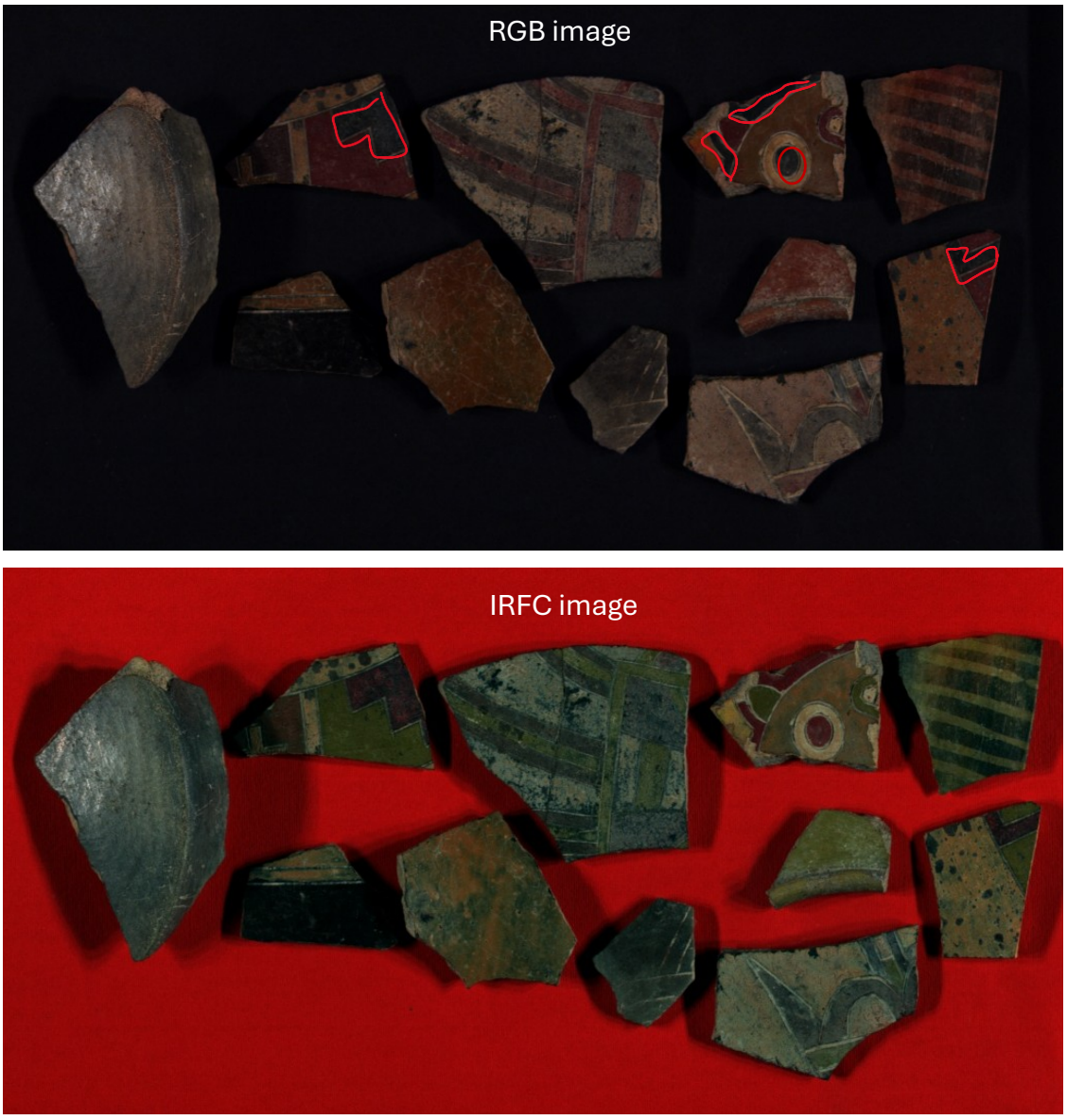

Figure 49. RGB and IRFC images highlight material differences: red areas appear greenish due to iron-based pigments, while indigo-rich blacks also shift to green, supporting spectral identification.

3.2 Colorimeter

The spectrophotometer recorded values in the CIELab system (L*, a*, b*) and derived CIELCh parameters (C*, h°) (Table 1) provided five-dimensional data for describing the decorative surface colors (Ly et al., 2020). We focused on decorative categories that were visually described by Aicha Bachir Bacha: black, red, yellow, orange, cream, gray, and beige.

3.2.1.1 Black Color Areas

Black samples present L* values from 26 to 42, confirming their general black color appearance. However, looking closer at a* (1.1 to 4.6) and b* (1.2 to 7.6) reveals some chromatic deviation towards warm colors, more evident in samples with b* > 6. C* values between 2.1 and 8 reflect low chroma, consistent with desaturated colors, while hue angles (53°–86°) are inclined towards the yellowish hue. While the low lightness values are generally in line with a black visual appearance, the high b* and moderate C* suggest that some samples can be darker brown or warm gray. In brief, while most black decorations are justifiably classified, a minority show pronounced chromatic warmth, warranting reclassification as very dark brown.

3.2.1.2 Red Color Areas

Red samples are medium dark, with L* values of 31 to 40, aligning with moderately to strongly saturated red hues. a* values that fall between 7 to 15 are consistent with a high red component. b* values (7–11) and hue angles (33°–47.7°) firmly place these colors in the red-orange class on the color wheel. Chroma (C*) of 12 to 18.5 suggests moderate to strong saturation. Together, these parameters support the classification of these pigments as saturated red to reddish orange.

3.2.1.3 Yellow Color Areas

Yellow samples have medium L* values (39 –43.5), consistent with medium-bright visual appearance. b* values are high (16–22), characteristic of yellow color. a* ranges between 6 and 9, indicating red-shifted yellows. Chroma values are among the highest in the database C*(17.26– 23.95), consistent with vividness. Hue angles between 68° and 72° place these pigments in the yellow to yellow-orange class. This highly supports visual identification of the samples as yellow, and consistency in chromatic coordinates reinforces their classification.

*Table 1. Average CIELab and CIELCh values from two zones of visually identified ceramic decorations. *Indicates monochrome samples*

Color	Sample	Site	L*(D65)	a*(D65)	b*(D65)	C*(D65)	h(D65)
red	BDX27677	Montículo 1	31.6	13.1	8.7	15.8	33.6
red	BDX27679	Montículo 1	40.1	8.3	9.1	12.4	47.7
red	BDX27680	Montículo 1	32.3	15.7	9.9	18.5	32.2
red	BDX27682	Montículo 1	35.7	9.5	10.3	14.0	47.4
red	BDX27683	Montículo 1	38.9	10.2	11.1	15.1	47.3
red	BDX27686	Montículo 25	38.7	7.1	7.2	10.1	45.4
red	BDX27690	El Panteón	31.2	10.8	8.9	14.0	39.7
orange*	BDX27687	Montículo 25	50.9	14.4	20.7	25.2	55.2
orange*	BDX27675	Montículo 1	45.7	11.8	14.4	18.6	50.7
orange	BDX27678	Montículo 1	39.2	9.8	14.4	17.5	55.6
orange*	BDX27684	Montículo 25	42.4	14.3	15.2	20.9	46.7
orange*	BDX27688	El Panteón	39.0	9.7	14.9	17.8	57.0
orange*	BDX27691	El Panteón	38.6	12.8	14.0	19.0	47.5
orange*	BDX27689	El Panteón	43.8	18.7	18.7	26.4	44.9
black	BDX27677	Montículo 1	26.7	0.7	2.3	2.4	73.1
black	BDX27678	Montículo 1	32.1	5.0	6.7	8.3	53.3
black	BDX27679	Montículo 1	42.5	1.3	6.4	6.5	78.6
black	BDX27680	Montículo 1	29.8	0.5	2.3	2.3	78.3
black	BDX27682	Montículo 1	39.5	2.6	8.4	8.8	72.7
black	BDX27683	Montículo 1	36.1	0.2	3.7	3.7	86.3
black	BDX27686	Montículo 25	34.7	2.2	4.6	5.1	65.0
black	BDX27690	El Panteón	34.8	2.0	6.2	6.6	71.9
black	BDX27698	Montículo 1	27.7	1.2	2.4	2.7	64.4
yellow	BDX27677	Montículo 1	42.3	8.9	22.2	24.0	68.2
yellow	BDX27680	Montículo 1	43.4	7.8	20.1	21.6	68.8
yellow*	BDX27681	Montículo 1	38.9	6.7	20.8	21.9	72.1
yellow	BDX27690	El Panteón	40.2	5.9	16.2	17.3	69.8
cream	BDX27686	Montículo 25	54.9	4.8	14.2	15.0	71.4
cream	BDX27679	Montículo 1	44.8	4.8	13.8	14.6	71.2
cream	BDX27682	Montículo 1	51.7	5.4	12.9	14.0	67.1
cream	BDX27683	Montículo 1	54.6	5.1	18.7	19.4	74.9
gray*	BDX27674	Montículo 1	39.9	2.1	6.4	6.8	71.9
gray*	BDX27676	Montículo 1	48.5	3.6	10.5	11.1	71.0
beige	BDX27683	Montículo 1	42.0	6.7	17.5	18.7	69.0
brown	BDX27680	Montículo 1	30.0	6.9	5.4	8.8	38.0

3.2.1.4 Orange Color Areas

Orange samples fall between yellow and red. L* values range from 38.6 to 51, slightly lighter than yellow. a* (9–18) and b* (13–20) show strong red and yellow contributions. C* values are high

(average ≈ 20.8), and h° values (45°–57°) place the hue in the true orange sector. These are the most chromatically rich pigments. The values agree confidently with orange pigments, as both hue and saturation support this classification.

3.2.1.5 Cream Color Areas

Cream colors have moderate to high L* values (45–55), indicating a light visual tone. a* values (4.7–5.5) suggest a mild red component, while high b* values (12.8–18.7) indicate strong yellow influence. These yield mild chroma (C* = 14–19), creating soft yet clear coloration. Hue angles between 67° and 75° place these pigments in the yellow orange to yellow region. Such a chromatic profile is fitting for the eye perception of "cream" pigments—warm, light, less saturated than yellow or orange. Although BDX27686(Montículo 25) and BDX27679(Montículo 1) were labeled as white by archaeologists, colorimetric data supports their classification as cream, based on their position in the CIELab space. These values clearly distinguish cream from muted yellows and less intense beiges, supporting its classification as a distinct series of pigments.

3.2.1.6 Gray Color Areas

Gray samples have middle lightness (L* = 40–48.5) with low a* (2–3.6) and moderate b* (6–10.5), indicating low chroma and overall desaturated look. Chroma values (C* = 6.8–11) reinforce their near-neutral color status. However, their hue angles (~71°) are within the yellow quadrant, which reveals a slight chromatic bias. These pigments are not neutral but lean toward warm gray or taupe. Although visually consistent with gray decoration, the data show that some of the samples would more accurately be described as warm-toned gray.

3.2.1.7 Beige and Brown Color Areas

There was just a single sample that was said to be beige. It has L* = 42.0, a* = 6.6, b* = 17.5, C* = 18.7, and h° = 69.0° and places it close to the yellow and cream classes in color space but darker and more saturated. It is an option for the cream class but darker and more saturated. While the beige class is visually reasonable, the colorimetric data suggests that it might more accurately be characterized as yellow brown or rich cream than as a specific beige.

In addition, one sample—BDX27680 from Montículo 1—was a brown, with L = 30.0*, a = 6.9*, b = 5.4*, C = 8.8*, and h° = 38.0°. These measurements define a low-lightness, low-chroma

color that lies in the red orange to brown area on the color wheel. Its low value, low saturation, and muted chromaticity overwhelmingly classify as brown, separating it from the red and orange classes.

Most color clusters defined by visual observation are generally supported by spectrophotometric measurement. The red, yellow, orange, and cream clusters are highly consistent internally. The "black" cluster, while generally consistent in lightness, includes samples with unexpected chromatic warmth, precluding strict neutral classification. Gray samples all also have a slightly yellow-biased color. All these findings indicate that while visual identification is largely accurate, objective colorimetric data enable greater subtlety, with nearer classification and the potential identification of misattributions.

In addition to the quantitative analysis, we plotted the color distribution in two color planes: the ab* (chromatic axes) and aL* (red-green vs. lightness) plots. These plots show the internal variability within each visually defined group of colors and assess the stability of their colorimetric attributes. The a*b* plane highlights the relationship between the yellow blue (b∗) and red-green (a∗) components, and the aL* plane indicates that red intensity is correlated with lightness (L∗). These plots are particularly helpful to identify pigment clusters and identify overlaps or transitional gradients between categories.

For example, the distribution of the red pigment samples is shown in (Fig.50) and demonstrates consistent clustering along both axes.

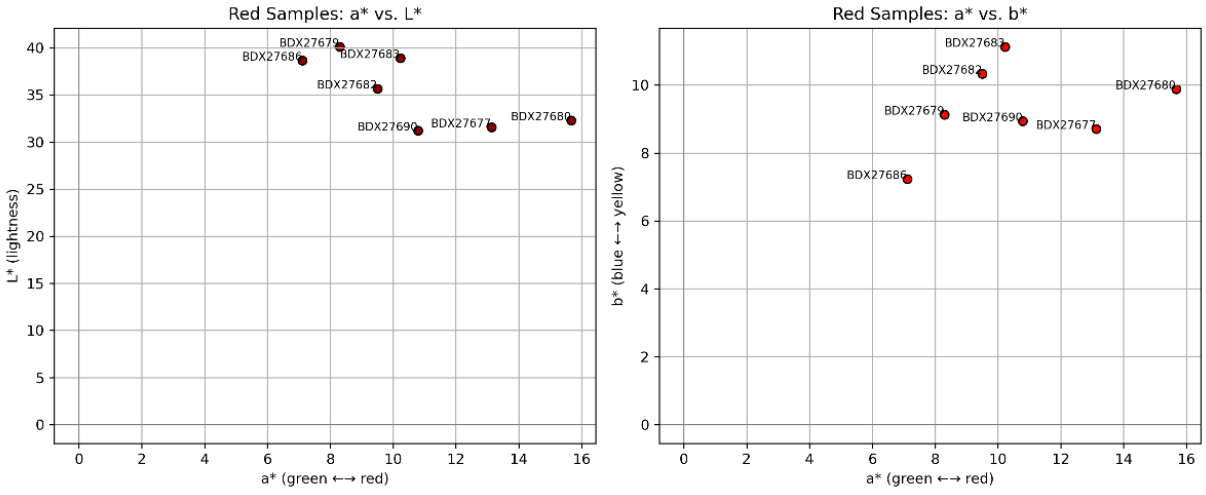

Figure 50. Distribution of red color measurements in CIELab space. Left: a vs. L* (red–green axis vs. lightness). Right: a* vs. b* (chromatic plane), illustrating hue direction and chroma variation among red samples.*

The ab plot (right) shows red samples cluster in the top-right quadrant, confirming high red (a*) and moderate yellow (b*) content, typical of red to reddish-orange pigments. The aL plot (left)

confirms the relationship between red colorimetry and lightness: most samples place at moderate lightness (L*) and high a* values, confirming their highly saturated red appearance. Together, these plots visually confirm the numerical data and confirm the chromatic similarity of the red pigment group.

Decorative color samples are plotted in CIELCh° polar coordinates (Fig. 51), where hue angle (h°) is plotted against chroma (C*) to define color direction and saturation.

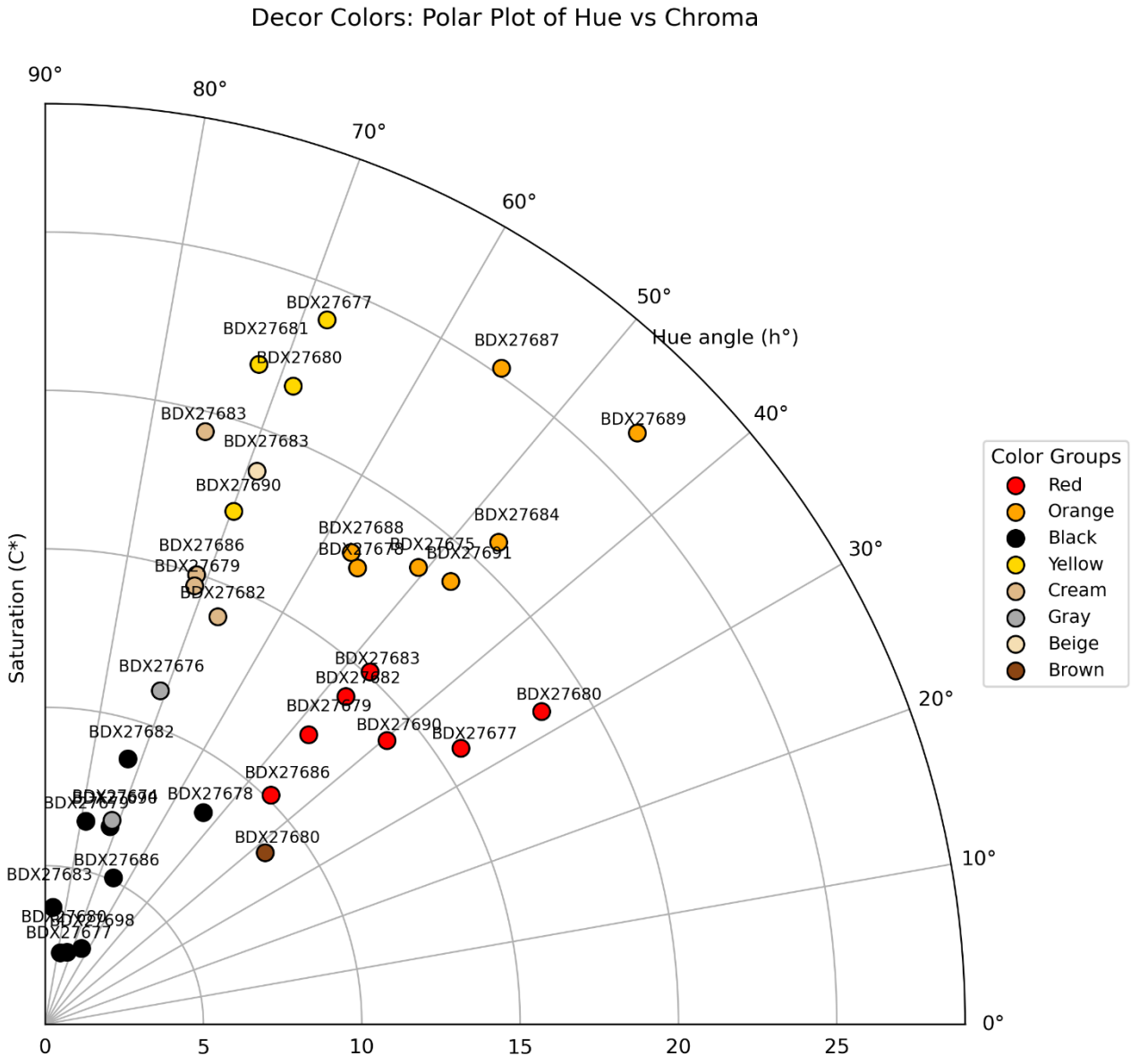

Figure 51. polar plot of all decorative color samples, showing hue angle (h°) and chroma (C) distributions across visually identified color groups.*

Red samples form a distinct cluster between 30° and 48°, with medium to high values for chroma (C* ≈ 8–18), as expected for their deep red to red-orange hue. Orange samples vary between

approximately 44° and 57° hue angles with some of the highest values of chroma (C* > 20), as would be expected of their intense, saturated appearance. Yellow samples cover the range between 67°–75° with slightly less chroma than orange but still firmly within the yellow range. Cream samples appear near the yellow cluster but with low chroma and slightly higher lightness, as expected to be in their position as lighter less saturated yellow orange. The gray and beige samples are in the lower chroma region (C* < 12), near hue angles of about 70°, which indicates low saturation but a poor warm tone—especially in beige.

Finally, black samples cluster close to the origin with low chroma values and diffuse hue directions, as one would expect for their dark and nearly neutral appearance. Polar visualization confirms overall visual coherence of classifications and shows nuanced tonal distinctions between the different groups of pigments.

To validate the spectrophotometric data, CIELab values were also extracted from hyperspectral RGB images using Python. The respective color differences (ΔE) between the datasets were calculated afterwards. While some samples, e.g., BDX27682 (ΔE ≈ 3) and BDX27690 (ΔE ≈ 3), show good consistency (ΔE < 5), most showed significant discrepancies. Interestingly, samples BDX27691 (ΔE ≈ 45.4) and BDX27684 (ΔE ≈ 31.1) contained high ΔE values, indicating major divergence (Paravina et al., 2015). These differences are probably results of variations in data manipulation between the hyperspectral and the spectrophotometric methods, and not of actual inconsistencies in decoration content.

A complete comparison of L*, a*, and b* values for the hyperspectral image (from Python) and ΔE values (compared to spectrophotometer data) and their corresponding visual color labels are provided in Appendix Table 2.

3.3 Chemical Analyses

This section focuses on the chemical analysis of the ceramic samples, with particular attention to the decorative elements, following an initial assessment of the paste composition. The analyses were conducted using a set of complementary techniques: SEM-EDS, pXRF, Raman spectroscopy, and FTIR.

3.3.1 Analysis of the Ceramic Paste

For the matrix, SEM-EDS and pXRF analysis were conducted to assess elemental composition between the three sites as well as between the polychrome and monochrome groups as these techniques widely adopted in archaeometric studies for their ability to identify major and minor elements(Tite, 2008).

3.3.1.1 pXRF

As a first step to our analytical approach, we conducted pXRF data on the 19 ceramic samples for analyzing compositional heterogeneity and assessing the capacity of pXRF to differentiate among the groups and polychrome and monochrome style.

- ✓ **Polychrome**

Though the sample set was limited, Principal Component Analysis (PCA) was applied to the log-transformed elemental data to explore patterns of geochemical variability, following the approach used by (Frerebeau et al., 2020) in their study of Iberian ceramic production. (Fig.52) is a presentation of the results, which are a score plot and a loading plot of both the distribution of samples and the contributions of specific elements to the principal components based on five elements (CaO, MgO, Mn, Cu, and Zr). PC1 explains 50.90% of the variance, and PC2 explains 29.89%, thus a total of 80.79% cumulative explanation. This implies that the majority of the compositional variation among the samples is captured in the first two axes.

Although the few samples—i.e., the individual polychrome pieces from Montículo 25 and El Panteón—preclude any strong statistical generalizations, the PCA reveals coherent patterns in their geochemical signatures.

The distribution of the samples testifies to the three contexts—Montículo 1, Montículo 25, and El Panteón—being generally alike in composition with only individual slight variations. Most of the sample's cluster are near the origin of the PCA space, indicating little differentiation. Two of the Montículo 1 samples vary: BDX27680 traverses the positive PC1 direction, directed by CaO and Cu, and other traverses the positive PC2 direction, indicating Mn.

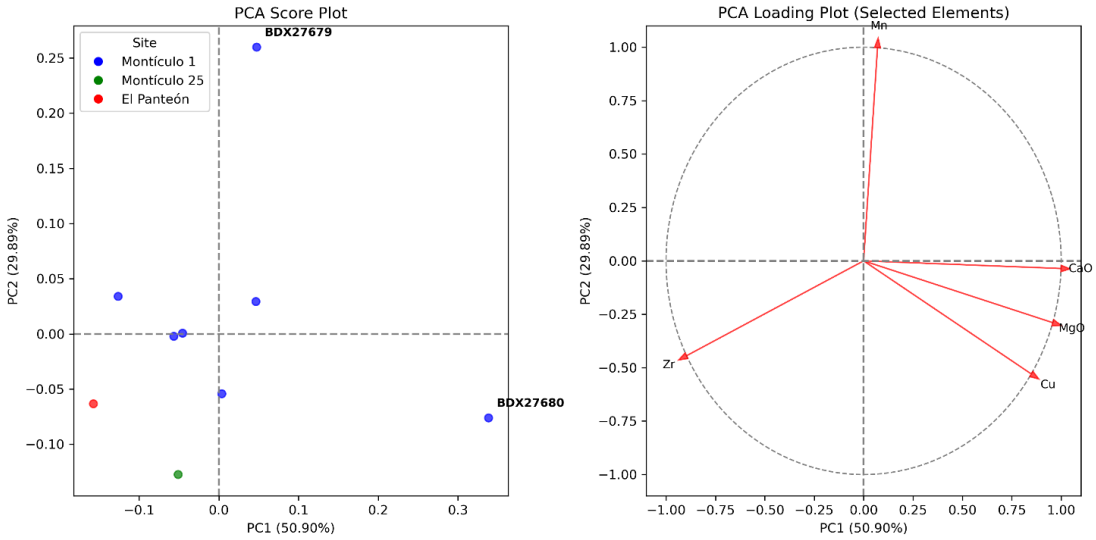

Figure 52. Principal Component Analysis (PCA) of the polychrome ceramic pastes based on the five most variable elements (CaO, MgO, Mn, Cu, and Zr).

To better characterize the geochemical heterogeneity of the polychrome ceramics, Table 2 presents mean concentrations and standard deviations for thee sites: Montículo 1, Montículo 25, El Panteón.

Table 2. Elemental concentrations of polychrome ceramic samples based on pXRF analysis. Major elements are expressed in weight percent (wt%), and trace elements in parts per million (ppm)

Site	Sample ID	MgO	Al_2O_3	SiO_2	K_2O	CaO	TiO_2	Fe_2O_3	Mn	Ni	Cu	Zn	Rb	Sr	Zr
Montículo 1	BDX27677	3.3	21.2	57.3	2.3	3.5	1.1	11.3	1321	55	213	194	127	295	173
	BDX27678	2.3	19.5	58.1	2.4	3.3	1.1	13.3	1140	55	183	216	135	307	186
	BDX27682	2.8	19.6	57.5	2.2	3.6	1.3	13.0	943	53	153	194	119	328	160
	BDX27683	2.5	20.3	58.5	2.8	3.0	1.2	11.7	1125	56	188	181	123	328	164
	BDX27698	2.2	20.7	57.3	2.4	2.6	1.1	13.6	1160	59	167	189	119	309	167
Montículo 25	BDX27686	3.1	20.8	58.3	2.4	2.9	1.0	11.5	794	67	158	225	129	309	156
El Panteón	BDX27690	2.2	21.4	59.2	2.5	3.0	1.1	10.8	981	52	160	207	124	294	246
	Mean	**2.6**	**20.5**	**58.0**	**2.4**	**3.1**	**1.1**	**12.2**	**1066**	**57**	**175**	**200**	**125**	**309**	**178**
	SD	0.4	0.7	0.7	0.2	0.4	0.1	1.1	173	5	21.3	16	6	14	31
Montículo 1	BDX27679	2.7	20.0	58.5	2.4	3.9	1.1	11.4	1992	51	148	184	119	322	145
	BDX27680	3.4	20.4	54.1	2.2	6.9	1.1	11.8	1053	55	264	171	99	286	140
	Mean	**2.4**	**17.8**	**49.5**	**2.1**	**3.3**	**0.9**	**10.3**	**1031**	**49**	**156**	**170**	**103**	**263.4**	**152**
	SD	0.9	7.5	21.6	0.8	2.0	0.4	4.2	538	20	71	70	43.9	111	64

Sample variation remains minimal for most components consistent with the clustering observed in the PCA score plot. SiO_2 and Al_2O_3 are the most concentrated of the oxides with minimal ranges and low standard deviations, indicating a broadly uniform silicate-based matrix throughout the assemblage. This overall homogeneity helps explain the tight grouping of most samples around the origin in PCA space.

However, there are two deviant Montículo 1 samples. Sample BDX27680, which plots further along PC1, is characterized by increased CaO and Cu content, while sample BDX27679, which plots along PC2, is characterized by a very high concentration of Mn.

The table thus confirms the inference that compositional difference between the samples is minimal and largely a result of a number of discrete elemental enrichments, rather than general differences between archaeological contexts.

- ✓ **Monochrome ceramics**

Following the analysis of the polychrome samples, the same methodology was applied to the monochrome group to ascertain if there were any compositional differences between the three sites.

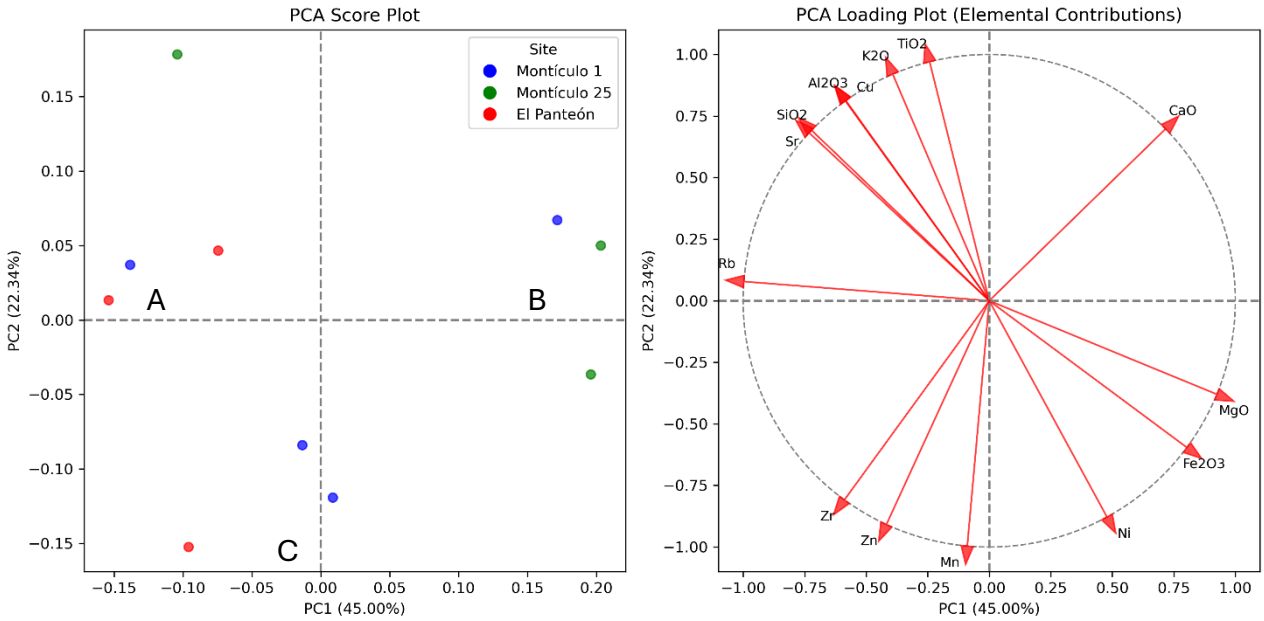

Figure 53. Principal Component Analysis (PCA) of the monochrome ceramic pastes based on their elemental composition (pXRF). We distinguish three groups (A, B and C).

The PCA of the monochrome group (Fig.53) shows that the variance of 67.34% is accounted for by PC1 and PC2 (45.00% and 22.34%, respectively), and this is an appropriate two-dimensional representation of the data.

The score plot suggests three compositional groupings. Group A, in the upper-left corner, is characterized by intermediate geochemical diversity and does not appear to be controlled by any single element. Group B, in the positive direction of PC1, is characterized by high MgO and CaO, as shown in the loading plot. Group C, in the lower-left quadrant, is where there are higher levels of Mn, Zn, and Zr, the factors which load negatively on PC1 and PC2, respectively.

Besides these three groups, one sample is distinctly separated from the rest, located at the upper edge of the PCA space along PC2. This positioning suggests an anomalous geochemical profile.

These associations suggest that although overall variance within the monochrome assemblage is fairly muted, specific elemental enrichments—particularly alkaline earths and trace metals—are responsible for the observed segregation. These distinctions can be explained by variation in clay sources, practices of incorporation, or technological preference among the contexts sampled.

Besides the multivariate analysis (PCA), a basic statistical summary for the major and trace elements of the monochrome samples was conducted (Table 3) to better delineate internal compositional heterogeneity.

Table 3. Descriptive statistics of ceramic monochrome paste composition by pXRF. Major elements in wt%, trace elements in ppm.

Site	Sample ID	MgO	Al_2O_3	SiO_2	K2O	CaO	TiO_2	Fe_2O_3	Mn	Ni	Cu	Zn	Rb	Sr	Zr	
Montículo 1	BDX27674	2.53	20.93	60.80	2.28	2.83	0.94	9.68	727	49	150	185	118	341	178	
	BDX27689	2.57	21.95	58.83	2.39	2.56	0.96	10.75	810	48	156	189	136	292	159	
El Panteón	BDX27691	3.05	20.68	59.89	2.60	2.82	1.03	9.93	793	52	154	178	124	329	155	A
	Mean	**2.72**	**21.19**	**59.84**	**2.42**	**2.74**	**0.98**	**10.12**	**777**	**50**	**153**	**184**	**126**	**321**	**164**	
	SD	0.29	0.67	0.99	0.17	0.16	0.05	0.56	44	2	3	5	9	26	13	
Montículo 1	BDX27681	3.80	20.11	56.77	2.28	5.01	0.95	11.08	939	53	151	167	100	263	147	
Montículo	BDX27685	5.36	19.95	58.01	2.29	3.59	0.94	9.86	652	44	135	165	116	323	137	
25	BDX27687	5.05	20.55	56.61	1.97	3.80	0.99	11.03	864	49	141	174	102	305	159	B
	Mean	**4.74**	**20.20**	**57.13**	**2.18**	**4.13**	**0.96**	**10.66**	**818**	**49**	**142**	**169**	**106**	**297**	**148**	
	SD	0.83	0.31	0.77	0.18	0.77	0.02	0.70	149	5	8	5	8	31	11	
	BDX27675	3.79	20.60	58.59	2.28	2.91	0.86	10.96	1073	64	161	218	118	305	158	
Montículo 1	BDX27676	3.64	21.48	57.77	2.34	2.85	0.90	11.02	1032	44	154	186	117	273	176	
El Panteón	BDX27688	3.40	19.40	61.21	2.02	2.75	0.98	10.25	1020	41	145	221	121	337	241	
	Mean	**3.52**	**20.44**	**59.49**	**2.18**	**2.80**	**0.94**	**10.64**	**1026**	**43**	**150**	**204**	**119**	**305**	**208**	C
	SD	0.17	1.47	2.43	0.23	0.07	0.05	0.55	9	2	6	24	3	45	46	
	Sample ID	MgO	Al2O3	SiO2	K2O	CaO	TiO2	Fe2O3	Mn	Ni	Cu	Zn	Rb	Sr	Zr	
Montículo 25	BDX27684	2.48	20.24	60.30	2.51	3.49	1.09	9.89	768	37	186	160	113	331	153	

SiO_2 and Al_2O_3 are confirmed to be the most prevalent oxides, with constantly high abundance and minimal variability, forming a typical silicate-based ceramic matrix.

Group B is characterized by high concentrations of MgO and CaO elements, averaging 4.74 wt% and 4.13 wt%, respectively, where CaO does not exceed 3.0 wt%. This could suggest a different source or tempering material.

Group C, in contrast, is defined by high Mn concentrations (mean ≈ 1011 ppm), considerably higher than Groups A and B (both <800 ppm), with both distinct Zn and Zr enrichments (205 ppm and 221 ppm, respectively), which compositionally delineate it.

Group A does not have the characteristic elemental enrichments, so perhaps this reflects a more compositionally typical ceramic paste. However, subtle Rb and Sr variation could reflect small differences in clay sources or processing choices. The outlier sample confirms off-site status with elevated SiO_2 and Al_2O_3 and substantially lower Cu (37 ppm) and Zr (39 ppm), showing discrimination from the dominant clusters in the PCA.

These results support the multivariate by showing that elemental enrichments in MgO, CaO, Mn, Zn, and Zr are the most important criterion for distinguishing within the monochrome group, whereas a general major silicate similarity points to a shared technological foundation.

✓ Compositional Analysis of Monochrome and Polychrome Ceramics

To see the compositional differences between monochrome and polychrome ceramics, a PCA was applied on five discriminating elements (Mn, Cu, CaO, MgO, Zn, Rb, and Zr) (Fig.54). The selective analysis was intended to enhance contrasts related to the composition of the paste and technological choice.

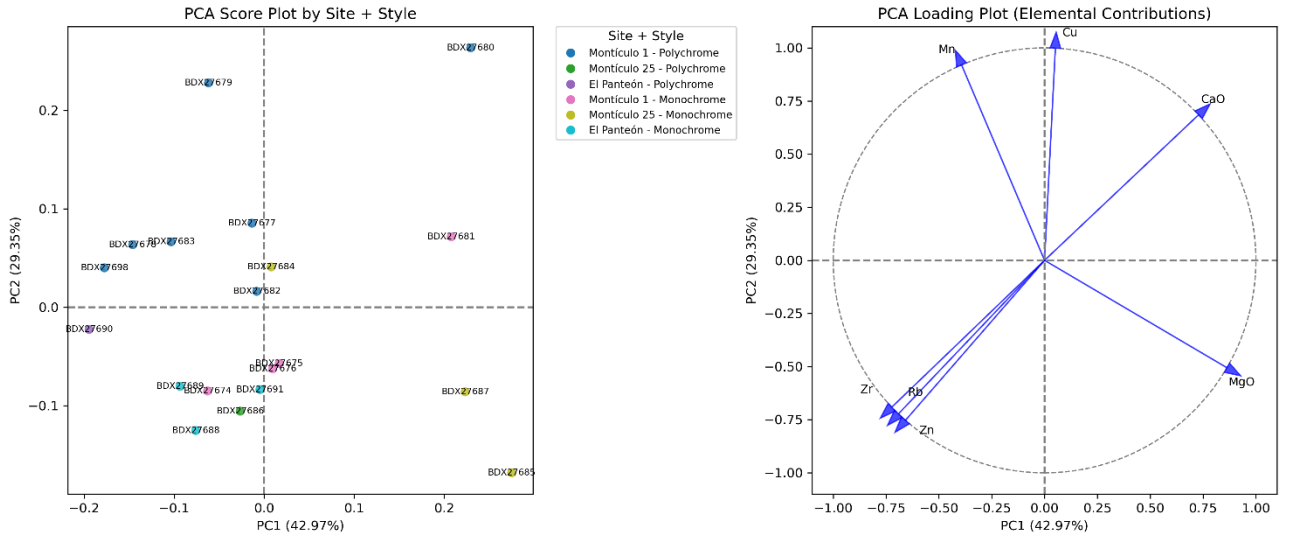

Figure 54. PCA score and loading plots based on Mn, Cu, CaO, MgO, Zn, Rb, and Zr, showing partial compositional separation between monochrome and polychrome ceramics.

The results show partial separation between the styles. There is a distinct cluster on the right of the PCA space (Group B), the monochrome samples that had already been found to be compositionally distinct. This group remains distinct in the reduced-variable PCA, with one other sample positioned a short distance away but still within the group.

The polychrome samples of Montículo 25 cluster together, reflecting internal compositional homogeneity. However, the two outliers from this group identified earlier (BDX27679 and BDX27680) continue to deviate outside of the main polychrome cluster, reinforcing their distinctiveness in elemental composition.

The remaining samples monochrome from El Panteón and Montículo 25 and polychrome Montículo 1 from different contexts—form an overlapping group, in which there is no differentiation by style and the samples are geochemically close, especially along PC1.

Overall, the PCA suggests that while some subgroups have compositional unity, the full dataset suggests some overlap among styles. This suggests that style alone cannot account for compositional variation, and that other processes—such as shared raw materials or cross-context production practices—were operating.

3.3.1.2 SEM-EDS

Following pXRF analysis, SEM-EDS was performed on the same samples to see if similar compositional patterns would be reproduced. PCA of major oxides (CaO, Na_2O, SiO_2, K_2O, Al_2O_3, MgO, Fe_2O_3, TiO_2) (Fig.55) shows that SEM-EDS cannot reproduce the partial groupings observed with pXRF. The SEM-based results show greater dispersion, with less clear separation by site or style.

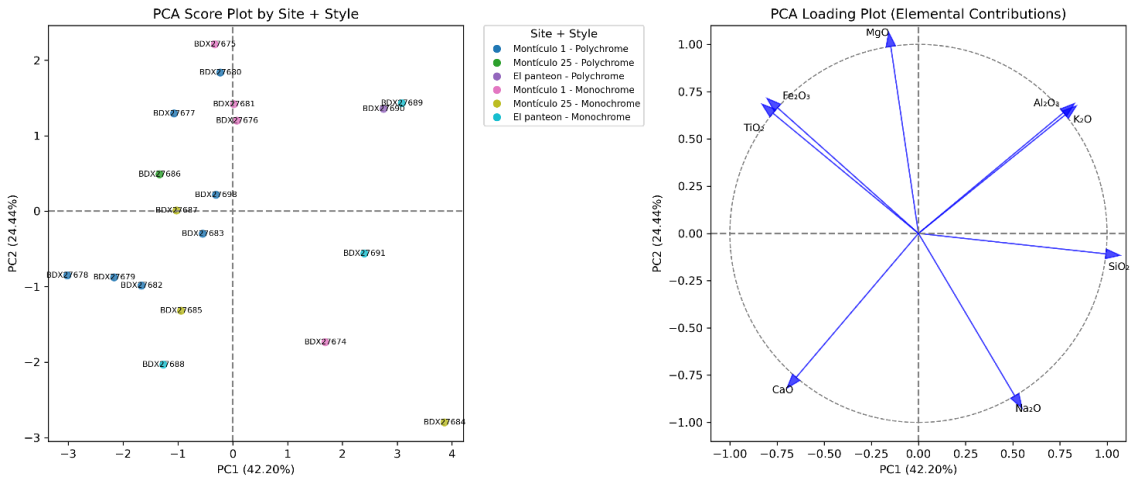

Figure 55. PCA based on SEM-EDS data (major oxides) shows no clear compositional grouping by site or style. The dispersion of samples reflects the homogeneous nature of the ceramic paste and the localized, trace-element-limited scope of SEM-EDS analysis.

This discrepancy likely stems from fundamental differences in analytical scope. pXRF is capable of identifying trace and major elements (e.g., Mn, Cu, Zn, Rb, Zr) *(Liritzis & Zacharias, 2011)*, its broader beam and deeper penetration can also incorporate contributions from surface slips, pigments, or weathered layers. SEM-EDS is limited in its sensitivity to trace elements and analyzes only a small, localized area usually a polished cross-section—means it is less likely to capture the heterogeneous inclusions*(Goldstein et al., 2018)*.

Table 4. SEM-EDS results for polychrome and monochrome ceramic pastes, measured on polished cross-sections. Values are expressed in weight percent (wt%) and represent the average of five representative analytical spots per sample.

Polychrome													
Site	Sample	Na_2O	MgO	Al_2O_3	SiO_2	P_2O_5	SO_3	Cl	K_2O	CaO	TiO_2	MnO	Fe_2O_3
Montículo 1	BDX27677	2.23	2.70	21.04	56.40	0.32	0.22	0.33	2.75	3.41	0.92	0.18	9.56
	BDX27678	2.36	2.84	19.34	54.60	0.35	1.73	0.51	2.57	4.92	0.86	0.15	9.83
	BDX27682	3.07	2.94	19.45	55.60	0.30	0.19	1.43	2.56	3.71	0.84	0.16	9.75
	BDX27683	2.63	2.90	19.54	56.50	0.28	0.31	1.27	2.86	3.80	0.81	0.18	8.87
	BDX27698	3.03	2.90	20.29	56.90	0.31	0.16	0.78	2.52	2.85	0.85	0.14	9.29
Montículo25	BDX27686	2.72	3.06	20.20	55.50	0.33	0.25	0.78	2.69	3.48	0.83	0.20	9.99
El Panteón	BDX27690	2.17	2.65	19.67	61.90	0.20	0.12	0.17	2.55	2.47	0.69	0.13	7.33
	Mean	**2.60**	**2.86**	**19.93**	**56.70**	**0.30**	**0.43**	**0.75**	**2.64**	**3.52**	**0.83**	**0.16**	**9.23**
	SD	0.37	0.14	0.61	2.38	0.05	0.58	0.47	0.13	0.78	0.07	0.02	0.92
Montículo 1	BDX27679	2.73	3.00	19.43	55.50	0.36	0.14	1.17	2.67	4.36	0.85	0.13	9.65
	BDX27680	2.20	2.94	21.34	56.70	0.34	0.15	0.33	2.65	3.19	0.82	0.21	9.13
	Mean	**2.47**	**2.97**	**20.39**	**56.10**	**0.35**	**0.15**	**0.75**	**2.66**	**3.78**	**0.84**	**0.17**	**9.39**
	SD	0.37	0.04	1.351	0.83	0.01	0.01	0.59	0.01	0.83	0.02	0.06	0.37
Monochrome													
Site		Na_2O	MgO	Al_2O_3	SiO_2	P_2O_5	SO_3	Cl	K_2O	CaO	TiO_2	MnO	Fe_2O_3
Montículo 1	BDX27674	3.10	2.65	19.64	60.30	0.30	0.15	0.25	2.36	3.06	0.72	0.11	7.44
El Panteón	BDX27689	2.40	2.81	21.08	59.70	0.26	0.14	0.23	2.65	2.50	0.68	0.09	7.44
	BDX27691	2.92	2.59	20.07	59.90	0.18	0.12	0.33	2.77	2.78	0.77	0.11	7.43
	Mean	**2.81**	**2.68**	**20.26**	**60.00**	**0.25**	**0.14**	**0.27**	**2.59**	**2.78**	**0.72**	**0.10**	**7.44**
	SD	0.36	0.11	0.73	0.26	0.06	0.02	0.05	0.21	0.28	0.05	0.01	0.01
Montículo 1	BDX27681	2.62	3.09	20.64	56.80	0.31	0.36	0.51	2.52	2.81	0.76	0.17	9.46
Montículo25	BDX27685	2.73	3.07	19.39	56.60	0.28	0.25	0.80	2.77	4.58	0.77	0.19	8.61
	BDX27687	2.73	3.14	20.51	56.20	0.30	0.19	0.85	2.47	3.63	0.82	0.14	8.99
	Mean	**2.69**	**3.10**	**20.18**	**56.50**	**0.30**	**0.27**	**0.72**	**2.59**	**3.67**	**0.78**	**0.17**	**9.02**
	SD	0.06	0.04	0.687	0.27	0.02	0.09	0.18	0.16	0.89	0.03	0.03	0.43
Montículo 1	BDX27675	2.61	2.97	20.36	56.70	0.26	0.38	0.48	2.91	2.56	0.94	0.15	9.66
	BDX27676	2.94	3.12	20.26	56.90	0.28	0.17	0.63	2.60	2.61	0.80	0.15	9.52
El Panteón	BDX27688	2.81	2.46	18.67	59.50	0.26	0.09	0.44	2.29	3.67	0.87	0.15	8.77
	Mean	**2.79**	**2.85**	**19.76**	**57.70**	**0.27**	**0.21**	**0.52**	**2.6**	**2.95**	**0.87**	**0.15**	**9.32**
	SD	0.17	0.35	0.948	1.56	0.01	0.15	0.10	0.31	0.63	0.07	0	0.48
Site		Na_2O	MgO	Al_2O_3	SiO_2	P_2O_5	SO_3	Cl	K_2O	CaO	TiO_2	MnO	Fe_2O_3
Montículo25	BDX27684	3.14	2.17	19.40	62.10	0.07	0.11	0.38	2.58	2.88	0.69	0.1	6.41

To further evaluate compositional homogeneity of the pastes, we constructed a statistical overview of the SEM-EDS information (Table 4), grouping samples based on the groupings suggested by the pXRF analysis. This allowed us to compare whether similar groupings are achieved irrespective of the methodological differences. The analyses indicate the pastes to be chemically homogeneous in terms of composition, with the consistently high levels of Fe_2O_3 (typically 7.4 wt% to 9.7 wt%) and low CaO (typically below 4.5 wt%), which testifies the use of non-calcareous, iron-rich clays. Additionally, the low relative standard deviations for major oxides such as SiO_2, Al_2O_3, and K_2O also confirm a highly uniform chemical composition for the assemblage.

3.3.2 Pigment and Decoration Analysis

After analyzing the ceramic paste with pXRF and SEM-EDS, we used these techniques again—along with Raman spectroscopy, and FTIR—to study the decorative surfaces.

3.3.2.1 SEM-EDS

We applied the SEM-EDS to the colored areas of the ceramics to investigate their elemental composition. As seen earlier in elemental mapping, the decorative layers show high amount carbon content.

To determine whether this carbon could originate from calcium carbonate (e.g., calcite), we compared the weight percentages of carbon in the decorative layers with both the ceramic paste and a reference calcite sample (BDX1712) from Spain. The theoretical carbon content of pure calcite is 11.99 wt%, but the SEM-EDS measurement of the calcite reference showed~26%, suggesting a systematic overestimation of carbon to the method.

However, SEM-EDS shows that the carbon content in the decorative layers is ranging from approximately 70% to over 90$, which is far above what could be attributed to carbonate minerals, even accounting for such instrumental bias. These results could probably support the presence of an organic in the decorative layer due to elevated amounts of carbon.

In contrast, a monochrome sample (BDX27688, orange) shows a moderately elevated carbon level (~53%), suggesting a different composition or degree of organic application. A representative comparison is presented in Table 5.

Table 5. Representative SEM-EDS values (wt%) of carbon and other elements in decorative layers, ceramic paste, and the calcite reference sample (BDX1712). ND = Not detected

Sample	C	Na_2O	MgO	Al_2O_3	SiO_2	P_2O_5	SO_3	Cl	K_2O	CaO	TiO_2	MnO	Fe_2O_3	As	Ba
BDX1712(Calcite)	**27.00**	0.17	ND	0.05	0.07	ND	ND	ND	0.05	71.80	ND	0.56	0.29	ND	ND
BDX27681(yellow)	**77.20**	0.60	0.18	3.04	11.80	ND	1.07	0.15	1.55	0.74	0.05	ND	0.61	3.02	0.03
BDX27677(red)	**72.90**	0.37	0.30	1.70	6.41	0.02	0.25	0.18	0.40	1.59	0.12	0.08	15.20	ND	0.47
BDX27677(black)	**88.90**	0.78	0.27	1.44	4.59	0.10	0.07	0.19	0.57	1.60	0.08	0.01	1.34	ND	0.02
BX27688 (orange)	**53.20**	2.01	0.92	9.66	24.00	0.11	0.07	0.35	2.80	1.57	0.25	0.14	4.95	ND	0.02
BDX27676 (gray)	**87.00**	0.53	0.48	2.37	5.72	0.03	0.05	0.71	0.51	0.77	0.12	0.04	1.72	ND	ND
BDX27681 (paste)	**26.50**	2.22	2.28	14.00	37.00	0.21	0.22	0.78	3.15	3.02	0.67	0.19	9.75	ND	0.03

For clarity, polychrome and monochrome decorations are discussed separately. The following sections examine each decorative color group in detail, beginning with the polychrome examples.

- ✓ **Polychrome ceramics**

The polychrome ceramics have five distinct colorations—red, black, yellow, cream, and beige. One exception is an orange decoration observed in sample BDX27678, which is discussed in Table 10 alongside the monochrome decorations.

3.3.2.1.1 Red decorations

Red decorations group (Table 6) relies on iron-based pigmentation exhibiting a broad range from 6.56% (BDX27686) up to 42.53% (BDX27677) with a mean of 29.9%. This is a clear indication that iron oxides were used intentionally, but with differing levels of pigment concentration.

Montículo 1 and El Panteón samples have higher iron content, supporting the hypothesis of rich, iron-charged applications, likely derived from hematite-rich material. Conversely, BDX27686 of Montículo 25 shows considerably lower iron content. SEM-EDS analysis of this sample also confirms that the pigment layer is not thinner, also macroscopic analysis reveals a visibly lighter red tone, which is indicative of the use of a more diluted pigment mixture or a less iron-content raw material.

SiO_2 content range 35.74% to 51.35% (mean:43%) and Al_2O_3 between 8.05% to 16.43%(mean:11%) within the decorative surface. Red decorations contain generally low concentrations of Mn (<0.25%) and no quantities of arsenic, with the only exception being BDX27682 with 3.39% As, potentially due to a unique pigment or accidental contamination by using the same painting brush for yellow and red.

Table 6. Results of SEM-EDS analysis of red and orange decorations. ND = Not detected.

	Red decoration														
Site	Sample	Na_2O	MgO	Al_2O_3	SiO_2	P_2O_5	SO_3	Cl	K_2O	CaO	TiO_2	MnO	Fe_2O_3	As	Ba
Montículo 1	BDX27677	1.72	1.41	9.69	35.74	0.00	1.68	0.53	1.26	3.85	0.43	0.18	42.53	ND	0.99
	BDX27679	1.48	1.61	12.18	47.41	0.33	1.68	0.31	1.79	3.79	0.50	2.12	25.71	ND	1.10
	BDX27680	1.05	1.26	8.05	41.30	ND	1.32	0.27	0.82	2.93	0.41	0.20	41.48	ND	0.93
	BDX27682	1.49	2.24	11.76	50.15	0.24	3.33	0.54	1.64	6.47	0.47	0.18	18.03	3.39	0.09
	BDX27683	1.40	1.96	9.42	40.70	ND	1.68	0.64	0.99	7.15	0.50	0.19	34.43	ND	0.95
Montículo 25	BDX27686	3.37	3.16	16.43	51.35	0.77	0.99	1.52	3.23	11.40	0.77	0.11	6.56	ND	0.35
El Panteón	BDX27690	1.64	2.47	10.51	36.23	0.22	1.07	0.39	1.61	3.24	0.53	0.20	41.02	ND	0.88
	Mean	1.73	2.02	11.15	43.27	0.26	1.68	0.60	1.62	5.55	0.51	0.45	29.96	3.39	0.76
	SD	0.75	0.67	2.72	6.41	0.28	0.79	0.43	0.80	3.05	0.12	0.74	13.79	n/a	0.38
Brown decoration															
Montículo 1	BDX27680	5.83	2.66	14.13	42.90	0.78	1.11	0.56	2.13	6.14	0.51	0.15	22.64	ND	0.47
El Panteón	BDX27690	4.55	3.44	18.67	51.25	0.37	1.75	0.95	3.77	6.44	0.73	0.33	7.71	ND	0.05
	Mean	2.98	2.40	12.27	38.57	0.45	1.23	0.74	2.19	5.97	0.53	0.33	20.28	3.39	0.48
	SD	1.95	0.99	5.61	16.76	0.26	0.39	0.43	1.11	3.03	0.23	0.24	13.55	n/a	0.30

Brown decorations are also derived from iron oxide rich materials the same as red color. In BDX27690, the amount of Fe_2O_3 is less as the layer was thinner to study on the cross section as result it was analyzed on the surface maybe it explains why it shows less Fe_2O_3.

3.3.2.1.2 Black decorations

As Table 7 shows, the black group is variable in elemental compositions. For example, Fe_2O_3 concentrations ranges from 6.11% to 19.24% (mean: 9%), which may reflect diverse strategies in pigment application or in firing techniques. In this group sample BDX 27679 is the most different sample due to its high concentration of manganese Mn (32.47%), which is far above background levels. This high amount of manganese oxide strongly suggests that they were intentionally used as a chromophore to achieve a deep black tone (Arriaza et al., 2025). The presence of Mn oxide in BDX 27679 as a technological outlier implies a locally distinct recipe or raw material source. BDX27698 and BDX27678 did not display a visible decorative layer in SEM or SEM-EDS on the polished cross-section, likely due to the extreme thinness of the application. For this reason, the analysis was conducted on the surface instead. The remaining black samples shows very low Mn concentrations (~0.25% or less), indicating that iron oxides were the dominant pigment in the majority of cases.

They also show considerable compositional heterogeneity with SiO_2 ranging from 36.25% to 56.35%, and Al_2O_3 from 12.40% to 19.15% can suggest the use of different clay materials or preparation standards throughout the assemblage. Arsenic (As) were also detected in two samples, BDX 27679 and BDX 27680. It may be a sign of mineralogical inclusions in the raw material or

cross-contamination through other pigment activities, but no clear correlation with intentional use exists.

Table 7. Results of SEM-EDS analysis of black and gray decorations. ND = Not detected.

Black decorations															
Site	Sample ID	Na_2O	MgO	Al_2O_3	SiO_2	P_2O_5	SO_3	Cl	K_2O	CaO	TiO_2	MnO	Fe_2O_3	As	Ba
Montículo 1	BDX27677	6.04	2.58	14.41	50.99	1.43	0.97	0.97	3.20	10.36	0.57	0.13	8.19	ND	0.15
	BDX27678	3.66	2.62	14.97	43.23	1.12	1.83	0.88	2.49	8.88	0.63	0.25	19.24	ND	0.21
	BDX27679	2.16	2.31	12.40	36.26	0.32	0.97	0.62	1.69	2.93	0.33	32.47	6.11	0.95	0.48
	BDX27680	5.66	2.83	16.64	53.51	0.73	1.07	1.09	2.63	7.40	0.65	ND	7.80	ND	ND
	BDX27682	3.39	3.03	16.01	53.16	1.16	1.80	1.64	2.56	9.47	0.66	0.11	7.01	ND	ND
	BDX27683	6.10	3.06	14.03	47.56	0.80	2.41	2.36	2.35	10.44	1.63	0.23	8.33	0.71	ND
	BDX27698	3.27	2.67	16.58	46.63	0.43	9.57	0.65	2.62	9.73	0.59	0.16	7.11	ND	ND
Montículo 25	BDX27686	2.55	3.34	16.94	56.35	0.43	0.93	1.58	2.21	6.80	1.01	0.12	7.74	ND	ND
El Panteón	BDX27690	2.39	3.64	19.15	53.90	0.59	0.89	0.46	3.30	4.11	1.00	0.17	10.32	ND	0.09
	Mean	**3.91**	**2.90**	**15.68**	**49.06**	**0.78**	**2.27**	**1.14**	**2.56**	**7.79**	**0.78**	**4.20**	**9.09**	**0.83**	**0.23**
	SD	1.60	0.41	1.97	6.35	0.38	2.79	0.61	0.49	2.73	0.38	11.42	3.98	0.17	0.17

3.3.2.1.3 Yellow decoration

Across six analyzed samples from Montículo 1 and El Panteón (Table 8), the yellow decorations display a consistently arsenic- and sulfur-rich composition that sets them apart from the iron-based systems used for red, orange, black, and gray surfaces. Arsenic (As) concentrations are between 2.37% to 26.67%, and sulfur (S) from 5.33% to 19.67%. This suggests the use of arsenic sulfide pigments, like orpiment (As_2S_3) or pararealgar (As_4S_4) (Vermeulen et al., 2015; De Keyser et al., 2024). Previous studies on Paracas ceramics, based on micro-Raman analysis, found pararealgar as the main arsenic sulfide pigment for yellow decorations (Kriss & DeLeonardis, 2018) that can support the possibility of its use in this assemblage.

Table 8. Results of SEM-EDS analysis of yellow decorations. ND = Not detected.

Yellow decoration															
Site	Sample ID	Na_2O	MgO	Al_2O_3	SiO_2	P_2O_5	SO_3	Cl	K_2O	CaO	TiO_2	MnO	Fe_2O_3	As	Ba
Montículo 1	BDX27677	1.75	0.67	11.54	56.49	ND	10.25	0.16	2.72	1.71	0.25	0.05	2.28	12.06	0.08
	BDX27680	1.71	0.55	11.47	51.28	ND	10.31	0.17	2.42	1.76	0.16	ND	1.63	11.16	ND
	BDX27681	1.99	0.68	13.71	59.86	ND	6.24	0.39	3.78	2.15	0.18	0.03	1.72	9.28	ND
	BDX27683	1.13	1.37	11.21	36.66	0.23	17.22	0.80	1.73	3.55	0.28	0.06	3.61	22.16	ND
	BDX27698	1.91	0.62	12.63	61.62	ND	6.21	0.32	3.72	2.71	0.17	0.04	1.59	8.47	ND
El Panteón	BDX27690	3.05	1.55	17.88	55.14	0.42	5.33	0.39	3.73	5.49	0.58	0.10	3.97	2.37	0.08
	Mean	**2.48**	**1.08**	**15.25**	**58.38**	**0.42**	**5.77**	**0.35**	**3.72**	**4.10**	**0.37**	**0.07**	**2.78**	**5.42**	**0.08**
	SD	0.806	0.654	3.711	4.577	n/a	0.619	0.055	0.008	1.964	0.286	0.04	1.684	4.315	n/a

Iron oxide levels remain consistently low across the group (typically below 5%), confirming that iron oxides were not the primary chromophores and manganese (Mn) is either extremely low or not detected.

The base composition of the decoration layers is silico-aluminous, with SiO_2 ranging from 31.94% to 61.79% and Al_2O_3 from 9.90% to 17.88%, indicating a variety of clay preparations.

Despite some minor variation in the arsenic and sulfur content, the widespread As–S-rich and Fe-poor signature across all samples suggests a systematic pigmenting approach using mineral-sourced coloring agents. The compositional uniformity across different mounds suggests a consistent technological tradition in the preparation and application of yellow pigments within the Paracas ceramic repertoire.

3.3.2.1.4 Cream and beige color

The cream-colored surfaces (Table 9), which are represented by samples BDX27679, BDX27682, BDX27683, and BDX27686, exhibit uniformly high silica levels between 49.99% and 66.45% (mean:59.60%) and alumina content between 6.72% and 11.95% (10%), indicating the use of a fine silico-aluminous clay.

Table 9. Results of SEM-EDS analysis of yellow decorations. ND = Not detected.

Cream decoration															
Site	Sample ID	Na_2O	MgO	Al_2O_3	SiO_2	P_2O_5	SO_3	Cl	K_2O	CaO	TiO_2	MnO	Fe_2O_3	As	Ba
Montículo 1	BDX27679	2.805	1.2	11.95	60.2	0	5.053	0.238	2.848	4.36	0.285	0.113	3.178	7.738	0.04
	BDX27682	2.00	0.77	10.89	61.79	ND	8.68	0.54	1.35	2.25	0.21	ND	1.84	9.64	ND
	BDX27683	1.215	0.918	6.718	66.45	0.145	10.05	0.75	1.193	3.27	0.915	ND	2.288	6.09	ND
Montículo 25	BDX27686	2.09	0.79	10.51	49.99	0.23	9.52	0.77	2.16	4.01	0.24	ND	4.84	14.86	ND
	Mean	**2.03**	**0.92**	**10.02**	**59.61**	**0.12**	**8.33**	**0.57**	**1.89**	**3.47**	**0.41**	**0.11**	**3.04**	**9.58**	**0.04**
	SD	0.65	0.20	2.28	6.94	0.12	2.25	0.25	0.77	0.93	0.34	n/a	1.32	3.81	n/a
Biege decoration															
Site	Sample ID	Na_2O	MgO	Al_2O_3	SiO_2	P_2O_5	SO_3	Cl	K_2O	CaO	TiO_2	MnO	Fe_2O_3	As	Ba
Montículo 1	BDX27683	8.448	1.988	11.1	40.21	0.728	6.294	2.13	5.154	9.632	0.614	ND	8.714	4.982	ND

All four samples have elevated levels of arsenic (6.09% to 14.86%) (mean:9.5%) and sulfur (5.05% to 10.05%) with the mean of 8.3%, those of which are extremely characteristic of the use of arsenic-sulfide pigments, such as orpiment or pararealgar, to produce the yellowish-cream coloration observed on the surface. Iron oxide content is relatively low, between 1.84% to 3.18%, indicating these were not the dominant chromophores within this group.

The beige decoration, analyzed on BDX27683 sample (monticulo1), presents slightly different chemical profiles. Silica is significantly lower at 40.21% and calcium significantly higher at 9.63%, the highest for this dataset. Iron oxide is also high at 8.71%, higher than for the cream category. Arsenic and sulfur remain at 4.98% and 6.29%, respectively, suggesting that arsenic-sulfide pigments continued in use, but possibly their optical effect had been changed by the presence of higher iron and calcium. Alumina remains at 11.10%, like the cream surfaces, and sodium and potassium are high too, particularly sodium at 8.45%. These differences imply the use of a different preparation technique on the beige surface, perhaps with a calcium-rich additive or clay that altered the pigment's color.

Overall, the evidence implies that beige as well as cream decorations were produced with arsenic- and sulfur-based pigments. In the cream samples, the combination of high silica and low iron resulted in a light, light-colored surface, while the beige zone would seem to have resulted from the reaction of arsenic-sulfide pigments with a more iron- and calcium-rich matrix, resulting in a warmer, darker color. All these points towards a shared pigmenting technique that was varied using different base materials or preparation techniques to create nuanced variations in color on the surface.

- ✓ **Monochrome ceramics**

Monochrome ceramic samples display only orange and gray decorations, with the exception of BDX27681, which features a yellow decoration (discussed in Table 8 with polychrome yellow decorations). In some cases, the monochrome decorations did not exhibit a distinct layer separable from the ceramic paste (BDX27684, BDX27688, BDX27689 orange, and BDX27674, BDX27676 gray). As a result, they were analyzed directly on the surface rather than on polished cross-sections.

3.3.2.1.5 Orange decoration

In contrast to the red decorations in the polychrome group, orange ones exhibit lower Fe_2O_3 concentrations ranging from 7.39% to 13.60% (mean:12%) (table. 10). This points towards the intentional usage of iron-based pigments with a smaller concentration like slip clay sediments, likely responsible for the lighter orange hue(Maggetti, 2001; Tite, 2008).

The SiO_2 ranges from 51.72% to 59.54% (mean:54.6%), while Al_2O_3 ranges from 16.31% to 21.80% (17.7%) higher than the red samples, revealing the use of a more alumino-silica. Overall, the mixture of the diluted pigment appears to be responsible for the normal orange tonality.

Table 10. Results of SEM-EDS analysis of orange decorations. ND = Not detected.

Orange decoration															
Site	Sample ID	Na_2O	MgO	Al_2O_3	SiO_2	P_2O_5	SO_3	Cl	K_2O	CaO	TiO_2	MnO	Fe_2O_3	As	Ba
	BDX27675	3.70	1.75	17.70	56.86	0.87	0.38	0.77	2.27	3.78	0.82	0.14	10.97	ND	ND
Montículo 1	BDX27678	3.96	2.54	14.14	44.27	0	0.51	0.71	2.09	4.38	0.48	0.25	26.39	ND	0.29
Montículo 25	BDX27684	3.85	2.44	16.31	54.92	0.59	0.71	0.73	2.58	3.37	0.71	0.22	13.60	ND	ND
	BDX27687	3.05	3.07	19.37	56.99	ND	0.57	2.46	2.33	4.05	0.61	0.13	7.39	ND	ND
El Panteón	BDX27688	3.33	2.01	21.80	58.05	0.30	0.21	0.38	3.39	2.38	0.49	0.18	7.44	ND	ND
	BDX27689	4.55	3.08	17.68	51.72	0.74	0.94	0.66	3.01	5.33	0.74	0.16	11.40	ND	ND
	BDX27691	3.28	2.37	17.37	59.54	0.68	0.48	0.43	3.13	4.40	0.83	0.08	7.42	ND	ND
	Mean	**3.67**	**2.47**	**17.77**	**54.62**	**0.53**	**0.54**	**0.87**	**2.68**	**3.95**	**0.67**	**0.16**	**12.09**	**n/a**	**0.29**
	SD	0.51	0.50	2.39	5.20	0.32	0.23	0.72	0.49	0.92	0.15	0.06	6.76	n/a	n/a

3.3.2.1.6 Gray decoration

The gray samples (BDX 27674 and BDX 27676) contain a more chemically uniform composition. Their Fe_2O_3 is characteristically distributed between 7.65% and 8.65%,. Low manganese contents (0.18–0.26%) confirm that Mn had not been a significant contributor to the gray hues. Instead, the color was likely due to surface treatment (polishing or smoothing) or caused by atmosphere control firing, i.e., partially oxidizing or partially reducing the atmosphere as described here (3.1.1.3 Decorative Layers) and you can refer to (Fig.29).

SiO_2 contents are between 53.66% and 54.75% and Al_2O_3 between 18.79% and 19.23%, pointing to a well-selected or refined silico-aluminous clay.

Table 11. Results of SEM-EDS analysis of gray decorations. ND = Not detected.

Gray decoration															
Site	Sample ID	Na_2O	MgO	Al_2O_3	SiO_2	P_2O_5	SO_3	Cl	K_2O	CaO	TiO_2	MnO	Fe_2O_3	As	Ba
Montículo 1	BDX27674	4.76	3.16	19.23	54.75	0.39	1.54	0.49	3.44	3.64	0.79	0.18	7.65	ND	ND
Montículo 1	BDX27676	4.88	3.20	18.79	53.66	0.50	1.05	2.49	2.53	3.29	0.72	0.26	8.65	ND	ND
	Mean	**4.82**	**3.18**	**19.01**	**54.20**	**0.45**	**1.30**	**1.49**	**2.98**	**3.46**	**0.75**	**0.22**	**8.15**	**n/a**	**n/a**
	SD	0.082	0.022	0.308	0.771	0.081	0.342	1.414	0.64	0.247	0.049	0.057	0.707	n/a	n/a

To compare more accurately the elemental concentration distribution between decorative groups, boxplots of the SEM-EDS data were generated (Fig. 56).

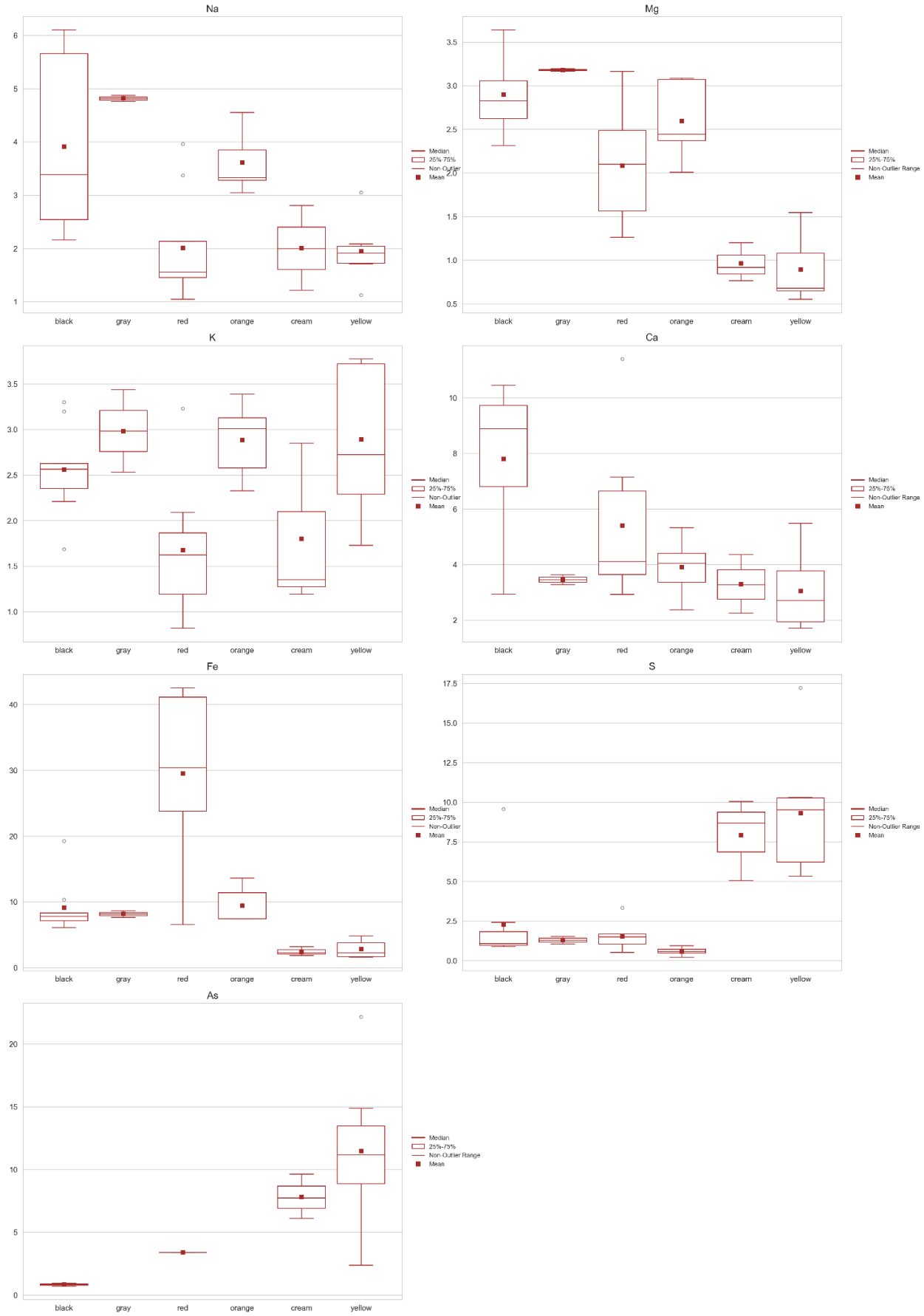

Figure 56. Boxplots of elemental concentrations (Na, Mg, K, Ca, Fe, S, As) by decorative group based on SEM-EDS data.

These indicate trends, outliers, and overlaps between color groups and clearly signal how specific elements correlate with different decorative treatments. By comparing the mean, range, and median values of the elements Na, Mg, K, Ca, Fe, Si, and As, it becomes possible to infer variations in pigment composition, clay selection, and production techniques.

Red decorations are marked by very high enrichment in iron (Fe), much higher than for all other groups. Orange decorations have intermediate values for most elements. for example, K, Fe, and Ca, show intermediate values, indicating possible dilution or mixture of red pigmentation. None of the elements stand out as clearly representative of orange.

Yellow and cream pigments are distinguished by their increased levels of potassium (K), sulfur (S), and arsenic (As). These reflect varying recipes of pigments or use of potassium- and sulfur-containing clays or minerals. Yellow, in particular, shows drastic variations in K and As. Calcium (Ca) is very variable for all groups, but black and red have the largest ranges. This may be the result of lime-based slips or calcareous inclusions in some color treatments, but no group is defined by Ca alone.

Briefly, the elemental signatures mark various decoration technologies: Fe indicates red; and K, S, and As mark cream and yellow decorations. They all argue in favor of the fact that each set of decorations was produced based on different material traditions and recipes for pigments.

3.3.2.2 pXRF

To assess the potential of pXRF for the non-destructive analysis of decorated ceramics, we conducted measurements directly on the surface of the decorative layers. This approach is particularly relevant in heritage and museum contexts, where sampling is not permitted. However, it is important to note that pXRF measurements inherently capture contributions from both the surface decoration and the underlying ceramic paste, which can complicate the interpretation of elemental data specific to the applied pigments permitted (Shackley, 2011; Liritzis & Zacharias, 2011; Tykot, 2016).

We aimed to determine whether pXRF could provide reliable quantitative results or whether it should be limited to qualitative or semi-quantitative interpretation. To evaluate this, we compared pXRF results with those obtained using SEM-EDS analysis on cross-sections of the same samples. SEM was used as a reference method due to its ability to target specific layers with higher spatial resolution and more controlled conditions.

For each sample, we calculated the relative deviation (%) between pXRF and SEM values for several major and minor elements: Al, Si, K, Ca, Ti, Fe, Mn, As, and S. This allowed us to quantify

the level of agreement between the two methods across different types of decorations (e.g., red, yellow, black).

Line graphs were generated based on these relative deviation values, allowing a visual comparison of the consistency between pXRF and SEM measurements across individual samples and elements.

For red decorations (Fig. 57), relative deviation values exhibit significant differences between SEM-EDS and pXRF. Silicon (Si) and aluminum (Al) exhibit moderate deviations on most samples, which normally occur within the range of 30% to 60%. Demonstrating a commendable, if not perfect, agreement between both methods.

Potassium (K) and calcium (Ca) vary more, relative deviations between about 40% to 90%. These two may be susceptible to post-depositional alteration or surface enrichment and therefore may have different detection efficiencies based on whether surface (pXRF) or cross-sectional (SEM-EDS) measurements are used.

Titanium (Ti) and iron (Fe) show the highest discrepancies between the two methods. For example, in (BDX27686), 4.1% Ti was detected by pXRF, whereas 0.77% was measured by SEM-EDS. Similarly, Fe was ~42% by pXRF and only ~6.56% by SEM. Such contrasts represent relative deviations greater than 400%.

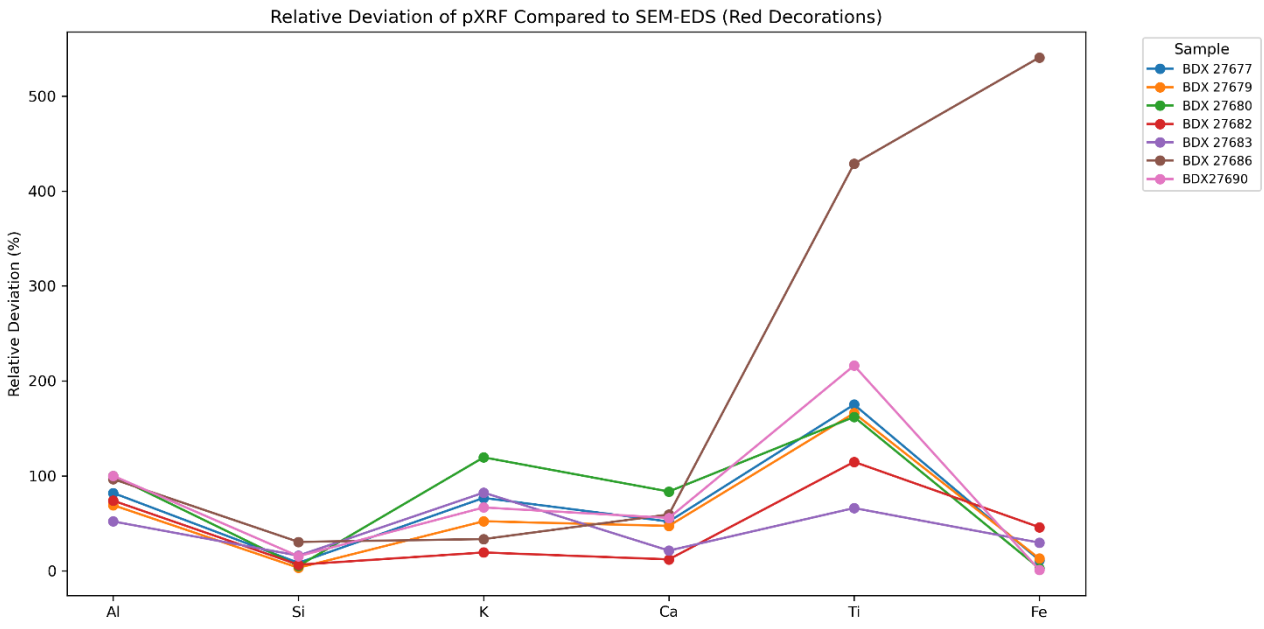

Figure 57. Relative deviations of values obtained by p-XRF compared to SEM-EDS for red decorations.

For black decorations (Fig. 58), relative discrepancies between SEM-EDS and pXRF measurements show element-dependent tendencies. Silicon (Si) exhibits the most consistent

concordance across samples with variations typically below 25% suggesting uniform matrix distribution and minimal surface enrichment.

\

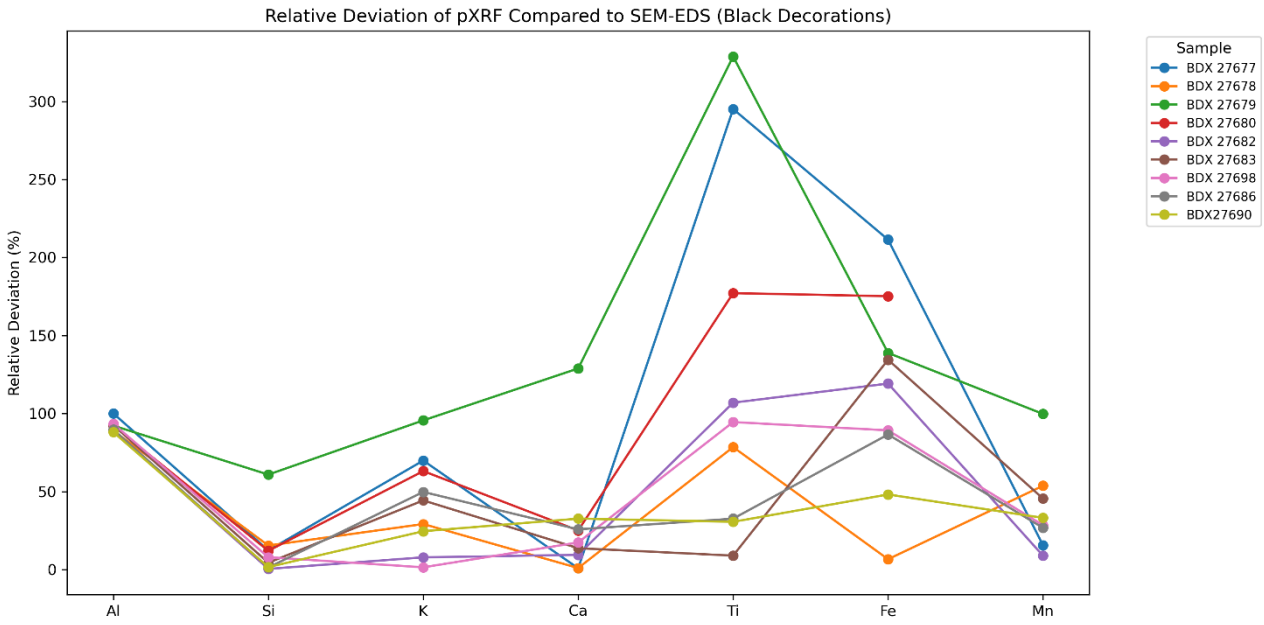

Figure 58. Relative deviations of values obtained by p-XRF compared to SEM-EDS for black decorations.

Aluminum (Al) is characterized by huge deviations (up to 100%), which may be caused by variation in detection efficiency for light elements and acceptance of surface and bulk signals by pXRF. Potassium (K) and calcium (Ca) show moderate to high deviations, ranging between 20% and 100%, and could reflect composition heterogeneity or post-depositional diagenesis.

The highest deviations are exhibited again for titanium (Ti) and iron (Fe) as red decorations with Ti deviations over 300% and Fe around 210% in some samples. Manganese (Mn) shows deviations between (20–60%).

Overall, these results show that pXRF is very sensitive to the elements present in the decorative layers of the surface. Because it could collect signals from both the decoration and some of the underlying ceramic due to its penetration depth, it often gives higher values for elements that are concentrated at the surface(Shackley, 2011; Tykot, 2016). In contrast, SEM-EDS analyzes cross-sections and provides more precise information about each layer, but it can miss or underestimate the surface pigments unless they are specifically targeted during analysis(Tite, 2008; Liritzis & Zacharias, 2011).

To further explore the interpretive potential of pXRF compared to SEM-EDS, we also examined whether monochrome outer decorative layer—particularly those exhibiting orange coloration—might be compositionally distinguished from the underlying paste. Although most of

these samples didn't show a distinct layer on SEM-EDS compared to the polychrome decorations, their comparative composition between the paste and outer decoration layer (Fig. 59) reveals considerable differences.

The decoration layer is richer in MgO, Fe_2O_3, K_2O, and CaO and poorer in Al_2O_3. These trends confirm that a second clay, likely iron- and magnesium-enriched, was used to produce the orange hue. High Fe_2O_3 supports the presence of iron-based pigments, and the high MgO may infer the utilization of magnesian clays or temper. The paste is more alumina-rich and reflects a different clay. The overall conclusion is that monochrome ceramics surface treatment involved a controlled material selection to create the desirable orange coloration and not merely a result of firing effects.

The complete chemical composition obtained by pXRF on the decorative layers is presented in Appendix Table 3.

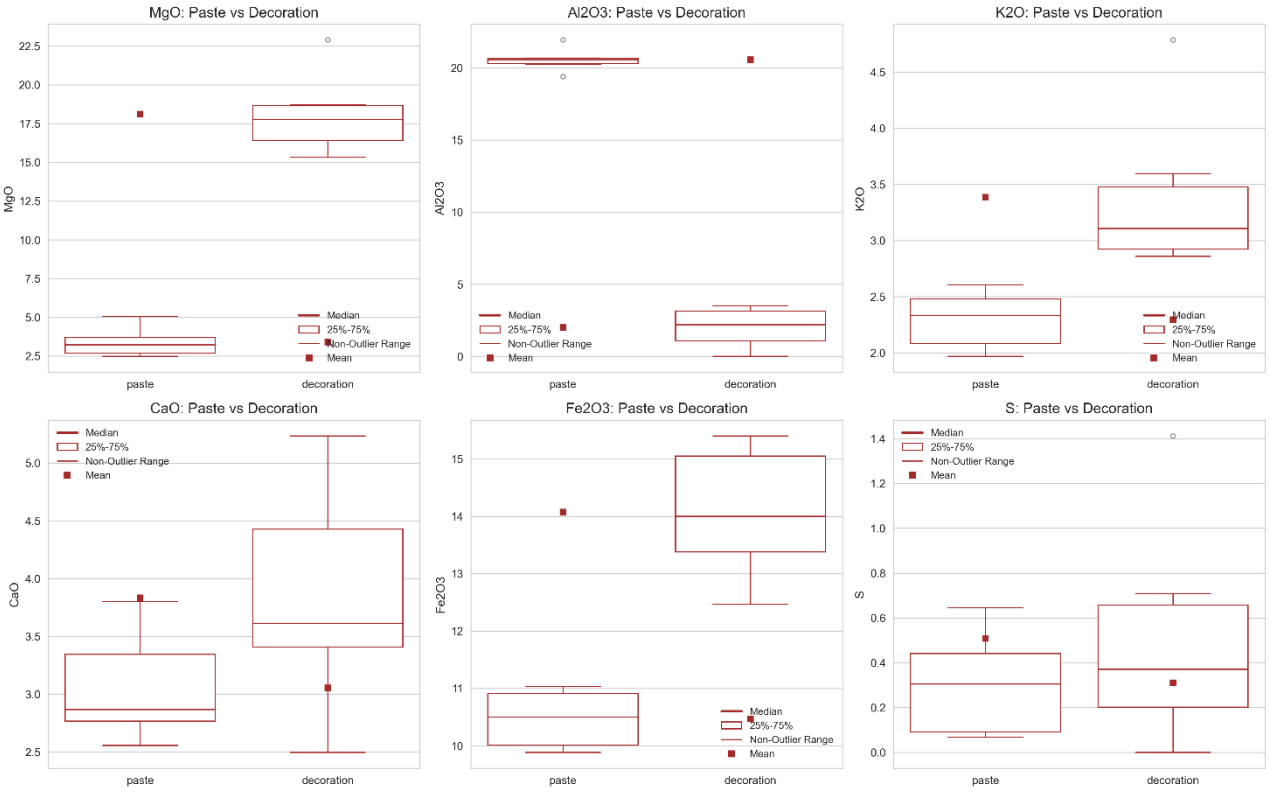

Figure 59. Boxplots showing elemental differences between paste and monochrome orange decoration. The decoration is enriched in MgO, Fe_2O_3, K_2O, and CaO, and depleted in Al_2O_3.

3.3.3 Raman Spectroscopy

Raman spectroscopy was carried out on various decorated surfaces to identify the molecular structure of the pigments(Bell et al., 1997; Smith & Clark, 2004; Vandenabeele et al., 2007). Preliminary analysis with handheld instruments using 785 nm and 532 nm laser

excitations did not yield interpretable data. Despite attempting a number of acquisition parameters to inhibit fluorescence and enhance signal detection, spectra acquired, such as the one in (Fig.60), were feeble in intensity and lacked features and did not present any signature Raman shifts.

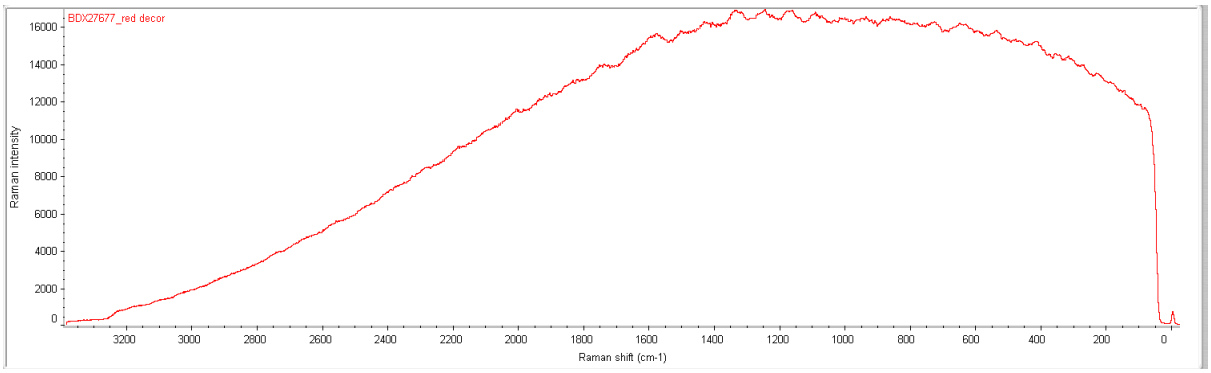

Figure 60. Raman spectrum collected from a red-decorated area, using a 785 nm laser (3 × 3 seconds at 50% power). The spectrum displays no distinct Raman peaks; the broad elevation is likely due to background fluorescence or instrument (BDX27677, Montículo 1).

Similarly, the benchtop system using the 532 nm laser also failed to produce conclusive spectrum. As is evident in (Fig.61), again, fluorescence dominated the spectral output and lacked diagnostically useful features. Such limitations are likely to be introduced through surface degradation, low pigment concentration, or matrix fluorescence, all of which complicate the detection of Raman-active constituents.

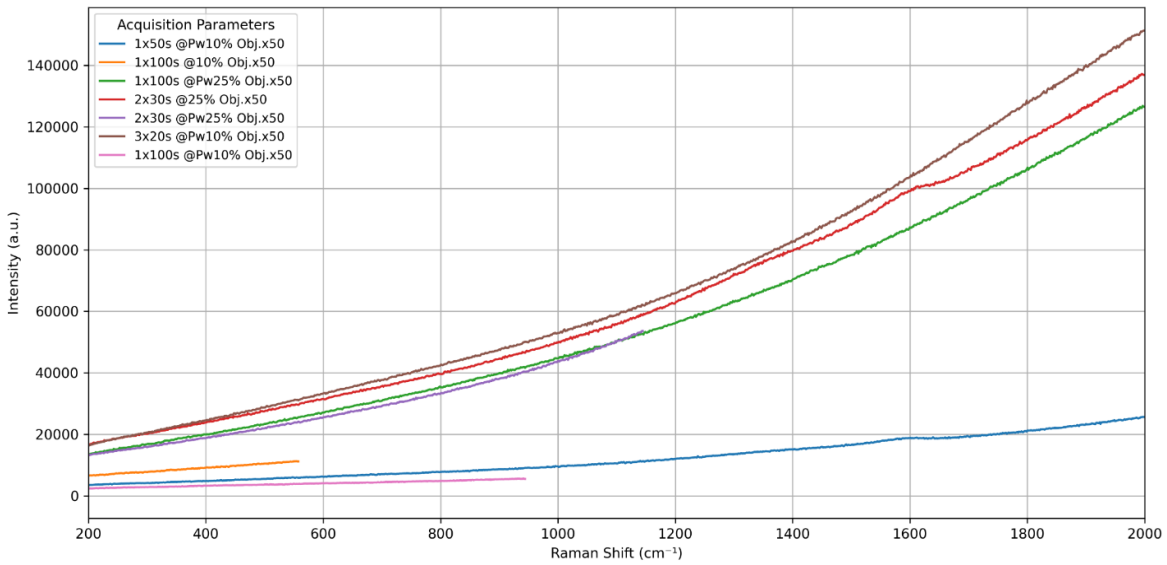

Figure 61. Raman spectra of brown-decorated area acquired using a 532 nm laser under various acquisition parameters. Despite differences in laser power and exposure time, none of the spectra exhibit distinct Raman bands, indicating a strong fluorescence (BDX27680, Montículo.1).

On the other hand, 785 nm excitation on the benchtop system produced significantly good results. Several of the decorated areas gave clear Raman spectra with interpretable shifts, enabling pigment characterization. The system's improved performance is a result of deeper penetration, reduced fluorescence, and improved signal-to-noise ratio.

The brown and red regions produced spectra with sharp, well-defined, and readily distinguishable peaks (Fig. 62a) characteristic of hematite (α-Fe_2O_3) as shown by the spectral overlay (Fig. 62b), suggesting the use of iron oxide pigments.

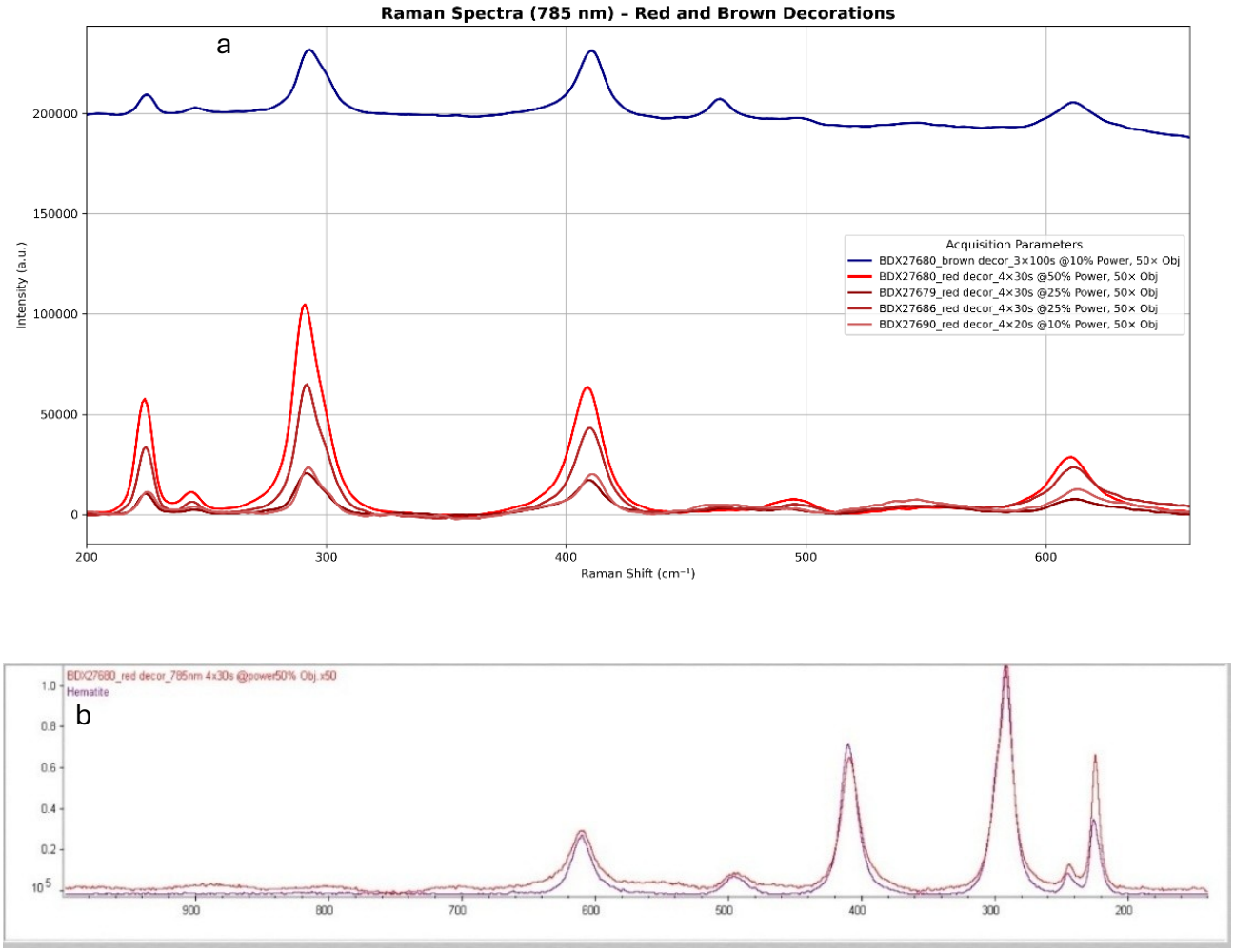

Figure 62. (a) Raman spectra of the brown and red decorative areas from (BDX27679, BDX27680, BDX27686 and BDX27690) (785 nm excitation), (b) Overlay of the red decorative area spectrum with a reference hematite spectrum from the Omnic RRUFF library, showing a strong spectral correlation that supports the identification of hematite as the red pigment (BDX27680, Montículo.1).

The peaks resulted by focusing laser directly on a small mineral grain embedded in the pigment layers (Fig. 63), features hypothesized to be the color-producing agent. This interpretation is also supported by SEM-EDS and pXRF analysis, which identified high levels

of iron (Fe) in the samples, setting up evidence for the occurrence of hematite as a likely coloring material.

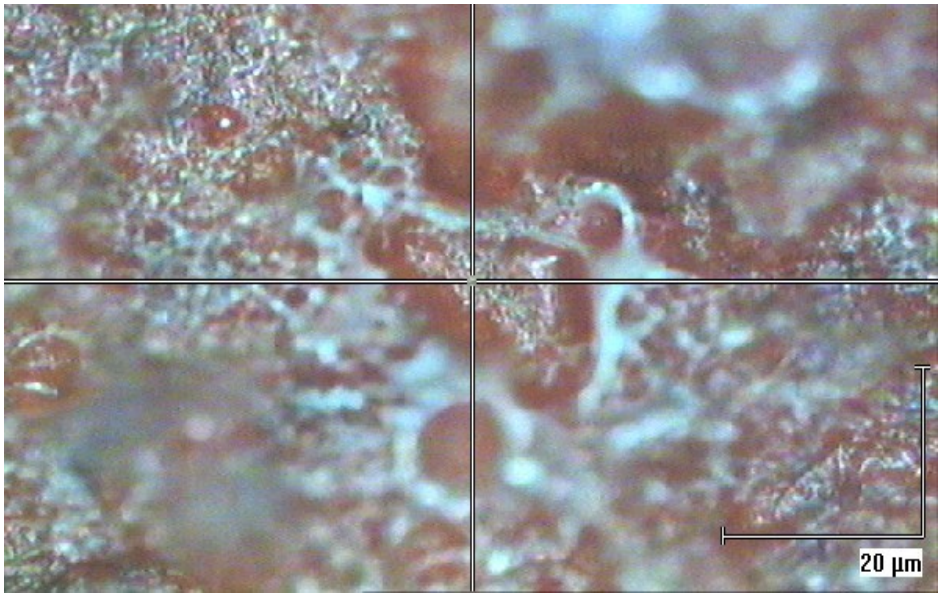

Figure 63. Mineral grain in the red decoration (50× objective, 20 µm scale), targeted for Raman analysis (BDX27680, Montículo.1).

In the yellow area (Fig. 64), the Raman spectrum revealed orpiment (As_2S_3) characteristic bands. This was confirmed by comparing it with the RRUFF reference library (Fig. 65). The presence of orpiment is also indicated by the detection of arsenic (As) and sulfur (S) in SEM-EDS and pXRF analysis.

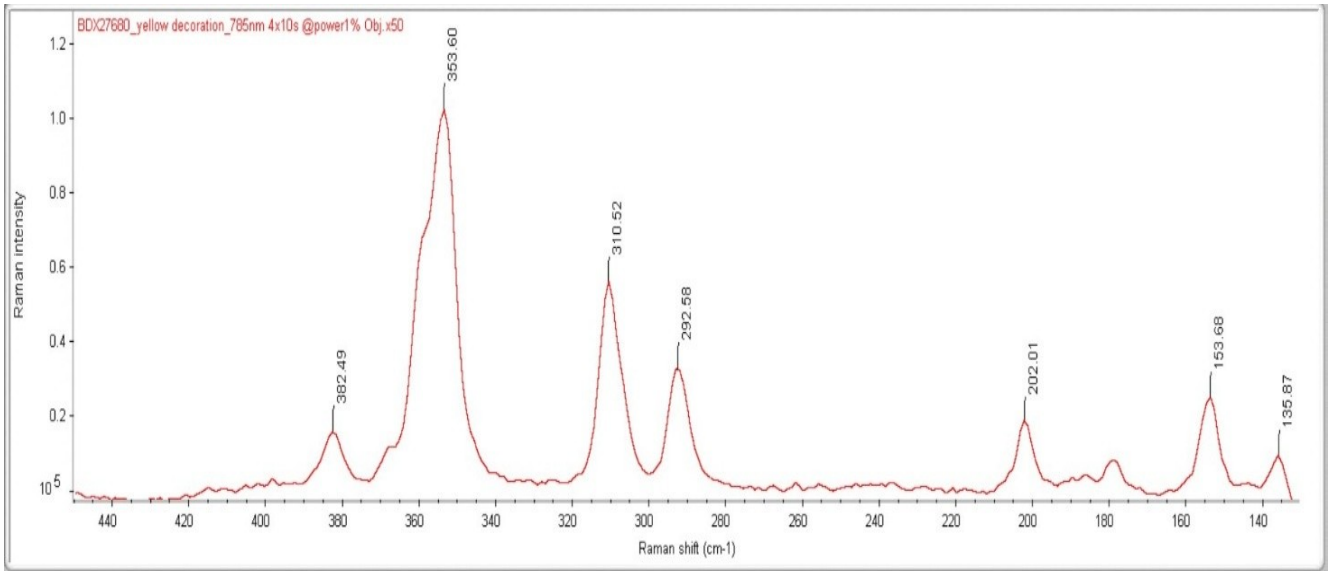

Figure 64. Raman spectrum—4×10s @1% power, 50× obj (785 nm), collected from a yellow-decorated area where the spectrum displays characteristic bands of orpiment (As_2S_3) (BDX27680, Montículo.1).

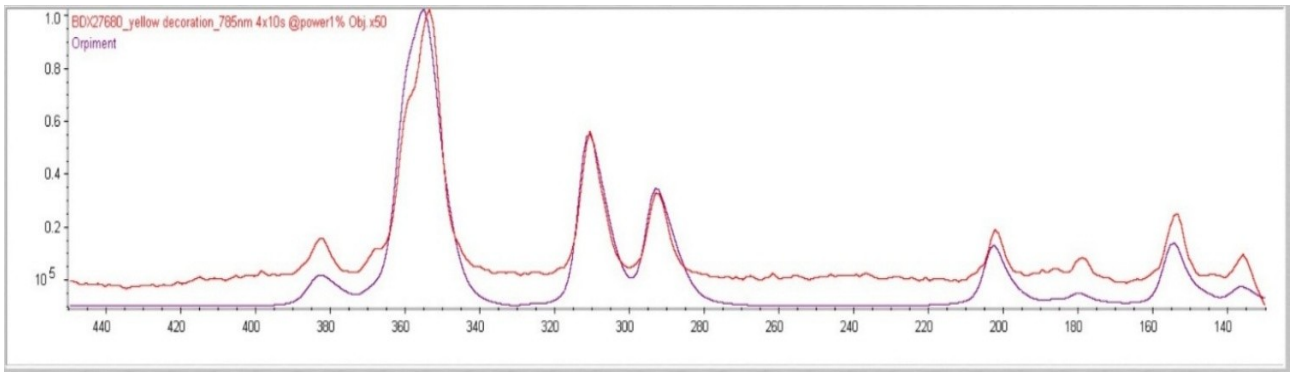

Figure 65. Comparison of the Raman spectrum from the yellow-decorated area (4×10s @1% power, 50× objective) (785 nm) with the reference spectrum of orpiment (As_2S_3) from the RRUFF database. The experimental spectrum shows strong bands at 135, 153, 202, 292, 310, 353, and 382 cm $^{-1}$, confirming the identification of orpiment (BDX27680, Montículo.1).

Although pararealgar (As_4S_4) is composed of arsenic and sulfur, the Raman spectral profile—particularly the sharp bands around 135 cm^{-1}, 1531 cm^{-1}, 202 cm^{-1}, 292 cm^{-1}, 310 cm^{-1}, 353 cm^{-1} and 382 cm^{-1}—clearly aligns with orpiment, resolving any ambiguity(Bell et al., 1997).

Several parameters of acquisition were attempted during yellow pigment analysis. At 50% of the laser power, the surface demonstrated interaction with laser radiation, leading to thermal alteration (Fig. 66). To avoid further damage and preserve the sample integrity, the power level was subsequently reduced for all remaining acquisitions in the yellow area.

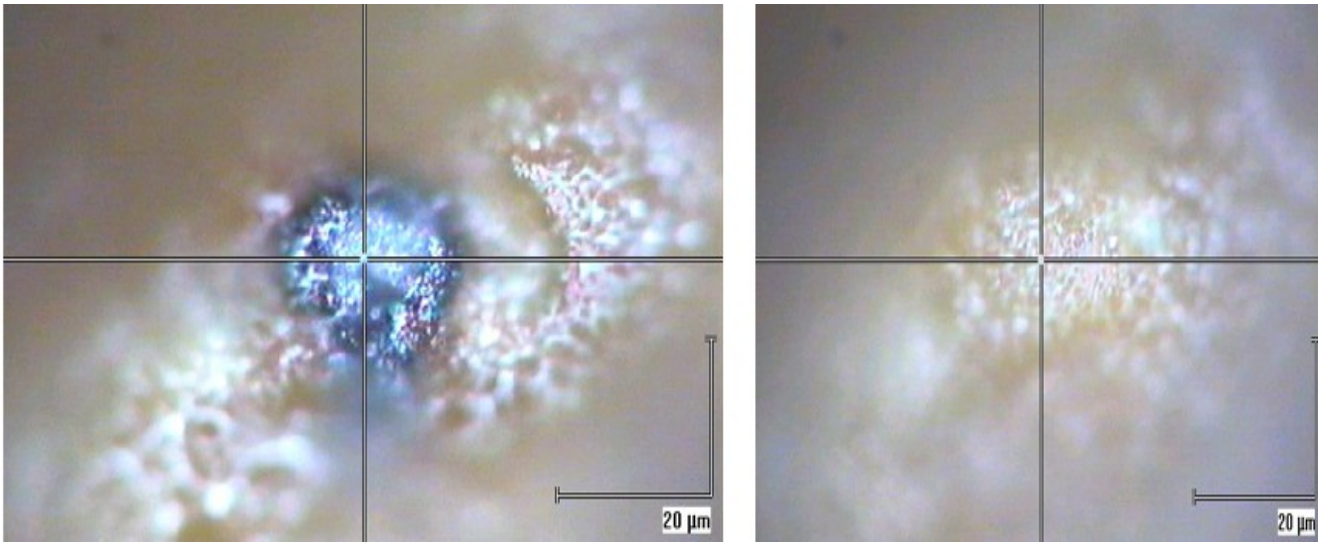

Figure 66. Microscope images of the yellow surface before (right) and after (left) exposure to the Raman laser at 50% power. The central darkened area in the left image shows clear evidence of laser-induced thermal damage, highlighting he sample's sensitivity and the need for reduced power settings in subsequent acquisitions (BDX27680, Montículo.1).

The spectrum of the cream decoration revealed orpiment (Fig.67) as yellow decoration. This is supported by SEM-EDS and pXRF analysis too due to the high amount of As and S.

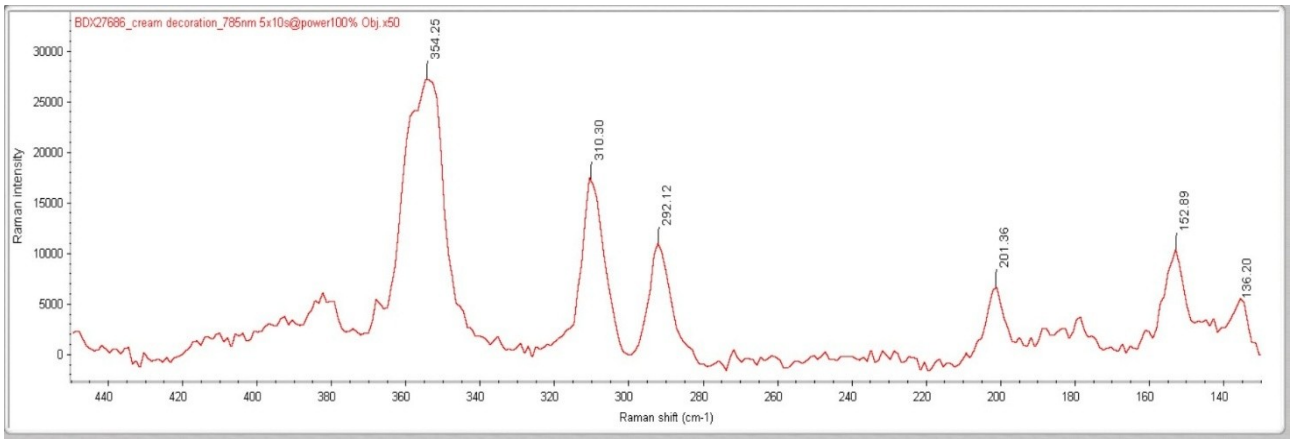

Figure 67. Spectrum collected from cream decoration matching with Orpiment (BDX27686, Monticulo25).

The Raman spectrum of black decoration, Figure 68, showed considerable baseline shift and noise, probably it's the result from fluorescence or pigment structure. Both are common when analyzing older or complex materials(Smith & Clark, 2004; Vandenabeele et al., 2007).

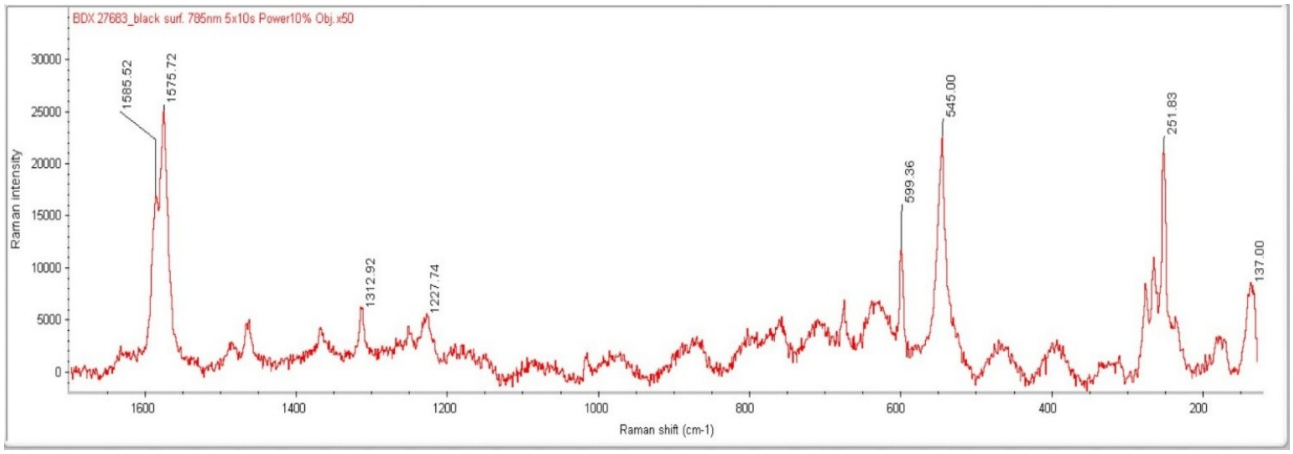

Figure 68. Raman spectrum collected from the black decoration displays characteristic bands of indigo. Prominent peaks at 1575 cm $^{-1}$, 1586 cm $^{-1}$, 1312 cm $^{-1}$,1227 cm $^{-1}$ and 545 cm^{-1} are clearly visible and are characteristics of indigo (BDX27683, Montículo 1).

Despite all of these disturbances, certain peaks characteristic of indigo are easily recognizable, most prominently at 1575 cm^{-1} and 1586 cm^{-1}, indicative of C=C stretching vibrations(Vandenabeele & Moens, 2003). These maxima look extremely close to the indigo reference spectrum (https://chsopensource.org/indigo-k-36005/), as reported in (Fig.69). As the same figure shows, bands at 545 cm^{-1} and 251 cm^{-1} are also present in both the black decor spectrum and in the indigo standard, which correspond to skeletal and ring deformation modes of the indigo molecule(Baran et al., 2010). These peaks were also achieved in FT-Raman analyses of indigo, confirming its identification.

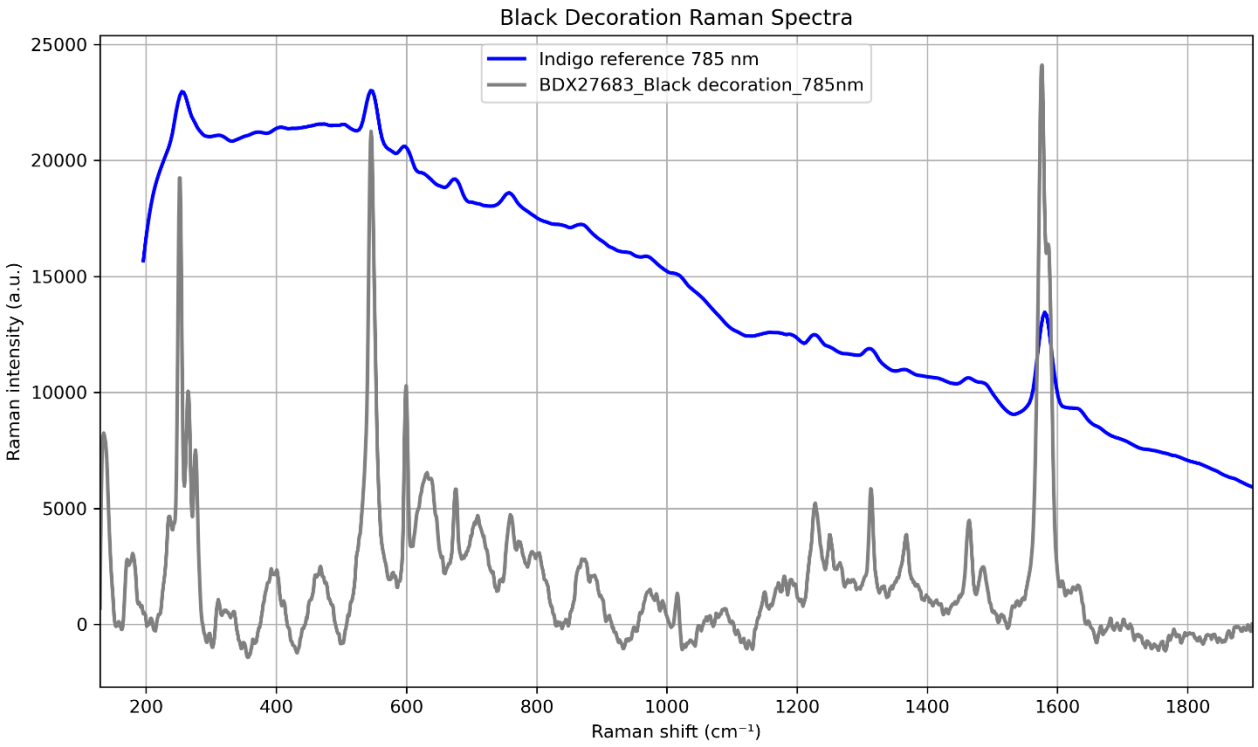

Figure 69. Comparison between the Raman spectrum of the black decoration and the Indigo reference spectrum (785 nm excitation). Showing a good alignment support indigo identification (DBX2783, Montículo 1).

Spectrum was collected from a small black grain, as indicated in Figure 70, Indigo-related peaks being present confirm that indigo contributes to the black pigment, alone or in combination with other materials. Noise and fluctuation in the spectrum may be a sign of degradation, chemical alteration, or mixtures of pigments in the original layer.

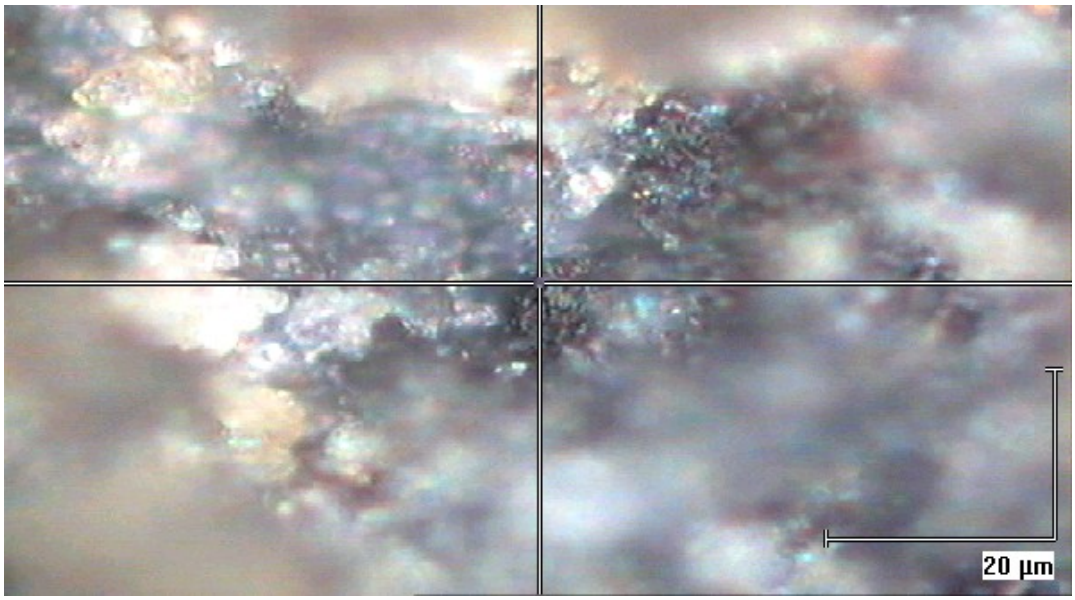

Figure 70.Optical image of the black area targeted for Raman analysis, confirming the source of the indigo signal (DBX2783, Montículo 1).

In addition to the indigo-related peaks observed in BDX27683, Raman spectroscopy on a second black-decorated sample (BDX27698) detected two peaks at 1590 cm^{-1} and 1356 cm^{-1} (Fig. 71). These are the G and D bands, respectively, typical of disordered carbon structures. The G band at ~1590 cm^{-1} is attributed to sp^2 carbon (graphitic domains) vibrations, and the D band at ~1356 cm^{-1} is caused by disorder in the carbon lattice and is assigned to sp^3-hybridized carbon(Bouchard-Abouchacra, 2001, p. 123).

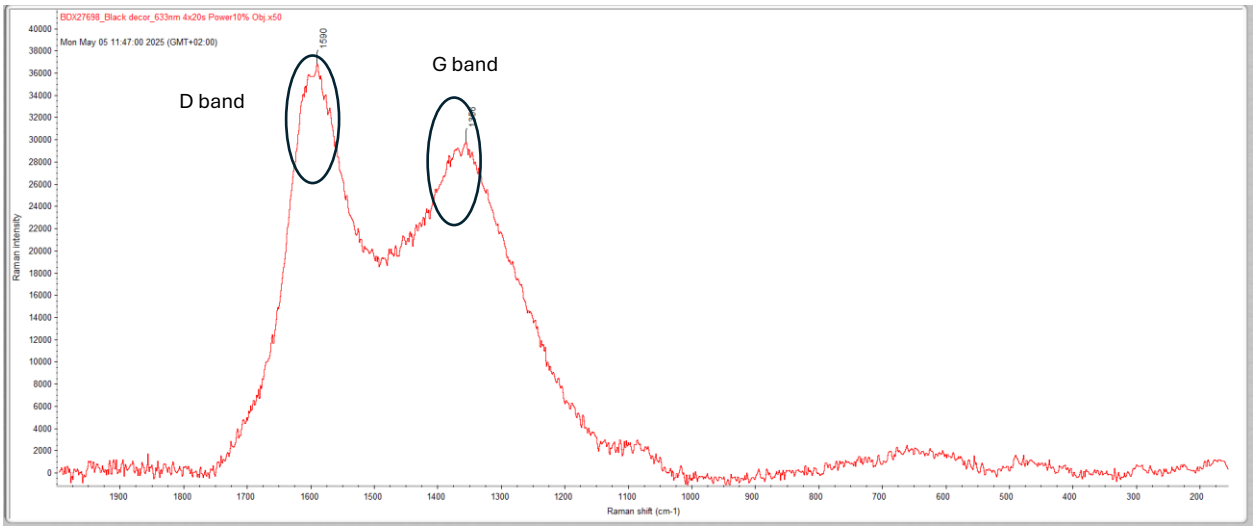

Figure 71.Raman spectrum of the black decoration, showing characteristic D and G bands of disordered (amorphous) carbon at 1356 cm $^{-1}$ and 1590 cm $^{-1}$, respectively. Spectrum acquired using a 633 nm laser (4 × 20 s, 10% laser power, 50×objective) BDX27698, Montículo 1).

This spectral signature agrees with that which *Bouchard-Abouchacra (2001)* described as amorphous carbon, from comparative Raman data originally published by (Dhamelincourt & Nakashima, 1996). Figure 72 shows that different types of carbon such as highly oriented graphite, polycrystalline graphite, amorphous carbon, and diamond-like carbon (DLC)—feature distinct spectral profiles as a function of crystallinity. The Raman spectrum of BDX27698 is most similar to the form of amorphous carbon (c), characterized by broad and overlapping D and G bands, characteristic of a structurally disordered carbon.

This supports the hypothesis that a carbon-based pigment, most probably of charred organic material, was used in ceramics decoration. The presence of amorphous carbon also reveals intentional carbonization processes in pigment preparation, as already observed in archaeometry studies of black pigments in archaeological contexts(Vandenabeele et al., 2007).

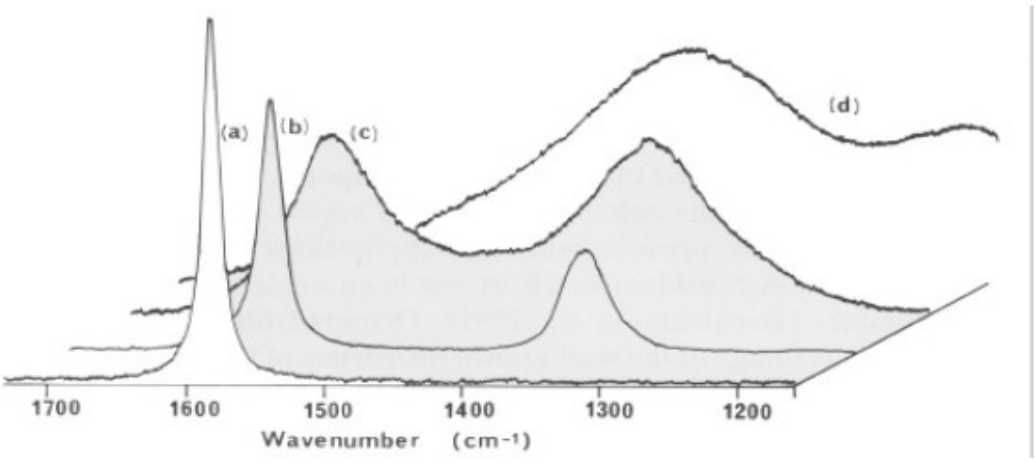

Figure 72. Raman spectra showing the sp^2 and sp^3 bands of graphite according to crystallinity: (a) highly oriented graphite, (b) polycrystalline graphite, (c) amorphous carbon, and (d) diamond-like carbon (DLC). Bouchard (2001)

In some cases, the hematite is found to be mixed with indigo (Fig. 73), which can be attributed to contamination while painting. This could have occurred if the same brush had been used for applying both the red(hematite-based) and the black (indigo- based) decorations, or if the hematite had been derived from the red decoration. There is a possibility that small amount of hematite were intentionally mixed to subtly change the chromatic tone of the black pigment, as seen in some other polychrome traditions where visual depth or warmth was achieved through pigment blending (Tite, 2008; Vandenabeele et al., 2007).

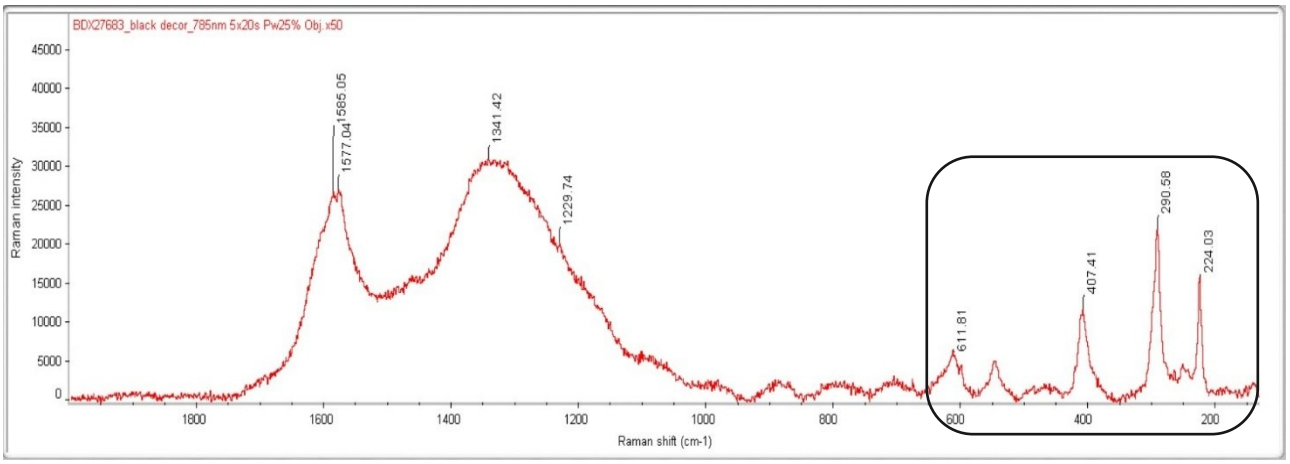

Figure 73. Raman spectrum of the black decoration showing a mixture of hematite and indigo. The characteristic Raman shifts of hematite are highlighted with black squares (BDX27683, Montículo 1).

3.3.4 FTIR Analysis

FTIR spectroscopy was applied to assess the presence of surface coatings or organic binders on the decorated ceramic areas including black, red, yellow, orange, cream, and brown regions(Michele R. Derrick, Dusan C. Stulik, and James M. Landry, 1999; Poliskie & Clevenger, 2008; Chua et al., 2017).

All spectra (Fig. 74) show a strong and clearly defined band near 1040 cm^{-1}, which is linked to Si–O stretching vibrations typical of silicate minerals like quartz and clay. These materials make up most of the ceramic body(Madejová, 2003; Michele R. Derrick, Dusan C. Stulik, and James M. Landry, 1999).

The bands around 460–470 cm^{-1} and 540–550 cm^{-1} in the FTIR spectra are due to bending vibrations of Si–O–Si and Si–O–Al bonds, which are commonly found clay minerals like smectite and kaolinite. Although these bands might partly overlap with signals from iron or manganese pigments, their consistent appearance in all samples suggests they mostly reflect the ceramic body itself(FARMER, 1974; Madejová, 2003).

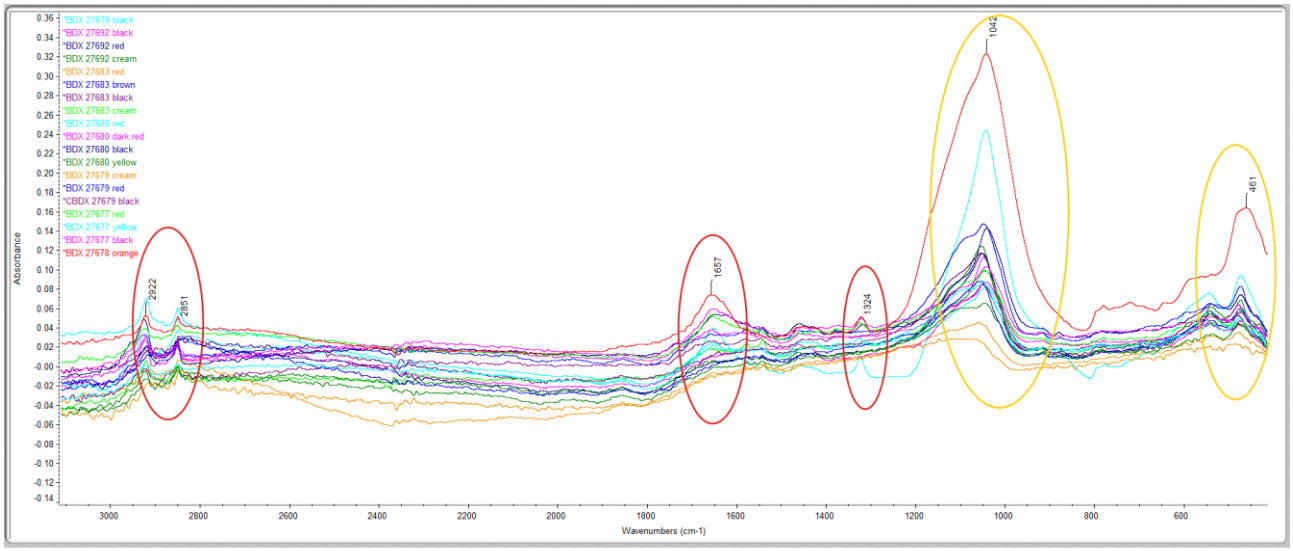

Figure 74. FTIR spectra of different decoration areas of ceramic fragments showing strong Si–O stretching bands near 1042 cm $^{-1}$ and a Si–O–Si bending band around 461 cm $^{-1}$, both characteristic of silicate minerals and pigments in the ceramic body. Weak absorptions at ~2920, 2851, 1657, and 1324 cm $^{-1}$ suggest traces of organic compounds such as aged resins or proteins, though these signals are faint and inconsistent across samples.

Several samples also display weak absorptions in regions typically associated with organic materials:

Bands near 2920 and 2852 cm^{-1}, present in many spectra, correspond to aliphatic C–H stretching modes (CH_2 and CH_3 groups)(Ciumac et al., 2017).

A weak peak near 1650–1657 cm^{-1} may be related to carbonyl (C=O) or aromatic (C=C) stretching are commonly associated with aged natural organic compounds such as plant resins or proteins (DERRICK (M.R.) et al., 1999).

A minor absorption around 1320–1325 cm^{-1} could be related to C–O stretching or CH_2 bending vibrations(Sammons et al., 2013).

However, these organic-related features are regularly weak and poorly resolved. Their relatively low intensity, especially when compared to the silicate band, makes it difficult to confidently confirm the presence of organic coatings or binders. These signals may instead be related to trace residues, degradation products or environmental contamination.

In some samples, like in the red (e.g., BDX 27677 red) and black (e.g., BDX 27678 black) regions, slightly stronger features in the organic region were observed. Though, the differences are minimal, and they do not follow a systematic pattern.

Overall, all the spectra are mainly shaped by silicate and mineral signals. The organic signals are too weak and inconsistent to confirm that any coating or binder was used. It is likely that organic materials were originally present but have degraded over time, which would explain why these signals are now so faint and difficult to detect or the FTIR can’t be a good choice for these samples.

4 Conclusions and Future Perspectives

This study presents a comprehensive archaeometric analysis of the pigment technologies and decorative techniques used in Paracas ceramics from the Ánimas Altas archaeological complex. Through the integration of multi-scale imaging, and a set of complementary analytical technologies—SEM-EDS, pXRF, Raman spectroscopy, and FTIR—the study reveals new findings regarding the material composition, pigment recipes, and technological choices employed by Paracas artisans between 300 BCE and 50 CE.

The analysis conducted shows the use of various types of pigments with varying chemical signatures and technological processing. Iron oxides are determined as the essential chromophores in red and orange colorants, wherein red pigments show higher iron oxide concentration and higher matrix composition variability, and orange pigments are dispersed more homogeneously onto finer slips, these all point to use of red ochre pigmen. The yellow and cream decorations exhibited high concentrations of arsenic and sulfur, indicating the intentional use of the arsenic sulfide mineral (orpiment). Raman spectroscopy revealed the existence of hematite for Red and orange, orpiment for yellow and cream, and indigo and carbon used independently or in conjunction with carbonaceous material to produce black surfaces. The presence of amorphous carbon micro-inclusions and the irregular occurrence of manganese oxide in micro-sample BDX27679 reflects specific compositional choices and possibly a deliberate technological practice in the ceramic pigments.

pXRF compositional analysis of the ceramic matrix revealed overall a partial grouping across the three excavation areas—Montículo 1, Montículo 25, and El Panteón, suggesting moderate differentiation in raw material selection, but overall paste compositions tended to be silico-aluminous with no to minimal calcareous content. Firing conditions ranged from full oxidation to partial or complete reduction, as would be anticipated from firing in open or semi-controlled environments. From a methodological perspective, the present work highlights the limitations and advantages of pXRF for non-destructive pigment analysis. While semi-quantitative correlation with SEM-EDS was determined for Ti, K, and Ca, greater divergence was noted for Al, Si, Fe, and Mn—especially in layered or heterogeneous pigments. Raman spectroscopy with a 785 nm benchtop instrument was very effective for the analysis of molecular pigments in spite of pervasive fluorescence issues, and detection of prominent chromophores such as hematite, indigo, and orpiment. In contrast, FTIR spectra were dominated by silicate signals and weakly suggested the presence of deteriorated organic binders, indicating either degraded preservation or original absence of such material.

In the future, several archaeometric methods must be undertaken in order to expand and improve this study. Raman, FTIR, and XRD need to be applied more extensively, with Raman and synchrotron-based spectroscopy applied to measure pigment phase composition, detect arsenic compounds and

organic dyes, and detect possible synthetic or modified organic material. FTIR substitutes such as ATR-FTIR, micro-FTIR, and synchrotron-based FTIR can enhance the detection of degraded or low-concentration organic compounds that were of low resolution in this study. Methods such as Gas Chromatography–Mass Spectrometry (GC-MS) and Pyrolysis–Gas Chromatography–Mass Spectrometry (Py-GC-MS) are highly recommended for identification of resinous binders, lipids, or proteins and compare them with the natural organics from the site. Expanded sampling among categories of ceramics enables testing whether pigment technologies were standardized or adapted depending on function, social context, or workshop conventions.

Moreover, the detection of organic material in the decorative layers presents an opportunity for radiocarbon (C^{14}) dating, potentially offering more accurate insight into the true chronology of the ceramic production.

Lastly, six geological samples arrived with the ceramics. These would be in situ pigment or mineral sources and ought to be strictly examined to determine their compositional equivalence to the pigments used for pigments. By comparison, local methods of sourcing could be confirmed or imported materials recognized, advancing raw material procurement and artisanal skill in the Paracas cultural setting.

5 Bibliography

Aceto, M., Agostino, A., Fenoglio, G., Idone, A., Gulmini, M., Picollo, M., Ricciardi, P., & Delaney, J. K. (2014). Characterisation of colourants on illuminated manuscripts by portable fibre optic UV-visible-NIR reflectance spectrophotometry. *Analytical Methods*, *6*(5), 1488–1500. https://doi.org/10.1039/C3AY41904E

Amicone, S., Forte, V., Solard, B., Berthold, C., Memmesheimer, A., & Mirković-Marić, N. (2021). Playing with fire: Exploring ceramic pyrotechnology in the Late Neolithic Balkans through an archaeometric and experimental approach. *Journal of Archaeological Science: Reports*, *37*, 102878. https://doi.org/10.1016/j.jasrep.2021.102878

Arriaza, B., Halcrow, S., Vizcarra, A., Gutiérrez, S., Ogalde, J. P., Standen, V., & Santos, M. (2025). The potential hazards of smoking pots: Quantification of the black paint on the ceramics in the Atacama Desert. *Journal of Archaeological Science: Reports*, *61*, 104955. https://doi.org/10.1016/j.jasrep.2024.104955

Bachir Bacha, A. (2017). El Edificio de los Frisos de Ánimas Altas. Ser paracas en el valle bajo de Ica. *Boletín de Arqueología PUCP*, *22*, 191–225. https://doi.org/10.18800/boletindearqueologiapucp.201701.008

Bachir Bacha, A. (2018). Paracas, Geography and Culture of. In *Encyclopedia of Global Archaeology* (pp. 1–13). Springer International Publishing. https://doi.org/10.1007/978-3-319-51726-1_2579-1

Bachir Bacha, A. (2022). Paracas et Nasca:Nouvelles données, nouvelles perspectives. *Atlas*, 58–59.

Bachir Bacha, A., & Llanos, D. (2013). ¿Hacia un urbanismo paracas en Ánimas Altas/Ánimas Bajas (valle de Ica)? *Boletín de Arqueología PUCP*, *17*, 169–204. https://doi.org/10.18800/boletindearqueologiapucp.201301.008

Bachir Bacha, A., & Llanos Jacinto, Ó. D. (2021). *Ánimas Altas, Ánimas Bajas. Archéologie d'un centre urbain paracas. Andes centrales (400 av. J.-C. - 100 ap. J.-C.)*. Enredars. http://hdl.handle.net/10433/9669

Baran, A., Fiedler, A., Schulz, H., & Baranska, M. (2010). In situ Raman and IR spectroscopic analysis of indigo dye. *Analytical Methods*, *2*(9), 1372–1376. https://doi.org/10.1039/C0AY00311E

Bell, I. M., Clark, R. J. H., & Gibbs, P. J. (1997). Raman spectroscopic library of natural and synthetic pigments (pre- ≈ 1850 AD). *Spectrochimica Acta Part A: Molecular and Biomolecular Spectroscopy*, *53*(12), 2159–2179. https://doi.org/10.1016/S1386-1425(97)00140-6

Bouchard-Abouchacra, M. (2001). *Evaluation des capacités de la microscopie Raman dans la caractérisation minéralogique et physico-chimique de matériaux archéologiques: Métaux, vitraux & pigments* [These de doctorat, Paris, Muséum national d'histoire naturelle]. https://theses.fr/2001MNHN0035

Casanova-González, E., Maynez-Rojas, M. Á., Mitrani, A., Rangel-Chávez, I., García-Bucio, M. A., Ruvalcaba-Sil, J. L., & Muñoz-Alcócer, K. (2020). An imaging and spectroscopic methodology for in situ analysis of ceiling and wall decorations in Colonial missions in Northern Mexico from XVII to XVIII centuries. *Heritage Science*, *8*(1), 1–14. https://doi.org/10.1186/s40494-020-00434-8

Chua, L., Head, K., Thomas, P., & Stuart, B. (2017). FTIR and Raman microscopy of organic binders and extraneous organic materials on painted ceremonial objects from the

Highlands of Papua New Guinea. *Microchemical Journal*, *134*, 246–256. https://doi.org/10.1016/j.microc.2017.06.018

Ciumac, D., Campbell, R. A., Clifton, L. A., Xu, H., Fragneto, G., & Lu, J. R. (2017). Influence of Acyl Chain Saturation on the Membrane-Binding Activity of a Short Antimicrobial Peptide. *ACS Omega*, *2*(11), 7482–7492. https://doi.org/10.1021/acsomega.7b01270

Courty, M. A., & Roux, V. (1995). Identification of wheel throwing on the basis of ceramic surface features and microfabrics. *Journal of Archaeological Science*, *22*(1), 17–50. https://doi.org/10.1016/S0305-4403(95)80161-8

De Keyser, N., Broers, F. T. H., Vanmeert, F., van Loon, A., Gabrieli, F., De Meyer, S., Gestels, A., Gonzalez, V., Hermens, E., Noble, P., Meirer, F., Janssens, K., & Keune, K. (2024). Discovery of pararealgar and semi-amorphous pararealgar in Rembrandt's The Night Watch: Analytical study and historical contextualization. *Heritage Science*, *12*(1), 1–20. https://doi.org/10.1186/s40494-024-01350-x

DERRICK (M.R.), STULIK (D.), & LANDRY (J.M.). (1999). *Infrared spectroscopy in conservation science*. Los Angeles : Getty conservation institute, 1999. https://www.lrmh.fr/Default/doc/SYRACUSE/72390/infrared-spectroscopy-in-conservation-science

Dhamelincourt, P., & Nakashima, S. (1996). 6—Application to Materials Science. In G. Turrell & J. Corset (Eds.), *Raman Microscopy* (pp. 243–287). Academic Press. https://doi.org/10.1016/B978-012189690-4/50026-0

Elias, M., Chartier, C., Prévot, G., Garay, H., & Vignaud, C. (2006). The colour of ochres explained by their composition. *Materials Science and Engineering: B*, *127*(1), 70–80. https://doi.org/10.1016/j.mseb.2005.09.061

FARMER, (V.C.). (1974). *The Infrared spectra of minerals*. London (41 Queen's Gate. SW7SHR) : Mineralogical Society, 1974. https://www.lrmh.fr/Default/doc/SYRACUSE/72374/the-infrared-spectra-of-minerals

Felipe, C. V., Bellón, J. M., & Bellón, B. (2019). CRAFTER: An Experimental Approach to Fire-Induced Alteration of Pottery Fabrics. *EXARC Journal*, *EXARC Journal Issue 2019/2*. https://exarc.net/issue-2019-2/mm/crafter-experimental-approach-fire-induced-alteration-pottery-fabrics

Frerebeau, N., Amara, A. B., & Cantin, N. (2020). Analyse de données de composition et identification des altérations géochimiques des matériaux céramiques: Le cas des productions d'un atelier ibérique (Teruel, Espagne ; IIe-Ier siècles avant J.-C.). *ArcheoSciences*, *441*(1), 33–50. https://doi.org/10.4000/archeosciences.7220

Goldstein, J. I., Newbury, D. E., Michael, J. R., Ritchie, N. W. M., Scott, J. H. J., & Joy, D. C. (2018). *Scanning Electron Microscopy and X-Ray Microanalysis*. Springer. https://doi.org/10.1007/978-1-4939-6676-9

Hayem-Ghez, A., Ravaud, E., Boust, C., Bastian, G., Menu, M., & Brodie-Linder, N. (2015). Characterizing pigments with hyperspectral imaging variable false-color composites. *Applied Physics A*, *121*(3), 939–947. https://doi.org/10.1007/s00339-015-9458-8

Ion, R.-M., Pungoi, A.-E., Iancu, L., Grigorescu, R. M., Vasilievici, G., Gheboianu, A. I., Slamnoiu-Teodorescu, S., & Alexandrescu, E. (2024). Compositional and Microstructural Investigations of Prehistoric Ceramics from Southern Romania (Middle Neolithic Pottery). *Applied Sciences*, *14*(13), Article 13. https://doi.org/10.3390/app14135755

Kastenholz, H. V., Topper, M. I., Warren, W. S., Fischer, M. C., & Grass, D. (2024). Noninvasive identification of carbon-based black pigments with pump-probe microscopy. *Science Advances*, *10*(50), eadp0005. https://doi.org/10.1126/sciadv.adp0005

Kriss, D., & DeLeonardis, L. (2018). A material and technical study of Paracas painted ceramics. *Antiquity*. https://www.academia.edu/39342006/A_material_and_technical_study_of_Paracas_painted_ceramics

Kubik, M. (2007). Chapter 5 Hyperspectral Imaging: A New Technique for the Non-Invasive Study of Artworks. In D. Creagh & D. Bradley (Eds.), *Physical Techniques in the Study of Art, Archaeology and Cultural Heritage* (Vol. 2, pp. 199–259). Elsevier. https://doi.org/10.1016/S1871-1731(07)80007-8

Li, X., Zhang, X., Du, J., Yang, J., & Han, J. (2025). Painting technique of red post-firing painted pottery from the Nanzuo Neolithic site in Qingyang, Gansu Province. *Npj Heritage Science*, *13*(1), 1–8. https://doi.org/10.1038/s40494-025-01661-7

Liritzis, I., & Zacharias, N. (2011). Portable XRF of Archaeological Artifacts: Current Research, Potentials and Limitations. In M. S. Shackley (Ed.), *X-Ray Fluorescence Spectrometry (XRF) in Geoarchaeology* (pp. 109–142). Springer. https://doi.org/10.1007/978-1-4419-6886-9_6

López Puértolas, C., Ruvalcaba-Sil, J. L., Padilla, E., Casanova-González, E., Darras, V., & The 89th Annual Meeting of the Society for American Archaeology. (2024). *Analyses of Pastes and Polychromy of Chupícuaro Pottery: A Diachronic Comparison Using a Noninvasive Approach*.

Ly, B. C. K., Dyer, E. B., Feig, J. L., Chien, A. L., & Del Bino, S. (2020). Research Techniques Made Simple: Cutaneous Colorimetry: A Reliable Technique for Objective Skin Color

Measurement. *Journal of Investigative Dermatology*, *140*(1), 3-12.e1. https://doi.org/10.1016/j.jid.2019.11.003

Madejová, J. (2003). FTIR techniques in clay mineral studies. *Vibrational Spectroscopy*, *31*(1), 1–10. https://doi.org/10.1016/S0924-2031(02)00065-6

Maggetti, M. (2001). Chemical Analyses of Ancient Ceramics: What for? *CHIMIA*, *55*(11), Article 11. https://doi.org/10.2533/chimia.2001.923

Mardi, G. H. (2014). An Experimental Approach to Studying the Technology of Pottery Decoration. *EXARC Journal*, *EXARC Journal Issue 2014/3*. https://exarc.net/issue-2014-3/ea/experimental-approach-studying-technology-pottery-decoration

Maritan, L., Nodari, L., Mazzoli, C., Milano, A., & Russo, U. (2006). Influence of firing conditions on ceramic products: Experimental study on clay rich in organic matter. *Applied Clay Science*, *31*(1), 1–15. https://doi.org/10.1016/j.clay.2005.08.007

Michele R. Derrick, Dusan C. Stulik, and James M. Landry. (1999). *Infrared Spectroscopy in Conservation Science:* https://www.getty.edu/publications/virtuallibrary/0892364696.html

Mounier, A., & and Daniel, F. (2015). Hyperspectral imaging for the study of two thirteenth-century Italian miniatures from the Marcadé collection, Treasury of the Saint-Andre Cathedral in Bordeaux, France. *Studies in Conservation*, *60*(sup1), S200–S209. https://doi.org/10.1179/0039363015Z.000000000225

Mounier, A., Le Bourdon, G., Aupetit, C., Belin, C., Servant, L., Lazare, S., Lefrais, Y., & Daniel, F. (2014). Hyperspectral imaging, spectrofluorimetry, FORS and XRF for the non-invasive study of medieval miniatures materials. *Heritage Science*, *2*(1), 1–12. https://doi.org/10.1186/s40494-014-0024-z

Paravina, R. D., Ghinea, R., Herrera, L. J., Bona, A. D., Igiel, C., Linninger, M., Sakai, M., Takahashi, H., Tashkandi, E., & Mar Perez, M. del. (2015). Color Difference Thresholds in Dentistry. *Journal of Esthetic and Restorative Dentistry*, *27*(S1), S1–S9. https://doi.org/10.1111/jerd.12149

Pei, Z., Huang, Y. M., & Zhou, T. (2023). Review on Analysis Methods Enabled by Hyperspectral Imaging for Cultural Relic Conservation. *Photonics*, *10*(10), Article 10. https://doi.org/10.3390/photonics10101104

Pendleton, M. W., Washburn, D. K., Ellis, E. A., & Pendleton, B. B. (2014). Comparing the detection of iron-based pottery pigment on a carbon-coated sherd by SEM-EDS and by Micro-XRF-SEM. *The Yale Journal of Biology and Medicine*, *87*(1), 15–20.

Perttula, Timothy K. (2022). *Native American Ceramic Vessel Sherds at the Joyful Horse Site (41BP691), Bastrop County, Texas*. ResearchGate. https://www.researchgate.net/publication/360951469_Native_American_Ceramic_Vessel_Sherds_at_the_Joyful_Horse_Site_41BP691_Bastrop_County_Texas

Picollo, M., Cucci, C., Casini, A., & Stefani, L. (2020). Hyper-Spectral Imaging Technique in the Cultural Heritage Field: New Possible Scenarios. *Sensors*, *20*(10), Article 10. https://doi.org/10.3390/s20102843

Poliskie, M., & Clevenger, J. O. (2008). Fourier transform infrared (FTIR) spectroscopy for coating characterization and failure analysis: Effective technique for initial identification of resins and other organic additives in paint systems. *Metal Finishing*, *106*(3), 46–49. https://doi.org/10.1016/S0026-0576(08)80059-1

Protective Perimeters: The Symbolism of Borders on Paracas Textiles. (2017, December 16). ResearchGate.

https://www.researchgate.net/publication/311779409_Protective_Perimeters_The_Symbolism_of_Borders_on_Paracas_Textiles

Sabatini, F., Bacigalupo, M., Degano, I., Javér, A., & Hacke, M. (2020). Revealing the organic dye and mordant composition of Paracas textiles by a combined analytical approach. *Heritage Science*, *8*(1), 1–17. https://doi.org/10.1186/s40494-020-00461-5

Sammons, R. J., Harper, D. P., Labbé, N., Bozell, J. J., Elder, T., & Rials, T. G. (2013). Characterization of Organosolv Lignins using Thermal and FT-IR Spectroscopic Analysis. *BioResources*, *8*(2), 2752–2767. https://doi.org/10.15376/biores.8.2.2752-2767

Shackley, M. S. (2011). An Introduction to X-Ray Fluorescence (XRF) Analysis in Archaeology. In M. S. Shackley (Ed.), *X-Ray Fluorescence Spectrometry (XRF) in Geoarchaeology* (pp. 7–44). Springer. https://doi.org/10.1007/978-1-4419-6886-9_2

Smith, G. D., & Clark, R. J. H. (2004). Raman microscopy in archaeological science. *Journal of Archaeological Science*, *31*(8), 1137–1160. https://doi.org/10.1016/j.jas.2004.02.008

Splitstoser, J. C., Dillehay, T. D., Wouters, J., & Claro, A. (2016). Early pre-Hispanic use of indigo blue in Peru. *Science Advances*, *2*(9), e1501623. https://doi.org/10.1126/sciadv.1501623

Teetaert, D. (2017). Food and Soot: Organic Residues on Outer Pottery Surfaces. *Radiocarbon*. https://doi.org/10.1017/RDC.2017.25

Tite, M. S. (2008). Ceramic Production, Provenance and Use—A Review. *Archaeometry*, *50*(2), 216–231. https://doi.org/10.1111/j.1475-4754.2008.00391.x

Tykot, R. H. (2016). Using Nondestructive Portable X-ray Fluorescence Spectrometers on Stone, Ceramics, Metals, and Other Materials in Museums: Advantages and

Limitations. *Applied Spectroscopy*, *70*(1), 42–56. https://doi.org/10.1177/0003702815616745

Vandenabeele, P., Edwards, H. G. M., & Moens, L. (2007). A Decade of Raman Spectroscopy in Art and Archaeology. *Chemical Reviews*, *107*(3), 675–686. https://doi.org/10.1021/cr068036i

Vandenabeele, P., & Moens, L. (2003). Micro-Raman spectroscopy of natural and synthetic indigo samples. *Analyst*, *128*(2), 187–193. https://doi.org/10.1039/B209630G

Vasco, G., Aureli, H., Fernández-Lizaranzu, I., Moreno-Soto, J., Križnar, A., Parrilla-Giraldez, R., Gómez-González, E., & Respaldiza Galisteo, M. A. (2024). Development of a Hyperspectral Imaging Protocol for Painting Applications at the University of Seville. *Heritage*, *7*(11), Article 11. https://doi.org/10.3390/heritage7110281

Vermeulen, M., Sanyova, J., & Janssens, K. (2015). Identification of artificial orpiment in the interior decorations of the Japanese tower in Laeken, Brussels, Belgium. *Heritage Science*, *3*(1), 1–9. https://doi.org/10.1186/s40494-015-0040-7

Zhushchikhovskaya, Irina S. (2022, December 23). *(PDF) Experimental Ceramics Firing in Archaeology: Current Studies*. ResearchGate. https://www.researchgate.net/publication/359396650_Experimental_Ceramics_Firing_in_Archaeology_Current_Studies

Zhushchikhovskaya, R. (n.d.). *POLYCHROME SCULPTURE: TOOL MARKS, CONSTRUCTION TECHNIQUES, DECORATIVE PRACTICE AND ARTISTIC TRADITION*. Retrieved May 23, 2025, from https://www.academia.edu/32881672/POLYCHROME_SCULPTURE_TOOL_MARKS_CONSTRUCTION_TECHNIQUES_DECORATIVE_PRACTICE_AND_ARTISTIC_TRADITION

6 Appendix

Appendix Table 1. Composition of the obsidian standard MAOA.STD in oxide wt% or in µg/g for the trace elements as determined by Inductive Coupled Plasma - Mass Spectrometry (ICP-MS) and Inductive Coupled Plasma - Optical Emission Spectrometry (ICP-OES) analyses.

%

SiO_2	Al_2O_3	Fe_2O_3	MnO	MgO	CaO	Na_2O	K_2O	TiO_2	P_2O_5
74.10	13.50	1.44	0.056	0.10	0.63	3.49	5.14	0.098	< L.D.

µg/g

As	Ba	Be	Bi	Cd	Co	Cr	Cs	Cu	Ga	Ge	Hf	In	Mo	Nb	Ni	Pb	Rb	Sb	Sc	Sn	Sr
2.80	130	5.61	0.11	0.26	0.43	3.8	3.9	4.4	25.2	1.71	3.82	0.08	1.71	42.3	< L.D.	30.3	244	0.20	4.25	2.81	28.7

µg/g

Ta	Th	U	V	W	Y	Zn	Zr	La	Ce	Pr	Nd	Sm	Eu	Gd	Tb	Dy	Ho	Er	Tm	Yb	Lu
4.30	16.1	5.26	1.1	2.57	35.0	91.5	88.8	22.4	51.9	6.54	24.5	7.15	0.364	6.13	1.08	6.54	1.28	3.24	0.476	2.96	0.399

Appendix Table 2. CIELAB color values (L, a*, b*) extracted from hyperspectral images using Python, alongside visual color labels and ΔE values calculated in comparison to spectrophotometric measurements. ΔE indicates the color difference between the hyperspectral and spectrophotometric data, with values below 5 generally considered acceptable for visual agreement.*

Sample	l*	a*	b*	color	ΔE
BDX27677	35.20	31.16	14.21		3.69
BDX27680	35.40	39.10	16.47		3.97
BDX27682	35.37	14.58	8.01		4.45
BDX27683	35.54	32.96	16.45		5.59
BDX27686	35.07	18.10	8.30		6.38
BDX27690	36.05	36.10	19.74	red	8.06
BDX27675	36.78	18.25	18.05		8.95
BDX27678	36.92	26.51	22.09		9.55
BDX27684	37.89	41.54	29.64		11.57
BDX27687	36.89	18.01	18.51		11.59
BDX27688	37.02	24.22	21.83		11.60
BDX27689	36.80	28.69	22.15		12.46
BDX27691	40.13	50.38	39.54	orange	12.68
BDX27677	24.09	13.83	1.11		13.45
BDX27678	34.19	14.63	0.62		14.63
BDX27679	36.47	3.41	6.21		15.27
BDX27680	35.52	-0.01	-5.39		16.25
BDX27683	36.19	-3.35	-5.27		18.53
BDX27682	36.43	3.26	5.74		19.20
BDX27686	35.73	6.47	4.12		20.03
BDX27690	36.66	4.67	8.56		21.03
BDX27698	32.64	10.56	-15.74	black	23.59
BDX27677	37.74	20.37	23.99		24.54
BDX27680	37.66	13.50	20.32		27.93
BDX27681	39.50	22.48	33.20		31.14
BDX27690	38.04	12.56	21.80	yellow	45.48

Appendix Table 3. Chemical composition (in wt.% for major oxides and ppm for trace elements) of decorative layers on ceramic sherds of various colors from three archaeological sites, obtained using portable X-ray fluorescence (pXRF). The dataset includes both monochrome

Sample	Color	Site	MgO	Al_2O_3	SiO_2	S	K_2O	CaO	TiO_2	Fe_2O_3	Mn	Ni	Cu	Zn	As	Rb	Sr	Zr
BDX27677	yellow	Montículo 1	12.9	8.1	58.1	5.8	3.2	3.3	0.5	8.1	562	41	86	119	16570	109	283	137
BDX27680			13.5	5.7	56.6	4.8	3.6	4.4	0.8	10.5	667	33	94	138	12709	107	292	123
BDX27681			11.9	2.6	61.0	5.8	5.7	3.7	0.6	8.7	533	41	75	95	15581	122	263	139
BDX27698		El pantheon	13.9	6.2	58.6	4.6	4.6	4.3	0.5	7.3	447	45	72	90	17273	110	256	130
BDX27690		Montículo 1	15.5	2.8	52.7	3.4	4.6	6.0	1.3	13.6	1015	50	102	221	2566	114	281	180
BDX27677	red		11.7	1.7	38.7	0.8	2.2	5.8	1.2	37.8	786	70	116	150	187	106	296	143
BDX27679			14.7	3.8	48.9	0.6	2.7	5.6	1.3	22.4	732	30	135	164	558	127	327	148
BDX27680			10.9	0.0	39.2	1.3	1.8	5.4	1.1	40.4	713	41	90	140	142	94	276	127
BDX27682			13.4	3.1	46.9	0.1	1.9	7.2	1.0	26.3	1102	64	143	157	368	102	287	137
BDX27683			14.8	4.5	47.2	1.0	1.8	5.6	0.8	24.2	1078	44	133	204	650	98	283	146
BDX27686		Montículo 25	9.8	0.6	35.7	1.0	2.2	4.6	4.1	42.0	952	156	201	345	4229	133	374	175
BDX27690		El Panteón	8.2	0.0	41.8	0.0	2.7	5.0	1.7	40.6	1448	111	229	276	135	140	415	222
BDX27678	orange	Montículo 1	17.4	2.7	51.9	0.6	3.4	7.4	1.2	15.4	1152	49	124	202	35	123	319	160
BDX27675			17.1	2.8	56.6	0.7	2.9	3.7	0.9	15.3	753	62	97	215	60	117	334	149
BDX27684		Montículo 25	15.3	0.0	61.5	0.2	3.1	3.4	1.0	15.4	932	54	109	111	63	108	369	135
BDX27687			18.7	3.3	56.0	0.2	3.1	3.5	1.4	13.8	975	54	150	165	36	114	310	162
BDX27688		Panteón El	22.9	1.6	53.8	0.0	3.6	2.5	1.4	14.2	1385	47	166	310	44	104	269	158
BDX27689			18.4	3.5	55.2	0.5	2.9	5.2	1.0	13.2	856	54	109	143	43	131	316	179
BDX27691			16.2	0.9	58.5	1.4	4.8	4.7	1.1	12.5	718	65	122	172	57	110	337	131
BDX27677	black	Montículo 1	11.6	0.0	44.7	0.2	5.4	10.3	2.3	25.5	1112	50	147	175	61	108	296	151
BDX27678			15.9	1.6	49.9	1.4	3.2	9.0	1.1	18.0	1146	75	147	196	32	118	297	163
BDX27679			14.1	1.0	58.3	0.6	3.3	6.7	1.4	14.6	854	61	135	158	1069	125	326	172
BDX27680			14.5	1.3	47.1	0.4	4.3	9.3	1.8	21.5	839	47	111	181	62	107	301	161
BDX27682			16.7	1.8	52.9	0.5	2.8	8.6	1.4	15.4	1002	60	139	174	359	108	305	149
BDX27683			15.5	1.1	45.5	1.7	3.4	11.9	1.5	19.5	1226	47	173	388	439	108	296	181
BDX27698			17.0	1.1	50.3	6.3	2.7	8.0	1.2	13.5	1130	48	152	160	58	112	288	140
BDX27686		Montículo 25	17.6	1.8	55.6	0.9	3.3	5.0	1.3	14.4	904	63	165	210	854	122	304	155
BDX27690			17.8	2.3	53.0	0.7	4.1	5.5	1.3	15.3	1120	56	125	178	112	121	288	162
BDX27674	gray	Montículo 1	19.9	2.5	57.9	0.5	3.2	3.7	1.1	11.1	813	37	130	176	42	113	363	171
BDX27676			19.4	2.7	56.0	1.3	2.6	4.7	1.1	12.3	1302	75	160	189	44	116	280	197
BDX27679	cream		8.0	2.9	38.0	1.3	2.6	4.6	3.2	39.4	1054	58	100	155	8742	125	334	166
BDX27682			16.6	3.7	62.6	2.2	2.5	4.4	0.6	7.5	489	32	70	92	20797	91	275	169
BDX27686		Montículo 25	18.2	5.1	57.9	2.1	2.6	4.3	0.8	8.9	429	26	90	106	20208	100	275	148
BDX27683		Montículo 1	15.3	4.3	44.1	3.2	3.9	10.2	1.3	17.7	988	29	248	1690	2616	99	293	295
BDX27680	brown		11.8	1.6	44.6	0.7	4.2	8.0	1.7	27.4	934	48	171	167	691	113	292	133
BDX27690			18.9	3.4	54.1	0.8	3.9	4.7	1.2	13.1	1380	48	147	180	45	113	286	190
BDX27683	beige		12.2	4.2	57.5	6.8	2.1	5.6	1.6	10.0	915	48	121	132	8095	100	386	135